

University of Kentucky

UKnowledge

Theses and Dissertations--Mathematics

Mathematics


2024

Solid Angle Measure Approximation Methods for Polyhedral Cones

Allison Fitisone

University of Kentucky, allisonfitisone@gmail.com

Author ORCID Identifier:

 <https://orcid.org/0000-0003-3803-1454>

Digital Object Identifier: <https://doi.org/10.13023/etd.2024.104>

[Right click to open a feedback form in a new tab to let us know how this document benefits you.](#)

Recommended Citation

Fitisone, Allison, "Solid Angle Measure Approximation Methods for Polyhedral Cones" (2024). *Theses and Dissertations--Mathematics*. 109.

https://uknowledge.uky.edu/math_etds/109

This Doctoral Dissertation is brought to you for free and open access by the Mathematics at UKnowledge. It has been accepted for inclusion in Theses and Dissertations--Mathematics by an authorized administrator of UKnowledge. For more information, please contact UKnowledge@lsv.uky.edu.

STUDENT AGREEMENT:

I represent that my thesis or dissertation and abstract are my original work. Proper attribution has been given to all outside sources. I understand that I am solely responsible for obtaining any needed copyright permissions. I have obtained needed written permission statement(s) from the owner(s) of each third-party copyrighted matter to be included in my work, allowing electronic distribution (if such use is not permitted by the fair use doctrine) which will be submitted to UKnowledge as Additional File.

I hereby grant to The University of Kentucky and its agents the irrevocable, non-exclusive, and royalty-free license to archive and make accessible my work in whole or in part in all forms of media, now or hereafter known. I agree that the document mentioned above may be made available immediately for worldwide access unless an embargo applies.

I retain all other ownership rights to the copyright of my work. I also retain the right to use in future works (such as articles or books) all or part of my work. I understand that I am free to register the copyright to my work.

REVIEW, APPROVAL AND ACCEPTANCE

The document mentioned above has been reviewed and accepted by the student's advisor, on behalf of the advisory committee, and by the Director of Graduate Studies (DGS), on behalf of the program; we verify that this is the final, approved version of the student's thesis including all changes required by the advisory committee. The undersigned agree to abide by the statements above.

Allison Fitisone, Student

Dr. Yuan Zhou, Major Professor

Dr. Benjamin Braun, Director of Graduate Studies

Solid Angle Measure Approximation Methods for Polyhedral Cones

DISSERTATION

A dissertation submitted in partial
fulfillment of the requirements for
the degree of Doctor of Philosophy
in the College of Arts and Sciences
at the University of Kentucky

By
Allison Marie Fitisone
Lexington, Kentucky

Director: Dr. Yuan Zhou, Professor of Mathematics
Lexington, Kentucky
2024

Copyright© Allison Marie Fitisone 2024

<https://orcid.org/0000-0003-3803-1454>

ABSTRACT OF DISSERTATION

Solid Angle Measure Approximation Methods for Polyhedral Cones

Polyhedral cones are of interest in many fields, like geometry and optimization. A simple, yet fundamental question we may ask about a cone is how large it is. As cones are unbounded, we consider their solid angle measure: the proportion of space that they occupy. Beyond dimension three, definitive formulas for this measure are unknown. Consequently, devising methods to estimate this quantity is imperative. In this dissertation, we endeavor to enhance our understanding of solid angle measures and provide valuable insights into the efficacy of various approximation techniques.

Ribando and Aomoto independently discovered a Taylor series formula for solid angle measures of certain simplicial cones. Leveraging Brion–Vergne Decomposition, we extend their findings, devising an algorithm for approximating solid angle measures of polyhedral cones, including those where the series is not applicable. We compare our method to other estimation techniques, and explore the practical applications of these methods within optimization.

Gomory and Johnson established the use of facets of master cyclic group polyhedra to derive cuts for integer programs. Within this framework, the size of the solid angle subtended by a facet determines its importance. We apply various approximation techniques to measure facet importance, provide computational results, and discuss their implications.

KEYWORDS: solid angle, polyhedral cone, spherical polytope

Allison Marie Fitisone

April 22, 2024

Solid Angle Measure Approximation Methods for Polyhedral Cones

By
Allison Marie Fitisone

Dr. Yuan Zhou
Director of Dissertation

Dr. Benjamin Braun
Director of Graduate Studies

April 22, 2024
Date

Dedicated to Xhafer

ACKNOWLEDGMENTS

I am grateful to all those who helped me throughout graduate school. I am profoundly thankful to my advisor, Dr. Yuan Zhou, for her unwavering support and invaluable guidance. I am extremely grateful to Dr. Ehrenborg for his willingness to offer assistance whenever needed. Thank you to Dr. Braun, Dr. Ehrenborg, Dr. Smith, Dr. Troland, and Dr. Zhou for agreeing to serve on my committee.

A special thanks to my wonderful family, especially my mom Kathy, dad Paulo, sisters Angella, Karalyn, and Marci, brother Randall, and my husband Xhafer for their continued love, prayers, and guidance.

TABLE OF CONTENTS

Acknowledgments	iii
List of Tables	vi
List of Figures	vii
Chapter 1 Introduction and Background	1
1.1 Convexity and Polyhedra	1
1.2 Master Cyclic Group Polyhedra and Group–Facet Polytopes	3
Chapter 2 Solid Angles and their Properties	11
2.1 Solid Angles	11
2.2 Solid Angle Measure Invariant Operations	12
2.3 Outer normal cones of $\Pi(q, f)$ and $\mathfrak{B}(q, f)$	16
Chapter 3 Solid Angle Approximation Methods	20
3.1 Cousins–Vempala Practical Volume Algorithm	20
3.1.1 Discussion	23
3.2 Shooting Experiments	24
3.3 The Power Series Method	27
Chapter 4 Cone Decompositions for Solid angle measure	29
4.1 First decomposition method	30
4.1.1 Brion–Vergne decomposition with respect to a hyperplane	30
4.1.2 Solid angle decomposition that includes cones containing lines	31
4.2 Second decomposition method	37
4.2.1 Brion–Vergne decomposition with respect to a line	37
4.2.2 Solid angle decomposition that includes lower dimensional cones	39
4.3 Asymptotic bound on the truncation error	41
4.3.1 Tridiagonal associated matrices	41
4.3.2 Eigenvalues and series truncation errors	43
Chapter 5 Implementation and Applications of Solid Angle Measure Approx- imation Methods	51
5.1 Implementation	51
5.1.1 Stopping Criterion	51
5.1.2 Constructing Polyhedra	51
5.1.3 Projecting out Lineality Space	51
5.1.4 Triangulation	52
5.1.5 Decomposition	53
5.1.6 Computing the Power Series	54

5.1.7	Discussion of Optimizations to Code	56
5.2	Computational Experiments	57
5.2.1	Simplicial Cones with Known Solid Angles	57
5.2.2	Outer Normal Cones of Group-Facet Polytopes	59
5.2.3	Outer Normal Cones of Blockers of Master Cyclic Group Poly- hedra	67
Appendices	78
Appendix A:	SageMath Program	78
Appendix B:	Cones and Triangulations	87
Bibliography	90
Vita	93

LIST OF TABLES

5.1	Solid angle measures of outer normal cones at vertices of $\tilde{\Pi}(7, 6)$	60
5.2	Solid angle measures of outer normal cones at vertices of $\tilde{\Pi}(8, 7)$	60
5.3	Solid angle measures of outer normal cones at vertices of $\tilde{\Pi}(9, 8)$	62
5.4	Solid angle measures of outer normal cones at vertices of $\tilde{\Pi}(10, 9)$	64
5.5	Solid angle measures of outer normal cones at vertices of $\tilde{\Pi}(11, 10)$	66
5.6	Solid angle measures of outer normal cones at vertices of $\Pi(7, 6) + \mathbb{R}_{>0}^6$.	67
5.7	Solid angle measures of outer normal cones at vertices of $\Pi(8, 2) + \mathbb{R}_{>0}^7$.	68
5.8	Solid angle measures of outer normal cones at vertices of $\Pi(8, 4) + \mathbb{R}_{>0}^7$.	68
5.9	Solid angle measures of outer normal cones at vertices of $\Pi(8, 7) + \mathbb{R}_{>0}^7$.	70
5.10	Solid angle measures of outer normal cones at vertices of $\Pi(9, 3) + \mathbb{R}_{>0}^8$.	72
5.11	Solid angle measures of outer normal cones at vertices of $\Pi(9, 8) + \mathbb{R}_{>0}^8$.	74
5.12	Solid angle measures of outer normal cones at vertices of $\Pi(10, 2) + \mathbb{R}_{>0}^9$.	76

LIST OF FIGURES

1.1	Left: The polyhedron $P(3, 2)$ with the line containing its nontrivial facet. Right: The template function h defined by the nontrivial facet of $P(3, 2)$.	7
1.2	Left: Feasible Region of the IP contains the dots. Integer hull is the darker region. Feasible region of the LPR is the lighter region. Right: Feasible region of the LPR with added cut is the lighter region.	8
4.1	The (b_1, b_2) -plane corresponding to the proof of Proposition 4.3.10. The region bounded by rays θ_1 and θ_2 shows where the ratio bounds in (4.29) hold; The region above the horizontal line at N_2 and the ray θ_2 and the region to the right of the vertical line at N_1 and below the ray θ_1 correspond to Claim 4.3.11 (1) and (2), respectively.	47
4.2	Planes of multiexponents $(b_1, b_2) \in \mathbb{N}^2$ for analyzing the series truncation errors $E(N_1, N_2)$ (left) and $E(N_1 + \ell, N_2 + \ell)$ (right). The regions indicate which series S_k the term $ A_{b_1, b_2} \beta_1^{b_1} \beta_2^{b_2} $ belongs to in (4.31) and (4.32). . .	49
5.1	Number of cones in decomposition of triangulated cones versus running time.	53
5.2	Target Absolute Error versus Absolute Error for polyhedral cones with known solid angle measures on log-log scale.	59

Chapter 1 Introduction and Background

The focus of this dissertation is to analyze various solid angle measure approximation methods to measure cones of interest. In Chapter 1, we establish essential terminology and notions that will be used frequently throughout the dissertation. In Chapter 2, we consider solid angles and transformations which preserve solid angle measures. In Chapter 3, we survey existing solid angle approximation methods. In Chapter 4, we establish a decomposition method to approximate solid angle measures of polyhedral cones in dimensions greater than three, expanding upon the work of Ribando and Aomoto. Finally, in Chapter 5, we discuss the implementation and application of the considered approximation methods, with descriptions and results of computational experiments conducted.

1.1 Convexity and Polyhedra

Recall that a convex set satisfies the property that the line segment between any two points in the set is completely contained within the set. Formally, a *convex set* $C \subseteq \mathbb{R}^d$ is a set of points such that if $\mathbf{x}, \mathbf{y} \in C$, then $\lambda\mathbf{x} + (1 - \lambda)\mathbf{y} \in C$ for all $0 \leq \lambda \leq 1$. A *convex combination* of $\mathbf{x}_1, \mathbf{x}_2, \dots, \mathbf{x}_n \in \mathbb{R}^d$ is a linear combination

$$\lambda_1\mathbf{x}_1 + \lambda_2\mathbf{x}_2 + \dots + \lambda_n\mathbf{x}_n$$

where $\lambda_i \in \mathbb{R}_{\geq 0}$ for $i = 1, 2, \dots, n$, and $\lambda_1 + \lambda_2 + \dots + \lambda_n = 1$. The set of all possible convex combinations of the elements of a set X is a convex set denoted by $\text{conv}(X)$, called the *convex hull* of X .

Polyhedra are a class of convex bodies that are of particular interest. A subset P of \mathbb{R}^d is a *polyhedron* if there exists $A \in \mathbb{R}^{m \times d}$ and $\mathbf{b} \in \mathbb{R}^m$ ($m \geq 0$) such that

$$P = \{\mathbf{x} \mid A\mathbf{x} \leq \mathbf{b}\},$$

so that P is the intersection of finitely many affine half-spaces. Above, we use the shorthand notation $A\mathbf{x} \leq \mathbf{b}$ which represents the system of *linear inequality constraints*

$$\mathbf{a}_1^t\mathbf{x} \leq b_1, \quad \mathbf{a}_2^t\mathbf{x} \leq b_2, \dots, \quad \mathbf{a}_m^t\mathbf{x} \leq b_m,$$

with $\mathbf{a}_1, \mathbf{a}_2, \dots, \mathbf{a}_m$ representing the row vectors of A and b_1, b_2, \dots, b_m being the components of \mathbf{b} . An inequality $\mathbf{a}^t\mathbf{x} \leq b$ (with nonzero \mathbf{a}) is a *valid inequality* of a polyhedron P if it is satisfied by every point in P . The intersection of P with the hyperplane $\{x \mid \mathbf{a}^t\mathbf{x} = b\}$, where $\mathbf{a}^t\mathbf{x} \leq b$ is a valid inequality of P , is called a *face* of P , and is itself a polyhedron. The *dimension* of a face of P is the dimension of its affine hull. A face of P having dimension one less than that of P is called a *facet* of P . A face of P having dimension 0 is called an *extreme point* or a *vertex* of P .

There are two fundamental subclasses of convex polyhedra: polytopes and polyhedral cones. A subset P of \mathbb{R}^d is a *polytope* if it is the convex hull of finitely many

points in \mathbb{R}^d , or equivalently, if it is a bounded polyhedron. A polytope in \mathbb{R}^d with dimension $n \leq d$ is called an n -polytope. A *cone* (not necessarily convex) is a nonempty set of points $C \subseteq \mathbb{R}^d$ such that if $\mathbf{x} \in C$, then $\lambda\mathbf{x} \in C$ for all $\lambda \geq 0$. Terminology for cones mirrors that of convex sets. A *conic combination* of $\mathbf{x}_1, \mathbf{x}_2, \dots, \mathbf{x}_n \in \mathbb{R}^d$ is a linear combination

$$\lambda_1\mathbf{x}_1 + \lambda_2\mathbf{x}_2 + \dots + \lambda_n\mathbf{x}_n$$

where $\lambda_i \in \mathbb{R}_{\geq 0}$ for $i = 1, 2, \dots, n$. The set of all possible conic combinations of the elements of a set X is a convex cone denoted by $\text{cone}(X)$, called the *conic hull* of X . We say $\text{cone}(X)$ is *generated* by X . When X is finite, we say C is *finitely generated*. A vector $\mathbf{r} \in C$ is an *extreme ray* of C if it satisfies the property: for any $\mathbf{x}, \mathbf{y} \in C$, $\mathbf{x} + \mathbf{y} \in \{\lambda\mathbf{r} \mid \lambda \geq 0\}$ implies $\mathbf{x}, \mathbf{y} \in \{\lambda\mathbf{r} \mid \lambda \geq 0\}$. A cone C is *polyhedral* if there exists a matrix A such that

$$C = \{\mathbf{x} \mid A\mathbf{x} \leq \mathbf{0}\},$$

or equivalently, C is the intersection of finitely many half-spaces. Note that this implies that polyhedral cones are closed. The well-known Minkowski-Weyl Theorem states that a convex cone is polyhedral if and only if it is finitely generated. Given $X \subseteq \mathbb{R}^d$ and $Y \subseteq \mathbb{R}^d$, the *Minkowski sum* of X and Y is

$$X + Y = \{\mathbf{x} + \mathbf{y} \mid \mathbf{x} \in X \text{ and } \mathbf{y} \in Y\}.$$

Every polyhedron $P \subseteq \mathbb{R}^d$ can be expressed as the Minkowski sum of a polytope and a cone:

$$P = \text{conv}(X) + \text{cone}(Y),$$

for some $X, Y \subseteq \mathbb{R}^d$.

Certain types of polyhedral cones are worth distinguishing. A *pointed cone* has the origin as a vertex, or equivalently, does not contain a linear subspace of dimension greater than zero. A *simplicial cone* is generated by a linearly independent set of vectors. Certain cones arise in relation to convex sets. Let $X \subset \mathbb{R}^d$ be a convex set and $\mathbf{z} \in X$. The *outer normal cone* of X at \mathbf{z} is

$$N_X(\mathbf{z}) = \{\mathbf{y} \in \mathbb{R}^d \mid \mathbf{y}^t\mathbf{z} \geq \mathbf{y}^t\mathbf{x} \text{ for all } \mathbf{x} \in X\}.$$

The *recession cone* of X is

$$\{\mathbf{y} \in \mathbb{R}^d \mid \mathbf{y} + X \subseteq X\}.$$

Let $C \subseteq \mathbb{R}^d$ be a convex cone. The *dual cone* of C is

$$C^* = \{\mathbf{y} \in \mathbb{R}^d \mid \mathbf{y}^t\mathbf{c} \geq 0 \text{ for all } \mathbf{c} \in C\}.$$

The *polar cone* of C is the negative of the dual cone of C .

We can restrict our study to pointed cones by making use of the well known cone decomposition theorem of Stoer and Witzgall [43]. A closed convex cone can be expressed as the Minkowski sum of two orthogonal sets: a pointed cone and a linear subspace. Let $C \subseteq \mathbb{R}^d$ be a cone. The *linear span* of C , denoted by $\text{lin}(C)$ is

the smallest linear subspace containing C and is given by $\text{lin}(C) = C + (-C)$. The *dimension* of C is the dimension of the linear span of C . If C is not pointed, then C contains the linear subspace $L = C \cap (-C)$ of dimension $d - \dim(\text{lin}(C))$. The subspace L is called the *lineality space* of C . Thus, the lineality space of any pointed cone is $\{\mathbf{0}\}$. If C/L denotes the orthogonal projection of C onto the orthogonal complement of L , that is $C/L = C \cap L^\perp$, then C/L is pointed and C can be expressed as the Minkowski sum $C = L + C/L$.

1.2 Master Cyclic Group Polyhedra and Group-Facet Polytopes

In this section, we will focus on two particular types of polyhedra which arise in the area of optimization, particularly in integer programming. We first give a brief introduction to integer programming to give context to these polyhedra.

An integer programming problem is a linear programming problem which requires variables to take on integer values. The goal of a linear program is to maximize or minimize some linear objective function, subject to certain linear constraints. A *linear programming problem* (LP) has the following standard form:

$$\begin{aligned} & \text{maximize } \mathbf{c}^t \mathbf{x} \\ & \text{subject to } A\mathbf{x} \leq \mathbf{b} \\ & \mathbf{x} \geq 0, \end{aligned} \tag{1.1}$$

where $\mathbf{x} = (x_1, x_2, \dots, x_n)$ is a vector of *decision variables*, A is a given $m \times n$ matrix, and \mathbf{c} and \mathbf{b} are given $n \times 1$ and $m \times 1$ vectors respectively. The vector \mathbf{c} is called the *objective vector*. A proposal of values for the entries of \mathbf{x} is a *solution*. A solution is *feasible* if it satisfies all of the constraints. The *feasible region* of a linear program is the set of all feasible solutions. Note that the feasible region of an LP is the intersection of halfspaces, and so it is a polyhedron. A feasible solution that attains the desired maximum is *optimal*. If a problem has no feasible solutions, it is called *infeasible*. When the problem has feasible solutions whose objective values can be arbitrarily large, it is called *unbounded*.

We may also view an LP in the equivalent form as a *dictionary*

$$\begin{aligned} z &= \sum_{j=1}^n c_j x_j \\ x_{n+i} &= b_i - \sum_{j=1}^n a_{ij} x_j \quad (i = 1, 2, \dots, m). \end{aligned}$$

The variables which appear in the objective function are called *nonbasic variables* and take on value 0. The variables that do not appear in the objective function are called *basic variables*.

An *integer programming problem* (IP) has the following standard form:

$$\begin{aligned}
& \text{maximize } \mathbf{c}^t \mathbf{x} \\
& \text{subject to } A\mathbf{x} \leq \mathbf{b} \\
& \mathbf{x} \geq 0 \\
& \mathbf{x} \in \mathbb{Z}^n,
\end{aligned} \tag{1.2}$$

Note that the integrality constraints of an IP imply that the feasible region is not convex, hence not a polyhedron. To extend the notion of a valid inequality to an IP we consider the convex hull of the feasible region of an IP, called the *integer hull*. A *valid inequality* for an IP is a valid inequality for the integer hull.

In practice, to solve (1.2), one ignores the integrality constraint and solves the *linear programming relaxation* (LPR) of (1.2), described in (1.1). Linear programs can be efficiently solved by applying the simplex algorithm, which moves from feasible dictionary to feasible dictionary by exchanging a basic variable for a nonbasic variable, while increasing the objective function at each step. If the optimal solution to the LPR is integral, then it is the optimal solution to the IP. If the LPR is infeasible, then the IP is infeasible. Otherwise, the optimal solution to (1.1) given by the simplex algorithm takes on fractional values and so is not a feasible solution to (1.2). To deal with the latter case, we delve into the realm of cutting plane theory.

The cutting plane approach to solve integer programs, established by Gomory [21], involves generating valid inequalities (also called *cutting planes* or *cuts*) for integer programs. When the current optimal solution is not integral, a cut (or cuts) is generated which is satisfied by all the feasible integer solutions, but not the current optimal solution. The cut (or cuts) is added to the LPR, and the process is repeated. There are many ways to generate cuts, but we focus our attention on those derived from facets of master cyclic group polyhedra.

Consider the feasible region of an IP (1.2). By introducing nonnegative slack variables, the feasible region of an IP is described by

$$A\mathbf{x} = \mathbf{b}, \quad \mathbf{x} \geq 0, \quad \mathbf{x} \text{ integer.} \tag{1.3}$$

By partitioning the variables into basic and nonbasic variables, one can rewrite (1.3) as

$$B\mathbf{x}_B + N\mathbf{x}_N = \mathbf{b}, \quad \mathbf{x}_B, \mathbf{x}_N \geq 0, \quad \mathbf{x}_B, \mathbf{x}_N \text{ integer.} \tag{1.4}$$

If \mathbf{x}_B is a vector of integer components, then $B^{-1}N\mathbf{x}_N \equiv B^{-1}\mathbf{b} \pmod{1}$. Note here that the requirement of nonnegativity for \mathbf{x}_B is dropped. If column i of $B^{-1}N$ is denoted by \mathbf{t}_i , $B^{-1}\mathbf{b} = \mathbf{b}'$ and $\mathbf{x}_N = (n_1, n_2, \dots, n_{|N|})$, then the relation is expressed as

$$\sum_{i=1}^{|N|} n_i \mathbf{t}_i \equiv \mathbf{b}' \pmod{1}. \tag{1.5}$$

Consider a *group character* χ , an addition preserving map sending column vectors such as the \mathbf{t}_i 's into a group G . Applying such a map χ to (1.5) gives

$$\sum_{i=1}^{|N|} \chi(n_i \mathbf{t}_i) \equiv \chi(\mathbf{b}') \pmod{1}. \tag{1.6}$$

Now, suppose G is a finite additive Abelian group which contains an identity element $\bar{0}$ and an element g_0 . Let t be a function which assigns to each element in G a nonnegative integer. A function π is a *valid function* with right hand side g_0 as defined in [23] if π is continuous, nonnegative, $\pi(\bar{0}) = 0$, $\pi(g_0) = 1$, and $\sum_{g \in G} t(g)g = g_0$ implies $\sum_{g \in G} t(g)\pi(g) \geq 1$. Thus, if π is a valid function with right hand side $\chi(\mathbf{b}')$, then

$$\sum_{i=1}^{|N|} \pi(\chi(\mathbf{t}_i))n_i \geq \sum_{i=1}^{|N|} \pi(\chi(n_i \mathbf{t}_i)) \geq 1. \quad (1.7)$$

With this, Gomory and Johnson [23] showed that if π is subadditive and χ is a group character which maps the columns of $B^{-1}N$ into a group G , then (1.7) is a cut for all IP's with constraints $B\mathbf{x}_B + N\mathbf{x}_N$. Thus, one is interested in valid functions π . In the Gomory–Johnson model, the valid functions of particular interest are called facets. The procedure to construct such valid functions π is described below.

Suppose in the optimal dictionary from applying the simplex algorithm to the LPR, we have a basic variable x which takes on a fractional value. If the data is all rational, we can express x as a sum of terms with common denominator q :

$$\sum_{j \in \mathcal{N}} \frac{r_j}{q} y_j + x = \frac{b}{q}, \quad (1.8)$$

where \mathcal{N} is the set of indices of the integer nonbasic variables $y_1, y_2, \dots, y_{|\mathcal{N}|}$. Given nonnegative integer b above, we consider $f \equiv b \pmod{q}$ where $0 < f < q$. With q and f determined, to generate a cut for the integer program, we consider the master cyclic group polyhedron $P(q, f)$. These polyhedra first appeared in [21]. The *master cyclic group polyhedron* is

$$P(q, f) = \text{conv} \left(\left\{ \mathbf{z} \in \mathbb{Z}_{\geq 0}^{q-1} \mid \sum_{i=1}^{q-1} i \cdot z_i \equiv f \pmod{q} \right\} \right).$$

The term “master cyclic group polyhedron” comes from the fact that we can view the set of coefficients in the summation above as the set of all nonzero elements of the cyclic group of order q . The nonnegativity conditions $\mathbf{z} \geq 0$ imply that $P(q, f)$ lies within $\mathbb{R}_{\geq 0}^{q-1}$, the first orthant of \mathbb{R}^{q-1} . Gomory [21] showed that $P(q, f)$ is full-dimensional and has $\mathbb{R}_{\geq 0}^{q-1}$ as its recession cone, that is

$$P(q, f) = P(q, f) + \mathbb{R}_{\geq 0}^{q-1}.$$

Cutting planes can be derived from facets of master cyclic group polyhedra via Gomory and Johnson’s interpolation procedure [22] which is described in detail in [11]. We briefly outline the interpolation procedure. Given a facet-defining inequality for the polyhedron $P(q, f)$:

$$\sum_{i=1}^{q-1} \pi_i z_i \geq 1,$$

define the piecewise linear function $h : \mathbb{R} \rightarrow [0, 1]$ by

$$h(v) = \begin{cases} 0 & \text{if } v = \lfloor v \rfloor \\ \pi_i & \text{if } v - \lfloor v \rfloor = \frac{i}{q} \text{ for } i \in \{1, 2, \dots, q-1\} \\ \varepsilon\pi_i + (1 - \varepsilon)\pi_{i+1} & \text{if } v - \lfloor v \rfloor = \frac{i+\varepsilon}{q} \text{ for } i \in \{1, 2, \dots, q-1\}, 0 < \varepsilon < 1. \end{cases}$$

The above function is called the *facet interpolated template function* and abbreviated as *template function* in [11]. It is sufficient to consider template functions on the interval $[0, 1]$ as they are periodic modulo 1. We apply h to (1.8) to obtain the following valid inequality of the IP:

$$\sum_{j \in \mathcal{N}} h\left(\frac{r_j}{q}\right) y_j \geq 1.$$

Thus, it is of interest to determine facet-defining inequalities of master cyclic group polyhedra. In what follows, we will use the terms “facet” and “facet-defining inequality” interchangeably.

We demonstrate the interpolation procedure to generate cutting planes in the example below.

Example 1.2.1. Consider the integer program

$$\begin{aligned} & \text{maximize } 4x_1 - 3x_2 \\ & \text{s.t. } 3x_1 + x_2 + y_1 = 5 \\ & \quad -2x_1 + x_2 + y_2 = 1 \\ & \quad x_1 + x_2 + y_3 = 3 \\ & \quad x_1, x_2, y_1, y_2, y_3 \geq 0 \\ & \quad x_1, x_2 \in \mathbb{Z}. \end{aligned}$$

Solving the LP-relaxation of the integer program yields a fractional optimal solution of $(\frac{5}{3}, 0)$. The row corresponding to x_1 in the optimal dictionary is

$$\frac{1}{3}y_1 + \frac{1}{3}x_2 + x_1 = \frac{5}{3} \tag{1.9}$$

Thus, we consider facets of $P(3, 2)$. This polyhedron has one nontrivial facet given by

$$\frac{1}{2}z_1 + z_2 \geq 1,$$

from which we obtain the template function h shown below.

Now, we apply h to the coefficients in (1.9) to obtain the following cut

$$h\left(\frac{1}{3}\right) y_1 + h\left(\frac{1}{3}\right) x_2 = \frac{1}{2}y_1 + \frac{1}{2}x_2 \geq 1.$$

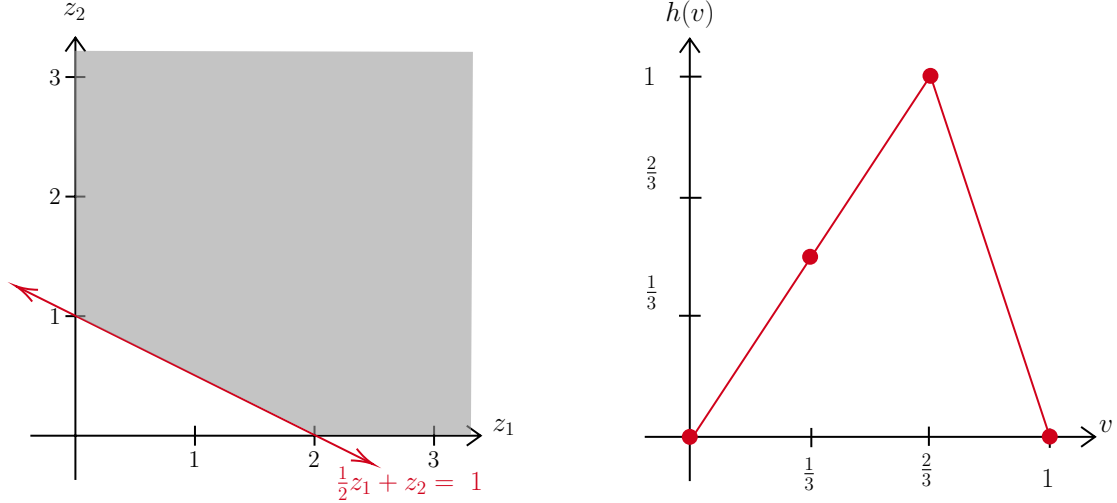


Figure 1.1: Left: The polyhedron $P(3, 2)$ with the line containing its nontrivial facet. Right: The template function h defined by the nontrivial facet of $P(3, 2)$.

which is equivalent to $x_1 \leq 1$. It is clear that this cut is valid for the integer hull and is violated by $(\frac{5}{3}, 0)$. Adding this cut gives another linear programming relaxation of the IP:

$$\begin{aligned}
 & \text{maximize } 4x_1 - 3x_2 \\
 & \text{s.t. } 3x_1 + x_2 + y_1 = 5 \\
 & \quad -2x_1 + x_2 + y_2 = 1 \\
 & \quad x_1 + x_2 + y_3 = 3 \\
 & \quad x_1 + y_4 = 1 \\
 & \quad x_1, x_2, y_1, y_2, y_3, y_4 \geq 0
 \end{aligned}$$

The feasible region of this new LPR is shown in Figure 1.2.1. Solving the new LPR yields an optimal solution of $(1, 0)$ which is integral and so optimal for the IP.

It is important to note that while our example only required the addition of one cut, in general, one may require multiple rounds of adding cuts, with multiple cuts added in each round.

The facets of master cyclic group polyhedra are typically grouped into two categories: trivial facets (facets corresponding to nonnegativity constraints) and nontrivial facets. Gomory [21] characterized the nontrivial facets of master cyclic group polyhedra in the following theorem:

Theorem 1.2.2 ([21, Structure Theorem], rephrased). *For positive integers $f < q$, $\pi^t \mathbf{z} \geq 1$ is a nontrivial facet of $P(q, f)$ if and only if $\pi^t = (\pi_1, \pi_2, \dots, \pi_{q-1})$ is an*

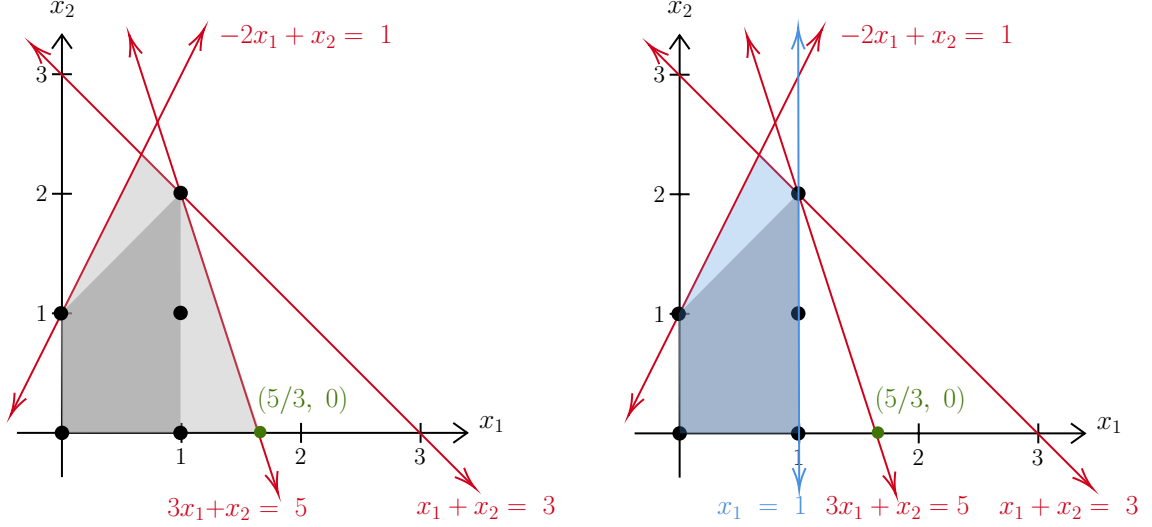


Figure 1.2: Left: Feasible Region of the IP contains the dots. Integer hull is the darker region. Feasible region of the LPR is the lighter region. Right: Feasible region of the LPR with added cut is the lighter region.

extreme point of the following system:

$$\pi_i \geq 0, \quad i = 1, \dots, q-1 \quad (\text{nonnegativity}) \quad (1.10a)$$

$$\pi_f = 1, \quad (1.10b)$$

$$\pi_i + \pi_j = 1, \quad i + j \equiv f \pmod{q} \quad (\text{complementarity}) \quad (1.10c)$$

$$\pi_i + \pi_j \geq \pi_k \quad k \equiv i + j \pmod{q} \quad (\text{subadditivity}). \quad (1.10d)$$

Gomory [21] showed that the underlying group structure of master cyclic group polyhedra allows one to relate facets of master cyclic group polyhedra via group homomorphisms.

Theorem 1.2.3 ([16, Theorem 2.4], rephrased). *Let q, f, s be positive integers with $f, s < q$. Let C_q denote the cyclic group of order q , and $\phi : C_q \rightarrow C_q$ be an automorphism such that $\phi(f) = s$. The facets of $P(q, f)$ are in one-to-one correspondence with the facets of $P(q, s)$. In particular, if*

$$(\pi_1, \pi_2, \dots, \pi_{q-1}) \cdot \mathbf{x} \geq \pi_f$$

is a facet of $P(q, f)$, then

$$(\pi_{\phi(1)}, \pi_{\phi(2)}, \dots, \pi_{\phi(q-1)}) \cdot \mathbf{x} \geq \pi_{\phi(s)}$$

is a facet of $P(q, s)$.

Thus, given a group automorphism $\phi : C_q \rightarrow C_q$, the facets of $P(q, \phi(f))$ are essentially the same as the facets of $P(q, f)$. As a consequence, we can understand the facial structure of the master cyclic group polyhedra $P(q, 1), P(q, 2), \dots, P(q, q-1)$

by considering only a subset of these $q - 1$ polyhedra. For instance, if $f_1, f_2 \in \{2, 4, 5, 7, 8\}$, then the facets of $P(9, f_1)$ and $P(9, f_2)$ are essentially the same; and the facets of $P(9, 3)$ and $P(9, 6)$ are essentially the same. Therefore, the facial structure of these eight polyhedra can be understood by looking at the facial structure of just two polyhedra; take, for instance, $P(9, 3)$ and $P(9, 8)$.

Theorem 1.2.4 ([16, Theorem 2.5], rephrased). *Let q, f, p, e be positive integers with $f, p < q$ and $e \equiv f \pmod{p}$, and where p divides q but p does not divide f . Let C_q denote the cyclic group of order q , C_p denote the cyclic group of order p and $\phi : C_q \rightarrow C_p$ be the group homomorphism defined by $\phi(j) = j \pmod{p}$. If*

$$(\pi_1, \pi_2, \dots, \pi_{p-1}) \cdot \mathbf{x} \geq \pi_e$$

is a facet of $P(p, e)$, then the facet of $P(q, f)$ obtained via homomorphic lifting is

$$(\pi_{\phi(1)}, \pi_{\phi(2)}, \dots, \pi_{\phi(q-1)}) \cdot \mathbf{x} \geq \pi_{\phi(e)},$$

where $\pi_0 = 0$.

As noted by Evans [16], the facets resulting from homomorphic lifting are characterized by the presence of zero(s) and cyclic repetitions. Consider the nontrivial facet $x_1 + 2x_2 \geq 2$ of $P(3, 2)$. As 3 divides 9 but does not divide 8, and $2 \equiv 8 \pmod{3}$, by Theorem 1.2.4, the facet

$$x_1 + 2x_2 \geq 2$$

of $P(3, 2)$ lifts to the facet

$$x_1 + 2x_2 + x_4 + 2x_5 + x_7 + 2x_8 \geq 2$$

of $P(9, 8)$. In general, a facet of $P(q, f)$ obtained by homomorphic lifting of a facet of $P(p, e)$ is the facet of $P(p, e)$ cyclically repeated $\frac{q}{p}$ times [16].

Since facets of the master cyclic group polyhedra can be used to generate valid inequalities for integer programs, we would like a method to generate these facets. We focus on the convex hull of the extreme points of the inequality system (1.10), as the components of the extreme points give coefficients for the desired facets. In the following, we borrow terminology and notation from [42].

Definition 1.2.5. The *group facet polytope*, $\Pi(q, f)$, is the convex hull of the extreme points of the inequality system (1.10).

The nonnegativity constraints (1.10a) imply that the group facet polytope also lies in the first orthant. However, unlike the master cyclic group polyhedron, the group facet polytope is not full-dimensional, due to the complementarity equations (1.10c).

As aforementioned, the recession cone of a master cyclic group polyhedron is the first orthant so that

$$P(q, f) = P(q, f) + \mathbb{R}_{\geq 0}^{q-1}.$$

Polyhedra of this type are of interest, particularly when viewed through the framework of blocking polyhedra which was introduced by Fulkerson. A thorough exposition of blocking polyhedra may be found in [40]. Shim [41] and Hunsaker [32] considered master cyclic group polyhedra within this framework. Let $X \subset \mathbb{R}^d$. The *blocker* of X is

$$\mathfrak{B}(X) = \{\mathbf{y} \in \mathbb{R}_{\geq 0}^d \mid \mathbf{y}^t \mathbf{x} \geq 1 \text{ for all } \mathbf{x} \in X\}.$$

Note that if X is a polyhedron of the form

$$X = \text{conv}(\mathbf{x}_1, \mathbf{x}_2, \dots, \mathbf{x}_s) + \mathbb{R}_{\geq 0}^d \quad (1.11)$$

then

$$\mathfrak{B}(X) = \{\mathbf{y} \in \mathbb{R}_{\geq 0}^d \mid \mathbf{y}^t \mathbf{x}_i \geq 1 \text{ for all } i = 1, 2, \dots, s\}$$

and $\mathfrak{B}(X)$ is called the *blocking polyhedron* of X . It is not difficult to see that for polyhedra of the form (1.11),

$$\mathfrak{B}(\mathfrak{B}(X)) = X,$$

that is, blocking polyhedra appear in pairs. More precisely, if there are vectors $\mathbf{c}_1, \mathbf{c}_2, \dots, \mathbf{c}_s, \mathbf{d}_1, \mathbf{d}_2, \dots, \mathbf{d}_t \in \mathbb{R}_{\geq 0}^d$ that satisfy

$$\text{conv}(\mathbf{c}_1, \mathbf{c}_2, \dots, \mathbf{c}_s) + \mathbb{R}_{\geq 0}^d = \{\mathbf{x} \in \mathbb{R}_{\geq 0}^d \mid \mathbf{d}_j^t \mathbf{x} \geq 1 \text{ for all } j = 1, \dots, t\},$$

then,

$$\text{conv}(\mathbf{d}_1, \mathbf{d}_2, \dots, \mathbf{d}_t) + \mathbb{R}_{\geq 0}^d = \{\mathbf{x} \in \mathbb{R}_{\geq 0}^d \mid \mathbf{c}_i^t \mathbf{x} \geq 1 \text{ for all } i = 1, \dots, s\}.$$

Moreover, $\text{conv}(\mathbf{c}_1, \mathbf{c}_2, \dots, \mathbf{c}_s) + \mathbb{R}_{\geq 0}^d$ and $\text{conv}(\mathbf{d}_1, \mathbf{d}_2, \dots, \mathbf{d}_t) + \mathbb{R}_{\geq 0}^d$ are called a *blocking pair* of polyhedra. As stated by Shim [41], we have the following characterization of the group facet polytope:

$$\mathfrak{B}(P(q, f)) = \Pi(q, f) + \mathbb{R}_{\geq 0}^{q-1},$$

that is, the group facet polytope is the convex hull of the vertices of the blocker of the master cyclic group polyhedron.

Gomory and Johnson [22] showed that the vertices of the blocker grow exponentially in q , and thus it is impractical to try to explain every facet. With the intuition that facets which appear larger on the surface of master cyclic group polyhedra will be more useful than those that do not, Gomory, Johnson, and Evans established the size of a facet, as seen from the origin, as a measure of its importance. In [2], it is noted that facets which appear larger on the surface of the polyhedron tend to exhibit a nicer structure than those which appear smaller. In the ensuing chapters, we consider and develop requisite tools to approximate the relative sizes of facets.

Chapter 2 Solid Angles and their Properties

In this chapter, we present essential definitions and background information regarding solid angles. We then establish results for solid angle measures of outer normal cones of $\Pi(q, f)$ and $\mathfrak{B}(q, f)$ at their vertices. The solid angle is a generalization of the two-dimensional plane angle. It is a measure of the proportion of space occupied by a cone in relation to some reference set, typically the ambient space in which the cone resides.

2.1 Solid Angles

We define the solid angle measure of a polyhedral cone according to [27], and we normalize it in such a way that the whole space has measure 1, according to [39].

Definition 2.1.1. The *normalized solid angle measure*, of a polyhedral cone $C \subseteq \mathbb{R}^d$ with respect to the space \mathbb{R}^d is defined as the ratio of the $(d-1)$ -dimensional volume of the intersection of the cone with the unit sphere S_{d-1} in \mathbb{R}^d centered around the origin to the volume of the unit sphere, i.e.,

$$\tilde{\Omega}_d(C) = \frac{\text{vol}_{d-1}(C \cap S_{d-1})}{\text{vol}_{d-1}(S_{d-1})}. \quad (2.1)$$

We note that the above definition works for convex non-polyhedral cones as well. When the cone C is of dimension $n < d$, let S_{n-1} denote the unit sphere centered around the origin in the n -dimensional linear space containing C . We define the normalized solid angle measure of C with respect to the linear span of C in a similar manner:

$$\tilde{\Omega}_n(C) = \frac{\text{vol}_{n-1}(C \cap S_{n-1})}{\text{vol}_{n-1}(S_{n-1})}.$$

We will refer to this measure as the *affine solid angle measure* of C .

Some authors prefer normalizing with respect to a half space [25] or the affine space [33]. Recall that a polyhedral cone is finitely generated. In dimensions two and three, we have easily understood formulas to compute solid angle measures of simplicial cones in terms of their extreme rays. In \mathbb{R}^2 , the solid (or plane) angle measure can be computed via the standard inner product. Assume that \mathbf{v}_1 and \mathbf{v}_2 are unit vectors in \mathbb{R}^2 . Then the normalized solid angle measure of the cone generated by \mathbf{v}_1 and \mathbf{v}_2 is

$$\frac{\cos^{-1}(\mathbf{v}_1 \cdot \mathbf{v}_2)}{2\pi}.$$

In \mathbb{R}^3 , the solid angle measure of a cone generated by three unit vectors is the area of the spherical triangle on the unit sphere formed by the unit vectors. There is a closed formula dating back to Euler and Lagrange which uses the scalar triple

product. Assume that $\mathbf{v}_1, \mathbf{v}_2$ and \mathbf{v}_3 are unit vectors in \mathbb{R}^3 . The solid angle measure of the cone generated by $\mathbf{v}_1, \mathbf{v}_2$ and \mathbf{v}_3 is given by [15]:

$$E := 2 \tan^{-1} \left(\frac{|\mathbf{v}_1 \cdot (\mathbf{v}_2 \times \mathbf{v}_3)|}{1 + \mathbf{v}_2 \cdot \mathbf{v}_3 + \mathbf{v}_2 \cdot \mathbf{v}_1 + \mathbf{v}_1 \cdot \mathbf{v}_3} \right),$$

and the normalized solid angle measure of the cone, which is the proportion of \mathbb{R}^3 that the cone occupies, is therefore $\frac{E}{4\pi}$. To the best of our knowledge, there currently does not exist a neat closed formula for the solid angle measure of polyhedral cones in dimensions greater than three.

The study of solid angles has gained a lot of traction in the past several years and has been investigated in several publications (see [5, 6, 19, 36, 39], etc.). Of particular interest is the solid angle measure of a polyhedral cone in dimensions beyond three. This measure has widespread potential applications, from computing the expected number of simplices in a triangulation of an n -cube [38], to calculating relative pixel purity index (PPI) scores [29], to computing the volume of the feasibility domain of an ecological community [35]. The various ways in which higher-dimensional solid angle measures appear in literature demonstrate the importance of the topic and necessitate a deeper understanding of it.

2.2 Solid Angle Measure Invariant Operations

In this section, we consider various maps as they relate to polyhedra and solid angle measures, namely, isometries, dilations, and embeddings into higher dimensions. We focus primarily on transformations on polyhedra where solid angle measures of outer normal cones at vertices are preserved. We then apply these transformations to the cones of interest to reduce the dimension of the solid angles we aim to measure.

We first demonstrate that the solid angle measure of an orthogonal direct sum of two cones is the product of their respective affine solid angle measures.

Lemma 2.2.1. *Let $C \subseteq \mathbb{R}^d$ be a polyhedral cone (or more generally, a convex cone) of dimension n . Suppose that $C = C_1 \oplus C_2$ is the orthogonal sum of cones C_1 and C_2 of dimensions n_1 and n_2 , respectively. Then, the normalized solid angle measure of C with respect to the linear span of C satisfies that*

$$\tilde{\Omega}_n(C) = \tilde{\Omega}_{n_1}(C_1) \cdot \tilde{\Omega}_{n_2}(C_2).$$

Proof. Since C_1 and C_2 are orthogonal, $n = n_1 + n_2$. Any $\mathbf{u} \in C$ can be uniquely expressed as $\mathbf{u} = \mathbf{v} + \mathbf{w}$ where $\mathbf{v} \in C_1, \mathbf{w} \in C_2$ and $\|\mathbf{u}\|^2 = \|\mathbf{v}\|^2 + \|\mathbf{w}\|^2$. Thus,

$$\int_C e^{-\|\mathbf{u}\|^2} d\mathbf{u} = \int_{C_1 \oplus C_2} e^{-\|\mathbf{v} + \mathbf{w}\|^2} d(\mathbf{v} + \mathbf{w}) = \int_{C_1} e^{-\|\mathbf{v}\|^2} d\mathbf{v} \int_{C_2} e^{-\|\mathbf{w}\|^2} d\mathbf{w}.$$

It then follows from (3.2) that

$$\tilde{\Omega}_n(C) = \frac{\int_C e^{-\|\mathbf{u}\|^2} d\mathbf{u}}{\pi^{n/2}} = \frac{\int_{C_1} e^{-\|\mathbf{v}\|^2} d\mathbf{v}}{\pi^{n_1/2}} \cdot \frac{\int_{C_2} e^{-\|\mathbf{w}\|^2} d\mathbf{w}}{\pi^{n_2/2}} = \tilde{\Omega}_{n_1}(C_1) \cdot \tilde{\Omega}_{n_2}(C_2). \quad \square$$

In the special case that one of the orthogonal parts is an ℓ -dimensional linear subspace L of \mathbb{R}^n , since $\tilde{\Omega}_\ell(L) = 1$, we enjoy the following corollary:

Corollary 2.2.2. *Let $C \subseteq \mathbb{R}^d$ be a polyhedral cone (or more generally, a convex cone) of dimension n , such that $C = C' \oplus L$ is the orthogonal sum of a cone C' of dimension $n' < n$ and a linear subspace L of \mathbb{R}^d . Then, $\tilde{\Omega}_n(C) = \tilde{\Omega}_{n'}(C')$.*

Corollary 2.2.2 demonstrates how computing solid angles of cones containing lines reduces to computing solid angles of lower dimensional cones. Further, by recalling the orthogonal decomposition of a cone $C = L + C/L$ as the Minkowski sum of its lineality space and its projection onto the orthogonal complement of its lineality space, we note that the normalized solid angle measure of C is equal to the affine solid angle measure of C/L .

Recall that an *isometry* h of \mathbb{R}^d is a function that is distance-preserving. Every isometry can be expressed as a composition $h(\mathbf{v}) = T(\mathbf{v}) + \mathbf{t}$, where T is a unique orthogonal linear transformation and \mathbf{t} is a unique translation vector. As translating a cone does not alter the proportion of space it occupies, we note that solid angle measures are invariant under translations. The same arguments used to show that orthogonal transformations preserve volumes can be used to show that they preserve solid angle measures.

Lemma 2.2.3. *Given a polyhedral cone $C \subset \mathbb{R}^d$, vectors $\mathbf{s}, \mathbf{t} \in \mathbb{R}^d$, and an isometry $h(\mathbf{x}) = T(\mathbf{x}) + \mathbf{t}$ of \mathbb{R}^d defined by an orthogonal transformation T , we have*

$$\tilde{\Omega}_d(h(C + \mathbf{s})) = \tilde{\Omega}_d(C).$$

Proof. By definition of isometry $h(C + \mathbf{s}) = T(C) + T(\mathbf{s}) + \mathbf{t}$ is a translation of the polyhedral cone $T(C)$. Thus, $h(C + \mathbf{s})$ and $T(C)$ have the same solid angle measure. It follows from properties of orthogonal transformations that

$$\text{vol}_{d-1}(T(C) \cap S_{d-1}) = \text{vol}_{d-1}(T(C \cap S_{d-1})) = \text{vol}_{d-1}(C \cap S_{d-1}).$$

Thus, by Definition 2.1.1 the statement holds. □

If a cone can be transformed to coincide with another cone by an isometry, the cones are said to have *congruent* solid angles. Cones with the same solid angle measure may not necessarily be congruent.

Recall that $N_P(\mathbf{v})$ denotes the outer normal cone of a polyhedron $P \in \mathbb{R}^d$ at $\mathbf{v} \in P$. We consider the image of a polytope and its outer normal cones at its vertices under isometries.

Lemma 2.2.4. *Let $P \subset \mathbb{R}^d$ be a polytope, and $h(\mathbf{x}) = T(\mathbf{x}) + \mathbf{t}$ be an isometry. The image of $N_P(\mathbf{v})$ under h is the outer normal cone of the polytope $h(P)$ at its vertex $h(\mathbf{v})$, translated by \mathbf{t} , that is*

$$h(N_P(\mathbf{v})) - \mathbf{t} = N_{h(P)}(h(\mathbf{v})).$$

Proof. It is clear that the vertices of $h(P)$ are the images of the vertices of P under h . Let \mathbf{v} be a vertex of P so that $h(\mathbf{v})$ is a vertex of $h(P)$.

Let $\mathbf{w} \in h(N_P(\mathbf{v})) - \mathbf{t}$ so that $\mathbf{w} = T(\mathbf{x})$ for some $\mathbf{x} \in N_P(\mathbf{v})$. Let $\mathbf{z} \in P$ and $\mathbf{y} = h(\mathbf{z})$. To show that \mathbf{w} lies in the outer normal cone of $h(P)$ at the vertex $h(\mathbf{v})$, it suffices to show that $\mathbf{w} \cdot (\mathbf{y} - h(\mathbf{v})) \leq 0$. Since T is an orthogonal linear transformation and \mathbf{x} is in the outer normal cone of P at \mathbf{v} , it follows that

$$\mathbf{w} \cdot (\mathbf{y} - h(\mathbf{v})) = T(\mathbf{x}) \cdot T(\mathbf{z} - \mathbf{v}) = \mathbf{x} \cdot (\mathbf{z} - \mathbf{v}) \leq 0.$$

If $\mathbf{w} \in N_{h(P)}(h(\mathbf{v}))$, then

$$\mathbf{w} \cdot (\mathbf{y} - h(\mathbf{v})) = \mathbf{w} \cdot (T(\mathbf{z}) - T(\mathbf{v})) \leq 0$$

holds. Since T is orthogonal, it is invertible with T^{-1} also being orthogonal. Thus,

$$T^{-1}(\mathbf{w}) \cdot T^{-1}(T(\mathbf{z}) - T(\mathbf{v})) = T^{-1}(\mathbf{w}) \cdot (\mathbf{z} - \mathbf{v}) \leq 0.$$

Thus,

$$T^{-1}(\mathbf{w}) \in N_P(\mathbf{v}) \text{ and } \mathbf{w} + \mathbf{t} = h(T^{-1}(\mathbf{w})) \in h(N_P(\mathbf{v})). \quad \square$$

The dilation of a polytope P by a positive scalar α has the same outer normal cones at its vertices as the original polytope P .

Lemma 2.2.5. *Let $P \subset \mathbb{R}^d$ be a polytope and $\alpha > 0$. The outer normal cone of P at a vertex \mathbf{x} is the outer normal cone of the polytope αP at the vertex $\alpha \mathbf{x}$.*

Proof. It is clear that the vertices of αP are the vertices of P scaled by α .

Let $\mathbf{p} \in P$, \mathbf{v} a vertex of P , and \mathbf{g} lie in the outer normal cone of P at \mathbf{v} . Then,

$$\mathbf{g} \cdot (\alpha \mathbf{p} - \alpha \mathbf{v}) = \alpha (\mathbf{g} \cdot (\mathbf{p} - \mathbf{v})) \leq 0.$$

Let \mathbf{h} be in the outer normal cone of αP at $\alpha \mathbf{v}$. Then,

$$\mathbf{h} \cdot (\mathbf{p} - \mathbf{v}) = \frac{1}{\alpha} (\mathbf{h} \cdot (\alpha \mathbf{p} - \alpha \mathbf{v})) \leq 0. \quad \square$$

The above lemma implies that scaling polytopes by positive factors preserves solid angle measures of outer normal cones at vertices. We establish an analogous result for higher-dimensional embeddings of polytopes.

Definition 2.2.6. Let $0 < d < n$ and $N = \{1, 2, \dots, n\}$. Let $D = (i_1, i_2, \dots, i_d)$ be a d -tuple of distinct elements of N . Define the linear embedding map $E_D: \mathbb{R}^d \rightarrow \mathbb{R}^n$ by

$$E_D(\mathbf{x} = (x_1, x_2, \dots, x_d)) := (a_1, a_2, \dots, a_n),$$

such that $a_k = x_j$ if $k = i_j \in D$, and $a_k = 0$ otherwise.

The next two assertions follow from Definitions 2.1.1 and 2.2.6.

Theorem 2.2.7. *Let $C \subset \mathbb{R}^d$ be a (translated) polyhedral cone, and $E_D: \mathbb{R}^d \rightarrow \mathbb{R}^n$ be an embedding map as defined in Definition 2.2.6. Then,*

$$\tilde{\Omega}_d(C) = \tilde{\Omega}_d(E_D(C)).$$

Proof. The above follows directly from Definition 2.1.1 by considering the solid angle measure of $E_D(C)$ with respect to its linear span. \square

Theorem 2.2.8. *Let $P \subset \mathbb{R}^d$ be a d -polytope and \mathbf{v} be a vertex of P . Let Q and \mathbf{w} be images of P and \mathbf{v} respectively, under an embedding map $E_D: \mathbb{R}^d \rightarrow \mathbb{R}^n$, as defined in Definition 2.2.6. Then, the outer normal cone of Q at \mathbf{w} is the orthogonal direct sum of the image of $N_P(\mathbf{v})$ under E_D and a linear subspace of \mathbb{R}^n .*

Proof. Given D , we define the linear subspace

$$L = \text{Span}(\{\mathbf{e}_i \mid i \notin D\}).$$

From Definition 2.2.6, it follows that for any $\mathbf{y}, \mathbf{z} \in \mathbb{R}^d$, and $\boldsymbol{\ell} \in L$,

$$E_D(\mathbf{y}) \cdot E_D(\mathbf{z}) = \mathbf{y} \cdot \mathbf{z}, \text{ and } E_D(\mathbf{y}) \cdot \boldsymbol{\ell} = 0.$$

Let $\mathbf{y} \in N_P(\mathbf{v})$, $\boldsymbol{\ell} \in L$, and $\mathbf{q} = E_D(\mathbf{p}) \in Q$, for some $\mathbf{p} \in P$. Then,

$$\begin{aligned} (E_D(\mathbf{y}) + \boldsymbol{\ell}) \cdot (\mathbf{q} - \mathbf{w}) &= (E_D(\mathbf{y}) + \boldsymbol{\ell}) \cdot (E_D(\mathbf{p}) - E_D(\mathbf{v})) \\ &= \mathbf{y} \cdot (\mathbf{p} - \mathbf{v}) + \boldsymbol{\ell} \cdot (E_D(\mathbf{p}) - E_D(\mathbf{v})) \\ &\leq 0. \end{aligned}$$

Now, any $\mathbf{x} \in \mathbb{R}^n$ can be uniquely expressed as $\mathbf{x} = \mathbf{m} + \boldsymbol{\ell}$ where $\mathbf{m} \in L^\perp$ and $\boldsymbol{\ell} \in L$. Since $\mathbf{m} \in L^\perp$, it is clear that $\mathbf{m} = E_D(\mathbf{r})$ for some $\mathbf{r} \in \mathbb{R}^d$. Suppose $\mathbf{x} \in N_Q(\mathbf{w})$ and $\mathbf{q} = E_D(\mathbf{p}) \in Q$ for some $\mathbf{p} \in P$. Then,

$$\mathbf{x} \cdot (\mathbf{q} - \mathbf{w}) = (E_D(\mathbf{r}) + \boldsymbol{\ell}) \cdot (E_D(\mathbf{p}) - E_D(\mathbf{v})) \leq 0.$$

Therefore,

$$E_D(\mathbf{r}) \cdot (E_D(\mathbf{p}) - E_D(\mathbf{v})) = \mathbf{r} \cdot (\mathbf{p} - \mathbf{v}) \leq 0,$$

so that $\mathbf{m} \in E_D(N_P(\mathbf{v}))$. \square

The following is a consequence of [18, Corollary 2.4] and the above theorems.

Corollary 2.2.9. *Let $P \subset \mathbb{R}^d$ be a d -polytope and \mathbf{v} be a vertex of P . Let Q and \mathbf{w} be images of P and \mathbf{v} respectively, under an embedding map $E_D: \mathbb{R}^d \rightarrow \mathbb{R}^n$ given in Definition 2.2.6. Then,*

$$\tilde{\Omega}_n(N_Q(\mathbf{w})) = \tilde{\Omega}_d(N_P(\mathbf{v})).$$

2.3 Outer normal cones of $\Pi(q, f)$ and $\mathfrak{B}(q, f)$

Hunsaker [32] showed that the solid angle subtended by a facet $\boldsymbol{\pi}^t \mathbf{x} \geq 1$ of $P(q, f)$ has equal measure to the outer normal cone of its blocker $\mathfrak{B}(q, f) = \Pi(q, f) + \mathbb{R}_{\geq 0}^{q-1}$ at its vertex $\boldsymbol{\pi}$. Thus, to measure facet importance for $P(q, f)$, we consider solid angle measures of outer normal cones of $\mathfrak{B}(q, f)$ at its vertices. Note that if $\boldsymbol{\pi}^t \mathbf{x} \geq 1$ is a facet of $P(q, f)$, then $\boldsymbol{\pi}$ is also a vertex of the group facet polytope $\Pi(q, f)$. Shim [41] considered and approximated solid and measure of the outer normal cone of the group facet polytope $\Pi(q, f)$ at its vertices as a measure of the importance of the corresponding facets of $P(q, f)$. We consider the latter case first.

Remark 2.3.1. In [42], it is shown that for any $(q, f) \notin \{(4, 3), (4, 1), (6, 2), (6, 3)\}$ the nonnegativity constraints (1.10a) of $\Pi(q, f)$ are redundant. As we do not consider these cases, we take this fact for granted. As such, we define $\Pi(q, f)$ as the set of $(\pi_1, \pi_2, \dots, \pi_{q-1})$ satisfying the system

$$\pi_f = 1, \tag{2.2a}$$

$$\pi_i + \pi_j = 1, \quad i + j \equiv f \pmod{q} \quad (\text{complementarity}) \tag{2.2b}$$

$$\pi_i + \pi_j \geq \pi_k \quad k \equiv i + j \pmod{q} \quad (\text{subadditivity}). \tag{2.2c}$$

We wish to compute the solid angle measures of two types of $(q-1)$ -dimensional cones: the outer normal cones of $\mathfrak{B}(q, f)$ at its vertices and the outer normal cones of $\Pi(q, f)$ at its vertices. As in the case of Shim [41], we first consider a partition of indices. Partition $\{1, 2, \dots, q-1\}$ into I, J, H and singleton $F = \{f\}$. For i, j such that $i + j \equiv f \pmod{q}$ if $i \neq j$, assign $i \in I$ and $j \in J$ (or vice versa), and if $i = j$, then $i \in H$. Following Shim's convention [41], we denote the *complement* of any any index k by \bar{k} , satisfying $k + \bar{k} \equiv f \pmod{q}$. Note that $|I|$ is at most $\lfloor \frac{q-2}{2} \rfloor$. Leveraging the dimension of group facet polytopes and Corollary 2.2.9, we reduce the computations of solid angle measures of the outer normal cones of group facet polytopes at their vertices and outer normal cones of blockers of master cyclic group polyhedra at their vertices to dimensions $|I|$ and $2|I|$ respectively. We note here that [42] consider a specific partition of indices. In the following, we make clear that in reducing the dimension, we still preserve the solid angle measures of the cones of interest. First, we introduce an additional polytope, the projection of $\Pi(q, f)$ onto the linear span of $\{\mathbf{e}_k \mid k \in I\}$:

$$\Pi_I(q, f) := \left\{ \sum_{i \in I} x_i \mathbf{e}_i \mid (x_1, x_2, \dots, x_{q-1}) \in \Pi(q, f) \right\} \subset \mathbb{R}^{q-1}.$$

Lemma 2.3.2. Consider the isometry $h(\mathbf{x}) = A(\mathbf{x}) + \mathbf{t}$ of \mathbb{R}^{q-1} , where the orthogonal matrix $A \in \mathbb{R}^{(q-1) \times (q-1)}$ has k^{th} column given by

$$A^{(k)} = \begin{cases} \frac{1}{\sqrt{2}}(\mathbf{e}_k - \mathbf{e}_{\bar{k}}), & \text{for } k \in I \\ -\frac{1}{\sqrt{2}}(\mathbf{e}_k + \mathbf{e}_{\bar{k}}), & \text{for } k \in J \\ \mathbf{e}_k, & \text{for } k \in H \cup F, \end{cases}$$

and where

$$\mathbf{t} = \sum_{k \in I} \frac{1}{\sqrt{2}} \mathbf{e}_k + \sum_{k \in J} \frac{1}{\sqrt{2}} \mathbf{e}_k - \sum_{k \in H} \frac{1}{2} \mathbf{e}_k - \mathbf{e}_f.$$

Then, the following holds: $h(\Pi(q, f)) = \sqrt{2} \Pi_I(q, f)$.

Note that by the results of the previous section, the above lemma implies that the outer normal cones of the two polytopes have congruent solid angles.

Proof of Lemma 2.3.2. First, note that h is indeed an isometry as A is an orthogonal matrix. Let $\boldsymbol{\pi} = (\pi_1, \pi_2, \dots, \pi_{q-1}) \in \Pi(q, f)$ so and $\boldsymbol{\pi}_I = \sum_{i \in I} \pi_i \mathbf{e}_i \in \Pi_I(q, f)$. We see that

$$\begin{aligned} \frac{1}{\sqrt{2}} h(\boldsymbol{\pi}) &= \frac{1}{\sqrt{2}} (A\boldsymbol{\pi} + \mathbf{t}) \\ &= \frac{1}{\sqrt{2}} \left(\sum_{i=1}^{q-1} \pi_i A^{(i)} + \mathbf{t} \right) \\ &= \frac{1}{\sqrt{2}} \left(\sum_{i \in I} \pi_i A^{(i)} + \sum_{j \in J} \pi_j A^{(j)} + \sum_{h \in H} \pi_h A^{(h)} + \pi_f A^{(f)} + \mathbf{t} \right) \\ &= \frac{1}{\sqrt{2}} \left(\sum_{i \in I} \frac{\pi_i}{\sqrt{2}} (\mathbf{e}_i - \mathbf{e}_{\bar{i}}) + \sum_{i \in I} \frac{1 - \pi_i}{\sqrt{2}} (-\mathbf{e}_i - \mathbf{e}_{\bar{i}}) + \sum_{h \in H} \frac{1}{2} \mathbf{e}_h + \mathbf{e}_f + \mathbf{t} \right) \\ &= \frac{1}{\sqrt{2}} \left(\sum_{i \in I} \frac{1}{\sqrt{2}} (2\pi_i - 1) \mathbf{e}_i + \sum_{j \in J} -\frac{1}{\sqrt{2}} \mathbf{e}_j + \sum_{h \in H} \frac{1}{2} \mathbf{e}_h + \mathbf{e}_f + \mathbf{t} \right) \\ &= \frac{1}{\sqrt{2}} \left(\sum_{i \in I} \sqrt{2} \pi_i \mathbf{e}_i \right) \\ &= \boldsymbol{\pi}_I. \end{aligned}$$

This shows the two polytopes are equal. \square

By substitution of the complementarities (2.2b) and (2.2a) in the characterization of the group-facet polytope $\Pi(q, f)$, each subadditivity (2.2c) can be expressed in terms of only variables with indices in I . The set of subadditivities in terms of variables with indices in I describes a polytope in $\mathbb{R}^{|I|}$. We refer to this polytope as the *reduced group facet polytope* and denote it by $\tilde{\Pi}(q, f)$.

At this stage, we recall that constraints $\mathbf{a}_1^t \mathbf{x} \leq b_1$ and $\mathbf{a}_2^t \mathbf{x} \leq b_2$ are *linearly independent* if \mathbf{a}_1 and \mathbf{a}_2 are. A constraint $\mathbf{a}^t \mathbf{x} \leq b$ is *tight* at $\bar{\mathbf{x}}$ if $\mathbf{a}^t \bar{\mathbf{x}} = b$. Thus, equality constraints $\mathbf{a}^t \mathbf{x} = b$ of a polyhedron are tight at every point in the polyhedron. For a polyhedron $P \subseteq \mathbb{R}^d$, a point $\mathbf{x} \in P$ is a vertex of P if there are d linearly independent constraints which are tight at \mathbf{x} . For convenience, we may suppose $|I| = s$ and index its elements: $I = \{i_1, i_2, \dots, i_s\}$.

Lemma 2.3.3. Let \mathbf{e}_i denote the i^{th} standard basis vector of \mathbb{R}^s . For a given point $\boldsymbol{\pi} = (\pi_1, \pi_2, \dots, \pi_{q-1}) \in \Pi(q, f)$, consider the corresponding point

$$\tilde{\boldsymbol{\pi}} = \sum_{\ell=1}^s \pi_{i_\ell} \mathbf{e}_\ell \in \tilde{\Pi}(q, f).$$

Then, $\boldsymbol{\pi}$ is vertex of $\Pi(q, f)$ if and only if $\tilde{\boldsymbol{\pi}}$ is a vertex of $\tilde{\Pi}(q, f)$.

Proof. If $\boldsymbol{\pi}$ is a vertex of $\Pi(q, f)$, then $q - 1$ linearly independent constraints are tight at $\boldsymbol{\pi}$. Since there are $q - 1 - s$ linearly independent equality constraints ((2.2a), (2.2b)), there are s linearly independent subadditivities (2.2c) which are tight at $\boldsymbol{\pi}$. Expressing these s subadditivities in terms of only variables with indices in I shows that $\tilde{\boldsymbol{\pi}}$ satisfies s linearly independent constraints of $\tilde{\Pi}(q, f)$, hence is a vertex.

If $\tilde{\boldsymbol{\pi}}$ is a vertex of $\tilde{\Pi}(q, f)$, then s linearly independent constraints are tight at $\tilde{\boldsymbol{\pi}}$. Since $\boldsymbol{\pi} \in \Pi(q, f)$, the $q - 1 - s$ equality constraints are tight at it. It is clear that a subadditivity of $\Pi(q, f)$ is tight at $\boldsymbol{\pi}$ if and only if the corresponding constraint (obtained from rewriting in terms of variable with indices in I) of $\tilde{\Pi}(q, f)$ is tight at $\tilde{\boldsymbol{\pi}}$. Furthermore, if a set of subadditivities of $\Pi(q, f)$ are linearly independent, then the corresponding constraints of $\tilde{\Pi}$ are linearly independent. Since s linearly independent constraints of $\tilde{\Pi}(q, f)$ are tight at $\tilde{\boldsymbol{\pi}}$, there are at least s linearly independent subadditivities which are tight at $\boldsymbol{\pi}$. Therefore, $\boldsymbol{\pi}$ is a vertex. \square

Example 2.3.4. We demonstrate this relationship with an example. By (1.10), the polytope $\Pi(5, 4) \subset \mathbb{R}^4$ is the set of $(\pi_1, \pi_2, \pi_3, \pi_4)$ satisfying:

$$\pi_1, \pi_3 \geq 0, \quad \pi_2 = \frac{1}{2}, \quad \pi_4 = 1, \quad \pi_1 + \pi_3 = 1, \quad 2\pi_1 \geq \pi_2, \quad \text{and} \quad 2\pi_3 \geq \pi_1.$$

Thus

$$\Pi(5, 4) = \text{conv} \left(\left\{ \left(\frac{1}{4}, \frac{1}{2}, \frac{3}{4}, 1 \right), \left(\frac{2}{3}, \frac{1}{2}, \frac{1}{3}, 1 \right) \right\} \right).$$

The partition of indices for this example is $I = \{1\}$, $J = \{3\}$, $H = \{2\}$, and $F = \{4\}$. After substitution using the equations, we have the inequality description of the reduced group facet polytope $\tilde{\Pi}(5, 4) \subset \mathbb{R}$:

$$\frac{1}{4} \leq \pi_1 \leq \frac{2}{3}.$$

Now, we can relate $\Pi_I(q, f)$ and $\tilde{\Pi}(q, f)$. The following corollary follows directly from previously established results and so is stated without proof.

Corollary 2.3.5. The polytope $\Pi_I(q, f) \subset \mathbb{R}^{q-1}$ is the image of $\tilde{\Pi}(q, f)$ under the embedding map $E_I : \mathbb{R}^s \rightarrow \mathbb{R}^{q-1}$.

Corollary 2.3.5 and Corollary 2.2.9 together show that measures of outer normal cones of $\Pi_I(q, f)$ at its vertices are the same as those of $\tilde{\Pi}(q, f)$ at its vertices. As a consequence, the following corollary shows that to obtain the solid angle measures of outer normal cones of vertices of $\Pi(q, f)$, it suffices to focus on the measure of the $|I|$ -dimensional solid angles subtended by the outer normal cones of the reduced group-facet polytope $\tilde{\Pi}(q, f)$ at its vertices.

Corollary 2.3.6. *Let $\mathbf{x} = (x_1, x_2, \dots, x_{q-1})$ be a vertex of the polytope $\Pi(q, f)$, and $\tilde{\mathbf{x}} = (x_{i_1}, x_{i_2}, \dots, x_{i_s})$ its corresponding vertex of $\tilde{\Pi}(q, f)$. Then,*

$$\tilde{\Omega}_{q-1} \left(N_{\Pi(q,f)}(\mathbf{x}) \right) = \tilde{\Omega}_{|I|} \left(N_{\tilde{\Pi}(q,f)}(\tilde{\mathbf{x}}) \right).$$

Proof. By Lemma 2.3.2, $N_{\Pi(q,f)}(\mathbf{x})$ has the same solid angle measure as $N_{\Pi_I(q,f)}(E_I(\tilde{\mathbf{x}}))$. By Corollary 2.3.5, $N_{\Pi_I(q,f)}(E_I(\tilde{\mathbf{x}}))$ has the same solid angle measure as $N_{\tilde{\Pi}(q,f)}(\tilde{\mathbf{x}})$. \square

Now, we focus our attention to outer normal cones of the blocker of $P(q, f)$ at its vertices. Using the structure of $\mathfrak{B}(q, f)$, we can simplify the computation of the solid angle measures of its outer normal cones at its vertices. The outer normal cones have the following form:

$$C \oplus \text{cone}(-\mathbf{e}_f) \oplus \bigoplus_{\{h \in H\}} \text{cone}(-\mathbf{e}_h)$$

for some $2|I|$ -dimensional cone C . By Lemma 2.2.1, the solid angle measure of the outer normal cone of $\mathfrak{B}(q, f)$ at a vertex is $2^{-(q-1-2|I|)}$ times the solid angle measure of C with respect to its $2|I|$ -dimensional linear span.

Chapter 3 Solid Angle Approximation Methods

The normalized solid angle of a cone $C \subseteq \mathbb{R}^d$ has many equivalent definitions, hence ways to measure it, including:

- 1: The proportion of a sphere, or ball centered at the origin which intersects C , in which case the problem of measuring the solid angle is that of finding the volume of a spherical polytope, which is a specific kind of convex body;
- 2: The probability that a randomly selected point in \mathbb{R}^d lies inside C , in which case Monte-Carlo estimates are appropriate for approximation;
- 3: or, in recognizing that volume is a special case of integration, viewing the ratio in Definition 2.1.1 as one of integrals. Doing so gives the following equivalent definitions of $\tilde{\Omega}_d$:

$$\tilde{\Omega}_d(C) = \frac{\text{vol}_{d-1}(C \cap S_{d-1})}{\text{vol}_{d-1}(S_{d-1})} = \frac{\int_C f(\mathbf{x}) d\mathbf{x}}{\int_{\mathbb{R}^d} f(\mathbf{x}) d\mathbf{x}}, \quad (3.1)$$

where $f: \mathbb{R}^d \rightarrow \mathbb{R}$ is any function that is invariant under rotations around the origin, and where $\int_{\mathbb{R}^d} f(\mathbf{x}) d\mathbf{x} < \infty$.

Viewing solid angle measures through the lens of Interpretation 1:, we consider the much celebrated practical randomized volume approximation algorithm of Cousins and Vempala [9]. For Interpretation 2:, we discuss the so called “shooting experiment” dating back to Kuhn [34] and popularized by Gomory, Johnson, and Evans [24]. For Interpretation 3:, we consider the work of Ribando [39], who choosing a particular form f , rediscovered Aomoto’s [1] solid angle measure formula, which takes the form of a hypergeometric power series. In this chapter, we survey these three methods.

3.1 Cousins–Vempala Practical Volume Algorithm

The normalized solid angle measure of a convex cone $C \subseteq \mathbb{R}^d$ is given by (2.1) which is equivalent to

$$\tilde{\Omega}_d(C) = \frac{\text{vol}_d(C \cap B_d)}{\text{vol}_d(B_d)} = \frac{\text{vol}_d(C \cap B_d)}{\frac{\sqrt{\pi}^d}{\Gamma(1+\frac{d}{2})}},$$

where B_d denotes the d -dimensional unit ball. Therefore, the problem of computing the normalized solid angle measure of C is reduced to computing $\text{vol}_d(C \cap B_d)$, the volume of a convex body. Computing volumes of convex bodies is a problem dating back to antiquity. The history of volume computation as an algorithmic problem dates back to at least the 1980s. In this context, a convex body is *given by an oracle* if there is a program which outputs whether a point is in the convex body or not. The early results of Elekes [14] and Bárány–Füredi [4] exhibited that no deterministic polynomial time algorithm could compute the volume of a convex set given by an

oracle to within less than exponential relative error. However, Dyer, Frieze, and Kannan [12] presented the first polynomial randomized algorithm to approximate the volume of a convex body to within any desired relative error. The algorithm is often referred to as the DFK algorithm. The primary tool used was Monte Carlo integration which relies on random sampling for the numerical estimation of an integral. This has been the main ingredient of the majority of randomized volume approximation algorithms since. The breakthrough result was an (ϵ, δ) approximation, which showed that given two positive numbers $0 < \delta, \epsilon < 1$, and a convex body $K \subset \mathbb{R}^d$ given by a *separation oracle* (a procedure which given $\mathbf{p} \in \mathbb{R}^d$ asserts that $\mathbf{p} \in K$ or returns a hyperplane that separates \mathbf{p} and K), one could determine a value ξ such that

$$(1 - \epsilon)\xi < \text{vol}(K) < (1 + \epsilon)\xi$$

with probability at least $1 - \delta$. The running time of the DFK algorithm is polynomial in $d, \frac{1}{\epsilon}$, and $\log(\frac{1}{\delta})$, in particular, it required

$$O^*(d^{23}) = O\left(d^{23} \log^5(d) \epsilon^{-2} \log\left(\frac{1}{\epsilon}\right) \log\left(\frac{1}{\delta}\right)\right)$$

membership tests. The soft- O notation $O^*(d^h)$ indicates that $\log^c(d)$ factors and constants depending on ϵ and δ are suppressed. The DFK algorithm became the impetus for the development of randomized (ϵ, δ) -volume approximation algorithms. Subsequent work in this field has largely been focused on improving the complexity growth with respect to dimension.

For solid angle measure computations, we will focus exclusively on the practical randomized volume approximation algorithm [9] by Cousins–Vempala, which is implemented in MATLAB [10], as its goal is to approximate volumes of intersections of polyhedra and ellipsoids, which is applicable for solid angle measure. We will delineate how the algorithm works and also discuss how we apply it to our cases. Here, we recall that a polyhedron can be expressed as the Minkowski sum of a cone and a polytope; each of which can be described as the convex hull of its extreme rays/points respectively, or by a system of equations and inequalities corresponding to the half-spaces of which the cone and polytope are the intersections of. The former case is called a *V-representation* of the polyhedron while the latter is called the *H-representation*.

One can assume that the convex bodies of interest are sufficiently round and that they contain the origin. Otherwise, translation and the rounding phase are performed as a pre-processing step in the volume approximation algorithm. Given the *H-representation* of a polyhedron (in particular, the matrices A, A_+ and the vectors \mathbf{b}, \mathbf{b}_+ such that the polyhedron satisfies $A\mathbf{x} \leq \mathbf{b}$ and $A_+\mathbf{x} = \mathbf{b}_+$), a point in the polyhedron, a description of an ellipsoid (the matrix E and center of the ellipsoid \mathbf{c} so that the ellipsoid is $(\mathbf{x} - \mathbf{c})^t E (\mathbf{x} - \mathbf{c}) \leq 1$), and a target relative error parameter ϵ , the Cousins–Vempala algorithm approximates the volume of the convex body K which is defined as the intersection of the polyhedron and the ellipsoid.

If f_m is the characteristic function of K , then for any functions f_0, f_1, \dots, f_{m-1} , the volume of K is given by the telescoping product:

$$\text{vol}(K) = \int_K f_0(\mathbf{x}) \, d\mathbf{x} \cdot \prod_{i=1}^m \frac{\int_K f_i(\mathbf{x}) \, d\mathbf{x}}{\int_K f_{i-1}(\mathbf{x}) \, d\mathbf{x}} = \int_K f_0(\mathbf{x}) \, d\mathbf{x} \cdot \prod_{i=1}^m R_i,$$

where each ratio of integrals is called a *phase*.

In this way, approximating the volume of K is broken down into approximating the initial phase $\int_K f_0(\mathbf{x}) \, d\mathbf{x}$ and approximating each phase R_i for $i = 1, 2, \dots, m$ appearing above. Cousins and Vempala [9] consider Gaussian functions of the form $f_i(\mathbf{x}) = e^{-a_i \|\mathbf{x}\|^2}$ for $i = 0, 1, \dots, m$, with f_0 being highly concentrated in K , so that most of the volume under the Gaussian lies above K . Since the integral of a Gaussian function over \mathbb{R}^d has a closed form, $\int_K f_0(\mathbf{x}) \, d\mathbf{x} \approx \int_{\mathbb{R}^d} f_0(\mathbf{x}) \, d\mathbf{x}$ gives an easily computable approximation for the first integral. To determine what the starting Gaussian should be, i.e., the value of a_0 , a percentage r (the default being 0.1) of the relative error ϵ is allotted. In [9], it is shown that for a given a , and a random variable X from $e^{-a\|\mathbf{x}\|^2}$ over \mathbb{R}^d , the probability that $X \notin K$ has upper bound given as a function of a :

$$p(a) := \sum_{H \in \mathcal{H}} \frac{e^{-ad_H^2}}{2d_H \sqrt{a\pi}} + e^{-\frac{d_E^2}{8}},$$

where \mathcal{H} represents the set of hyperplanes bounding the polyhedron, d_H is the distance from the origin to the hyperplane H , and d_E is the minimum distance from the origin to the boundary of the ellipsoid. Initial bounds of 0 and 1 are imposed upon a and binary search is performed to find a_0 such that $p(a_0) = r\epsilon$.

For each $i = 1, 2, \dots, m-1$, the phase R_i is the expectation of a random variable. If $X^{(i)}$ is a random variable with probability density function

$$\frac{f_{i-1}(x)}{\int_K f_{i-1}(y) dy} 1_K(x),$$

then the expected value of the random variable

$$Y^{(i)} = \frac{f_i(X^{(i)})}{f_{i-1}(X^{(i)})}$$

is

$$E[Y^{(i)}] = \int_K \frac{f_i(\mathbf{x})}{f_{i-1}(\mathbf{x})} \cdot \frac{f_{i-1}(\mathbf{x})}{\int_K f_{i-1}(\mathbf{x}) d\mathbf{x}} d\mathbf{x} = R_i.$$

To estimate the expected value of $Y^{(i)}$, random samples $\{X_1^{(i)}, X_2^{(i)}, \dots, X_{s_i}^{(i)}\}$ are obtained via a random walk. The s_i random samples correspond to $\{Y_1^{(i)}, Y_2^{(i)}, \dots, Y_{s_i}^{(i)}\}$ where, for $j = 1, 2, \dots, s_i$,

$$Y_j^{(i)} = \frac{f_i(X_j^{(i)})}{f_{i-1}(X_j^{(i)})}.$$

The Monte-Carlo estimator of R_i for $i = 1, 2, \dots, m$ is

$$R_i = E [Y^{(i)}] \approx \frac{1}{s_i} \sum_{j=1}^{s_i} Y_j^{(i)}.$$

For each $i = 1, 2, \dots, m$, to determine the quantity s_i of samples to take, Cousins and Vempala introduce a stopping criterion which uses a sliding window size W (in their implementation, the sliding window size is $400 + d^2$). If the maximum difference between any of the last W partial sums of the Monte-Carlo estimator of R_i :

$$\frac{1}{k-W+1} \sum_{j=1}^{k-W+1} Y_j^{(i)}, \frac{1}{k-W+2} \sum_{j=1}^{k-W+2} Y_j^{(i)}, \dots, \frac{1}{k} \sum_{j=1}^k Y_j^{(i)},$$

is at most $\frac{\epsilon}{2\sqrt{m}}$, then s_i is set to k , and the Monte-Carlo estimator is output as the approximation for R_i .

The values a_1, a_2, \dots, a_m are determined recursively so that

$$a_i = a_{i-1} \left(1 - \frac{1}{n}\right)^{r_i}$$

for $i = 1, \dots, m$, where $r_i \geq 1$ is the maximum value where

$$\frac{\text{Var}[Y^{(i)}]}{E[Y^{(i)}]^2} \leq 2$$

holds. In the MATLAB implementation, the initial value of r_i is 1. To test whether the bound on the variance holds, a fixed number of samples ($1000 + \frac{d^2}{2}$) is used. If the bound holds, the current value of r_i is doubled until the constraint is violated, at which r_i is set to the last value at which the bound held. To determine m , the number of phases which is sufficient, the MATLAB implementation computes the Monte-Carlo estimator of R_i using a fixed number of samples ($\lceil \frac{150}{\epsilon} \rceil$). If the estimation is sufficiently close to 1 (in practice, if it is less than 1.001), then m is set to $i + 1$ and a_m is set to 0.

3.1.1 Discussion

To apply the Cousins–Vempala algorithm to approximate the solid angle measure of a polyhedral cones in \mathbb{R}^d , we must provide the H -representation of the cone. In our use cases, we typically deal with the V -representation of the cone, and describe it by its extreme rays. For instance, Gomory’s characterization of the nontrivial facets of $P(q, f)$ provides a non-minimal H -representation of $\Pi(q, f)$ which encodes the generators of the outer normal cones of $\Pi(q, f)$ at its vertices, hence a non-minimal V -representation of the outer normal cones. Thus, in this framework, it is more natural to consider V -representations. To convert from the V -representation to an irredundant H -representation, we use the facet enumeration method of the Polyhedron class in the Multi-Parametric Toolbox 3.0 [28]. The ellipsoid will always

be the unit ball centered at the origin. Thus, \mathbf{c} is the d -dimensional zero vector and E is the $d \times d$ identity matrix. It is also necessary to find a point in the intersection of the cone and the unit ball. To determine this point, we sum up the extreme rays of the cone, so that the resultant vector is in the relative interior of the cone. To ensure that it also lies in the unit ball, we scale it by a factor of $\frac{1}{1+n}$ where n is the norm of the vector. Cousins and Vempala [9] note that while the heuristic stopping criterion experimentally provides a reasonable estimate, it cannot guarantee accuracy. One method to increase the probability of an accurate answer is to average over multiple trials. In the experiments reported in [9], at least 100 trials are conducted. As such, we consider 100 trials for our cases. Furthermore, as aforementioned, the convex bodies undergo a rounding pre-processing step before volume estimation. In the MATLAB implementation, the rounding step is performed after the convex body is already constructed, hence rounding is performed in each of the 100 trials. The authors note that the rounding phase is computationally expensive, but ensures that the volume approximation is efficient. It is also important to note that in the MATLAB implementation of the algorithm, three random walks are available for sampling: ball walk, hit-and-run, and the default random walk, coordinate hit-and-run. We use hit-and-run as it is the random walk of primary focus in [9].

For the purposes of our study, we are interested in absolute error rather than relative error. However, the Cousins–Vempala algorithm takes as input a target relative error parameter. For a target absolute error parameter δ , we input the relative error parameter $\frac{\delta}{V}$ where V is an estimation of the volume of the convex body of interest. For cones of dimension at most 4, we use estimates of the solid angle measure obtained from the power series method to obtain V . For cones of higher dimension, we use estimates of the solid angle measure obtained from existing empirical data from shooting experiments performed in [32] and [41] to obtain V .

3.2 Shooting Experiments

A “shooting experiment” on a polyhedron $P \subset \mathbb{R}^d$ is a randomized procedure whereby rays are “shot” from a particular point and the number of shots which “hit” a facet of P are recorded. The point from which the rays emanate is called the *shooting point*. The shooting point may be interior to the polyhedron (as in [34, 41]) or exterior to the polyhedron (as in [16, 24]). A random direction vector $\mathbf{d} \in \mathbb{R}^d$ is generated. If a facet f of P is the first facet of P which the ray \mathbf{d} intersects, we say f is *hit* by \mathbf{d} . The process is repeated and the frequency with which a facet is hit is recorded. The percentage of shots received by a facet gives an approximation for the measure of the solid angle subtended by that facet. Shooting experiments have been the primary method for measuring solid angles subtended by facets of master cyclic group polyhedra (see [11, 16, 32, 41] for example).

While the term “shooting experiment” is often attributed to Gomory, use of shooting experiments date back to at least the 1950s with Harold Kuhn [34] and his work on the traveling salesman problem. In 1953, Kuhn devised a shooting experiment to generate faces of an 11-dimensional polytope embedded in \mathbb{R}^{20} . Kuhn stated “To

generate faces of this polytope, I proposed the following ‘experiment’ in the summer of 1953: Sit at the center of gravity \bar{x} of the polytope and fire a pistol in a random direction d . Your shot will go out through a face with a probability 1.” For these shooting experiments, Kuhn considered shooting random direction vectors from a point in the interior of the polytope, out to the faces of the polytope. He posed the shooting experiment as a linear program whose optimal solution provided the equation of the face through which the shot exited. In this way, the ratio of the shooting experiment size of a facet (number of shots hit by a facet) to the total number of shots performed, is an estimate of the solid angle subtended by the facet at the interior shooting point.

In his initial shooting experiment in 1953, Kuhn shot 10 direction vectors, each obtained by “sticking a pin at random in the Los Angeles telephone book” [34]. He noted that all ten shots went through “trivial” faces, i.e. faces arising from nonnegativity constraints. In 1991, Kuhn revisited the same 11-dimensional polytope, performing another shooting experiment, this time with 152,636 shots, where the random direction vectors were obtained from a uniform distribution over the unit sphere in \mathbb{R}^{11} . From Kuhn’s latter shooting experiment, he was able to determine that the class of trivial faces, consisting of 20 out of the total 390 faces, subtended approximately 80 percent of the central spherical angle of the polytope. The variance in the results of Kuhn’s two shooting experiments reify the caution that is necessitated when drawing conclusions based on shooting experiments, as well as the need for a large number of shots to draw accurate conclusions.

In contrast to Kuhn’s shooting experiments, Gomory’s shooting experiments were conducted on unbounded master cyclic group polyhedra, with the shooting point being the origin, lying outside of the polyhedra. Moreover, in Kuhn’s shooting experiment, direction vectors are shot from the interior point \bar{x} in random directions coming from a uniform distribution over the unit sphere, whereas in Gomory’s shooting experiment, because the polyhedra of interest lie completely within the nonnegative orthant, the direction vectors are limited to the nonnegative orthant. Therefore, while Kuhn’s shooting experiment estimates the measure of the solid angle subtended by a facet of a polytope at the point \bar{x} normalized so that the solid angle of all of space has measure 1, Gomory’s shooting experiment estimates the measure of the solid angle subtended by a facet of a blocking polyhedron at the origin, normalized so that the solid angle of an orthant is 1.

For the shooting experiment established by [24], random direction vectors were generated uniformly on the nonnegative orthant of \mathbb{R}^{q-1} [16]. They were able to determine the facet hit by a random direction vector by use of the following theorem:

Theorem 3.2.1 ([24, Theorem 3 (Shooting Theorem)], rephrased). *For positive integers $f < q$, the facet $\boldsymbol{\pi}^t \mathbf{z} \geq 1$ of $P(q, f)$ (with $\boldsymbol{\pi} = (\pi_1, \pi_2, \dots, \pi_{q-1})$) hit by the*

random direction vector $\mathbf{v} \geq 0$ is the solution to the linear program:

$$\begin{aligned}
& \text{minimize } \mathbf{v}^t \boldsymbol{\pi} \\
& \text{such that } \pi_i \geq 0, \quad i = 1, \dots, q-1 \\
& \quad \pi_f = 1, \\
& \quad \pi_i + \pi_j = 1, \quad i + j \equiv f \pmod{q} \\
& \quad \pi_i + \pi_j \geq \pi_k, \quad k \equiv i + j \pmod{q}.
\end{aligned}$$

Thus, to perform one shot in the shooting experiment, one solves the LP above, and records the optimal solution corresponding to the facet hit. Hunsaker [32] proved a more general result:

Theorem 3.2.2 ([32, Theorem 3.2], rephrased). *Given a blocking polyhedron P and a nonnegative objective vector \mathbf{c} for minimization, \mathbf{x}_j is an optimal extreme point of P if and only if $\mathbf{z}^t \mathbf{x}_j \geq 1$ defines a facet of $B(P)$ that is intersected by the ray from the origin in direction \mathbf{c} .*

In the above, $B(P)$ is the blocker of P . This implies that a facet $\boldsymbol{\pi}^t \mathbf{z} \geq 1$ of $P(q, f)$ is hit by a direction vector \mathbf{v} in the shooting experiment if and only if \mathbf{v} lies in the negative of the outer normal cone of $\mathfrak{B}(q, f) = \Pi(q, f) + \mathbb{R}_{\geq 0}^{q-1}$ at its vertex $\boldsymbol{\pi}$. Therefore, the measure of the solid angle subtended by the facet $\boldsymbol{\pi}^t \mathbf{z} \geq 1$ of $P(q, f)$ is equal to the solid angle measure of the outer normal cone of $\mathfrak{B}(q, f)$ at its vertex $\boldsymbol{\pi}$.

As aforementioned, rather than considering outer normal cones of the polyhedron $\mathfrak{B}(q, f)$, Shim[41] considered outer normal cones of the polytope $\tilde{\Pi}(q, f) \subset \mathbb{R}^{|I|}$, with the partition of indices $\{1, 2, \dots, q-1\} = I \sqcup J \sqcup F \sqcup H$ and $I = \{i_1, i_2, \dots, i_s\}$. The polytope is first translated so that the point $(\frac{1}{2}, \frac{1}{2}, \dots, \frac{1}{2})$ which lies in its interior is translated to the origin. Then, for a single shot of Shim's shooting experiment, a random direction \mathbf{w} is generated from a uniform distribution on the unit sphere of \mathbb{R}^s . The shot is performed by solving the LP:

$$\begin{aligned}
& \text{maximize } \mathbf{w}^t \boldsymbol{\phi} \\
& \text{such that } \boldsymbol{\phi} \in \tilde{\Pi}(q, f) - \left(\frac{1}{2}, \frac{1}{2}, \dots, \frac{1}{2}\right).
\end{aligned}$$

Suppose the optimal solution to the LP above is $\bar{\boldsymbol{\phi}} = \tilde{\boldsymbol{\pi}} - \left(\frac{1}{2}, \frac{1}{2}, \dots, \frac{1}{2}\right)$, then we think of \mathbf{w} as lying in the outer normal cone $\tilde{\Pi}(q, f)$ at $\tilde{\boldsymbol{\pi}}$ and the facet $\boldsymbol{\pi}^t \mathbf{z} \geq 1$ of $P(q, f)$ as being hit, where $\tilde{\boldsymbol{\pi}} = \sum_{i=1}^s \pi_{i_\ell} \mathbf{e}_\ell$ and \mathbf{e}_i denotes the i^{th} standard basis vector of \mathbb{R}^s . In his thesis [41], Shim posited the question of whether the two shooting experiments were equivalent noting that ‘‘Experimental results boost the equivalence.’’ We can re-frame this question as asking whether the solid angle measure of an outer normal cone of $\tilde{\Pi}(q, f)$ at a vertex is equal to the solid angle measure of the outer normal cone of $\mathfrak{B}(q, f)$ at the corresponding vertex, where the former solid angle measure is normalized so that $\mathbb{R}^{|I|}$ has measure 1, while the latter solid angle measure is normalized so that an orthant $\mathbb{R}_{\geq 0}^{q-1}$ has measure 1.

For this project, we use existing data from prior shooting experiments for comparisons.

3.3 The Power Series Method

Ribando considered the function $f(\mathbf{x}) = e^{-\|\mathbf{x}\|^2}$ to express the normalized solid angle measure of an n -dimensional cone $C \subset \mathbb{R}^n$ as

$$\tilde{\Omega}_n(C) = \frac{\int_C e^{-\|\mathbf{x}\|^2} d\mathbf{x}}{\int_{\mathbb{R}^n} e^{-\|\mathbf{x}\|^2} d\mathbf{x}} = \frac{\int_C e^{-\|\mathbf{x}\|^2} d\mathbf{x}}{\pi^{n/2}}, \quad (3.2)$$

which when simplified and expanded gave rise to a hypergeometric series. Furthermore, Ribando showed that the convergence of the power series was dependent on a certain matrix, which we call the *associated matrix*.

Ribando's results are presented in Theorem 3.3.2 below.

Definition 3.3.1. Let C be a simplicial cone in \mathbb{R}^n , whose generators are the linearly independent unit vectors $\mathbf{v}_1, \dots, \mathbf{v}_n \in \mathbb{R}^n$. Then, the *associated matrix* of C , denoted by $M_n(C)$, is the $n \times n$ matrix whose (i, j) -th entry is $-|\mathbf{v}_i \cdot \mathbf{v}_j|$ for $i \neq j$, and whose diagonal (i, i) -th entry is 1.

$$M_n(C) = \begin{bmatrix} 1 & -|\mathbf{v}_1 \cdot \mathbf{v}_2| & \cdots & -|\mathbf{v}_1 \cdot \mathbf{v}_n| \\ -|\mathbf{v}_2 \cdot \mathbf{v}_1| & 1 & \cdots & -|\mathbf{v}_2 \cdot \mathbf{v}_n| \\ \vdots & \vdots & \ddots & \vdots \\ -|\mathbf{v}_n \cdot \mathbf{v}_1| & -|\mathbf{v}_n \cdot \mathbf{v}_2| & \cdots & 1 \end{bmatrix}. \quad (3.3)$$

Theorem 3.3.2 ([39, Theorem 2.2 and Corollary 3.3], rephrased). *Let $C \subseteq \mathbb{R}^n$ be the simplicial cone generated by the unit vectors $\mathbf{v}_1, \dots, \mathbf{v}_n$. Let $V \in \mathbb{R}^{n \times n}$ be the matrix whose i^{th} column is \mathbf{v}_i . Let $\alpha_{ij} = \mathbf{v}_i \cdot \mathbf{v}_j$ for $1 \leq i, j \leq n$. Let*

$$T_{\alpha} = \frac{|\det V|}{(4\pi)^{n/2}} \sum_{\mathbf{a} \in \mathbb{N}^{\binom{n}{2}}} \left[\frac{(-2)^{\sum_{1 \leq i < j \leq n} a_{ij}}}{\prod_{1 \leq i < j \leq n} a_{ij}!} \prod_{i=1}^n \Gamma \left(\frac{1 + \sum_{m \neq i} a_{im}}{2} \right) \right] \alpha^{\mathbf{a}}. \quad (3.4)$$

Then, T_{α} converges absolutely to the normalized solid angle measure $\tilde{\Omega}_n(C)$ of the cone if and only if its associated matrix $M_n(C)$ is positive definite.

In the above series (3.4), Γ is the Euler-Gamma function; $\alpha = (\alpha_{12}, \alpha_{13}, \dots, \alpha_{n-1,n})$ is a multivariable in $\binom{n}{2}$ variables; and $\mathbf{a} = (a_{12}, a_{13}, \dots, a_{n-1,n})$ is a multiexponent. We define

$$\alpha^{\mathbf{a}} := \prod_{1 \leq i < j \leq d} \alpha_{ij}^{a_{ij}}.$$

When $i > j$, we set $a_{ij} = a_{ji}$, and we define $\sum_{m \neq i} a_{im}$ to be the sum over all the terms in the multiexponent where i appears as either the first or second index.

Other functionals f have been used in (3.1) to represent high-dimensional solid angle measures as integrals. Hajja and Walker [27, Theorem 1] use $f(\mathbf{x}) = 1$ and consider a standard change of variables, to obtain an integral formula for the solid angle measures, where the integral is taken over the portion of the unit sphere in the positive orthant. Kabluchko and Zaporozhets [33, Proposition 1.1] use a form related

to Gaussian distribution to present an equivalent formula for the solid angle measures of a specific class of cones. For the purposes of this paper, we will focus exclusively on Ribando's hypergeometric series formula.

Chapter 4 Cone Decompositions for Solid Angle measure

In this chapter, we extend use of the power series formula to arbitrary polyhedral cones. The power series formula gives the solid angle measure of simplicial cones whose associated matrices are positive definite. Given a polyhedral cone, we may project it onto the orthogonal complement of its lineality space to obtain a pointed cone whose affine solid angle measure is the same as the normalized solid angle measure of the original cone. If the pointed cone is not simplicial, we can triangulate it simplicial cones, so that the solid angle measure of the pointed cone is the sum of the solid angle measures of the simplicial cones in the triangulation. In the next chapter, we discuss this projection and our choice of triangulation in depth. Thus, the task at hand is to determine solid angle measures of simplicial cones whose solid angles do not have convergent power series (3.4). In this chapter, we consider systematically decomposing such simplicial cones into cones whose associated matrices are positive definite. The content of this chapter appears in [18], which is collaborative work with Yuan Zhou.

Regarding the power series formula in (3.4), Ribando noted that there are two significant issues in applying the power series method [39]. The first major issue is that in higher dimensions, computational feasibility is hindered by the large number of coordinates needed to use the formula. To compute the normalized solid angle measure of an n -dimensional simplicial cone, one needs $\binom{n}{2}$ coordinates. Several authors make reference to the power series, but often cite it being computationally untractable for high dimensions. The second issue is that the positive definite-ness of the associated matrix is an essential assumption for applying the power-series formula. When this criterion is not met, α lies outside of the domain of convergence of the series, and the formula cannot be used in a way that is meaningful.

We present a method that allows one to compute the normalized solid angle measure of any polyhedral cone via the power series method. Moreover, we address the two major issues standing in the way of widespread use of the power series method as a means to compute solid angle measures.

We address the positive-definite-ness criterion via signed decompositions of cones. In Section 4.1, we investigate Brion–Vergne decomposition of cones with respect to hyperplanes. We demonstrate in Theorem 4.1.3 and Corollary 4.1.4 that Brion–Vergne decomposition of a simplicial cone with respect to a particular hyperplane results in finitely many cones that either have a positive definite associated matrix (and so their solid angle measures can be computed directly via the power series formula), or contain lines (and so by applying Corollary 2.2.2, the computation of solid angle measures can be simplified to a lower-dimensional problem, which can be addressed using induction on dimension). In Section 4.2, we consider Brion–Vergne decomposition of cones with respect to lines. We demonstrate in Theorem 4.2.3 that Brion–Vergne decomposition with respect to a particular line leads to a second decomposition of a simplicial cone into finitely many cones, each of which has a positive definite associated matrix. This theorem gives a method to decompose solid

angles lying outside the domain of convergence into solid angles lying within the domain of convergence of the series in Theorem 3.3.2.

We also address the computational feasibility of the power series method by reducing the number of coordinates needed. In Section 4.3, we explore the properties of cones resulting from the application of a stronger version of Theorem 4.2.3. These cones have associated matrices that are not only positive-definite but also tridiagonal, reducing the number of required coordinates for the power series formula from $\binom{n}{2}$ to $n - 1$. Theorem 4.3.1 shows that under the tridiagonal assumption, the power series formula always converges to the solid angle measure. In Theorem 4.3.9, we examine the asymptotic error of the power series formula for cones with tridiagonal associated matrices.

4.1 First decomposition method

4.1.1 Brion–Vergne decomposition with respect to a hyperplane

We will make use of Brion–Vergne (B–V) decomposition (see [8], [3]) with respect to a hyperplane. B–V decomposition is a signed decomposition of a simplicial cone into a finite family of full-dimensional simplicial cones. The hyperplane determines a facet for each of the cones in the decomposition. We adopt some of the notation used in [3] and reformulate the decomposition below.

Definition 4.1.1. Let $\mathbf{w}_1, \dots, \mathbf{w}_d$ be vectors in \mathbb{R}^n . We denote by $\langle \mathbf{w}_1, \dots, \mathbf{w}_d \rangle$ the linear span of $\mathbf{w}_1, \dots, \mathbf{w}_d$. We denote by $\mathbf{c}(\mathbf{w}_1, \dots, \mathbf{w}_d)$ the cone generated by the vectors $\mathbf{w}_1, \dots, \mathbf{w}_d$.

Let $L \subseteq \mathbb{R}^n$ be a hyperplane, and $\mathbf{w}_i \in \mathbb{R}^n \setminus L$. We denote by $\rho_i: \mathbb{R}^n \rightarrow L$ the projection onto L , parallel to \mathbf{w}_i .

Let C be a cone. We denote by $[C]$ the indicator function of the cone C . We say that a cone C can be decomposed into cones C_1, \dots, C_k , if their indicator functions satisfy the relation

$$[C] \equiv \sum_{i=1}^k s_i [C_i], \text{ where } s_i \in \{\pm 1\},$$

modulo indicator functions of cones containing lines (in Section 4.1) or modulo indicator functions of lower-dimensional cones (in Section 4.2).

Theorem 4.1.2 (Brion–Vergne decomposition with respect to a hyperplane [3, Proposition 15b]). *Let $\mathbf{w}_1, \dots, \mathbf{w}_n$ form a basis of \mathbb{R}^n and let cone $C = \mathbf{c}(\mathbf{w}_1, \dots, \mathbf{w}_n)$. Let $L \subseteq \mathbb{R}^n$ be a hyperplane. Assume that $\mathbf{w}_i \in L$ if and only if $r + 1 \leq i \leq s$ and that \mathbf{w}_i lie on one side of L for $1 \leq i \leq r$, and on the other side for $s + 1 \leq i \leq n$. Then, we have the following relation modulo indicator functions of cones containing lines.*

$$[C] \equiv \sum_{i=1}^r [\mathbb{R}_{\geq 0} \mathbf{w}_i + \rho_i(C)] - \sum_{i=s+1}^n [\mathbb{R}_{\geq 0}(-\mathbf{w}_i) + \rho_i(C)].$$

4.1.2 Solid angle decomposition that includes cones containing lines

We now present a signed decomposition of a given full-dimensional simplicial cone whose solid angle measure is of interest, in a way that the resulting cones either contain lines so that Corollary 2.2.2 applies, or have positive definite associated matrices so that Theorem 3.3.2 applies.

Theorem 4.1.3. *Given linearly independent unit vectors $\mathbf{w}_1, \mathbf{w}_2, \dots, \mathbf{w}_n \in \mathbb{R}^n$, the cone $\mathbf{c}(\mathbf{w}_1, \mathbf{w}_2, \dots, \mathbf{w}_n)$ can be decomposed into a finite family of cones, each of which is either:*

(I) *a cone containing lines, or*

(II) *a cone $\mathbf{c}(\mathbf{v}_1, \mathbf{v}_2, \dots, \mathbf{v}_n)$ of dimension n whose associated matrix*

$$M_n = \begin{bmatrix} 1 & -|\mathbf{v}_1 \cdot \mathbf{v}_2| & \cdots & -|\mathbf{v}_1 \cdot \mathbf{v}_n| \\ -|\mathbf{v}_2 \cdot \mathbf{v}_1| & 1 & \cdots & -|\mathbf{v}_2 \cdot \mathbf{v}_n| \\ \vdots & \vdots & \ddots & \vdots \\ -|\mathbf{v}_n \cdot \mathbf{v}_1| & -|\mathbf{v}_n \cdot \mathbf{v}_2| & \cdots & 1 \end{bmatrix}$$

is positive definite. In particular,

(a) $\|\mathbf{v}_i\| = 1$ for $i = 1, 2, \dots, n$

(b) $\mathbf{v}_n = \mathbf{w}_n$

(c) $\langle \mathbf{v}_1, \mathbf{v}_2, \dots, \mathbf{v}_{n-1} \rangle = \langle \mathbf{w}_1, \mathbf{w}_2, \dots, \mathbf{w}_{n-1} \rangle$

(d) $\mathbf{v}_i \cdot \mathbf{v}_n = 0$ for $i = 1, 2, \dots, n-2$

(e) $\mathbf{x}^T M_n \mathbf{x} = \left\| [\epsilon_1 \mathbf{v}_1, \dots, \epsilon_n \mathbf{v}_n] \mathbf{x} \right\|^2$ holds for every $\mathbf{x} \in \mathbb{R}^n$, where $\epsilon_i = \pm 1$.

Before proving the theorem, we point out that the property (e) ensures the positive definiteness of the associated matrix M_n given by (3.3). Indeed, for any nonzero vector $\mathbf{x} := (x_1, \dots, x_n)$, since $\mathbf{v}_1, \dots, \mathbf{v}_n$ are linearly independent,

$$[\epsilon_1 \mathbf{v}_1, \dots, \epsilon_n \mathbf{v}_n] \mathbf{x} = \sum_{i=1}^n \epsilon_i x_i \mathbf{v}_i \neq \mathbf{0},$$

and hence $\mathbf{x}^T M_n \mathbf{x} = \left\| [\epsilon_1 \mathbf{v}_1, \dots, \epsilon_n \mathbf{v}_n] \mathbf{x} \right\|^2 > 0$. As a consequence, the solid angle formula (3.4) for a cone in the decomposition, which is of the latter form (II), is a convergent power series.

Proof of Theorem 4.1.3. We proceed by induction on the dimension.

Consider the base case $n = 2$. Let $\mathbf{w}_1 = (w_{11}, w_{12})$ and $\mathbf{w}_2 = (w_{21}, w_{22})$ be linearly independent unit vectors. We show that the cone $\mathbf{c}(\mathbf{w}_1, \mathbf{w}_2)$ is already of the form (II). The cone satisfies the properties (a) through (d) trivially. Let $\mathbf{x} = (x_1, x_2) \in \mathbb{R}^2$. The equation in property (e) has the left-hand-side

$$\mathbf{x}^T M_n \mathbf{x} = \begin{bmatrix} x_1 & x_2 \end{bmatrix} \cdot \begin{bmatrix} 1 & -|\mathbf{w}_1 \cdot \mathbf{w}_2| \\ -|\mathbf{w}_1 \cdot \mathbf{w}_2| & 1 \end{bmatrix} \cdot \begin{bmatrix} x_1 \\ x_2 \end{bmatrix} = x_1^2 + x_2^2 - 2x_1x_2|\mathbf{w}_1 \cdot \mathbf{w}_2|,$$

and the right-hand side

$$\begin{aligned}
\|[\epsilon_1 \mathbf{w}_1, \epsilon_2 \mathbf{w}_2] \mathbf{x}\|^2 &= \left\| \begin{bmatrix} \epsilon_1 w_{11} & \epsilon_2 w_{21} \\ \epsilon_1 w_{12} & \epsilon_2 w_{22} \end{bmatrix} \cdot \begin{bmatrix} x_1 \\ x_2 \end{bmatrix} \right\|^2 \\
&= (\epsilon_1 x_1 w_{11} + \epsilon_2 x_2 w_{21})^2 + (\epsilon_1 x_1 w_{12} + \epsilon_2 x_2 w_{22})^2 \\
&= x_1^2 (w_{11}^2 + w_{12}^2) + x_2^2 (w_{21}^2 + w_{22}^2) + 2\epsilon_1 \epsilon_2 x_1 x_2 (w_{11} w_{21} + w_{12} w_{22}) \\
&= x_1^2 + x_2^2 + 2\epsilon_1 \epsilon_2 x_1 x_2 (\mathbf{w}_1 \cdot \mathbf{w}_2).
\end{aligned}$$

Thus, for appropriate choices of ϵ_1 and ϵ_2 , we see that property (e) is satisfied.

Suppose the statement is true for dimension $n - 1$. Now consider the cone $\mathbf{c}(\mathbf{w}_1, \mathbf{w}_2, \dots, \mathbf{w}_n)$ in dimension n which is not already of the form (I) or (II). We distinguish two cases depending on the orthogonality of \mathbf{w}_n .

Case 1: Suppose that \mathbf{w}_n is orthogonal to all \mathbf{w}_i for $1 \leq i \leq n - 1$. Set $\mathbf{v}_n = \mathbf{w}_n$. By the inductive hypothesis, there is a (signed) decomposition of the cone $\mathbf{c}(\mathbf{w}_1, \dots, \mathbf{w}_{n-1})$ into finitely many cones $\mathfrak{k}_1, \dots, \mathfrak{k}_N$ that either contain lines or are of the second form and satisfy the desired properties. Then, it is clear that the cones

$$C_1 := \mathfrak{k}_1 + \mathbf{c}(\mathbf{v}_n), C_2 := \mathfrak{k}_2 + \mathbf{c}(\mathbf{v}_n), \dots, C_N := \mathfrak{k}_N + \mathbf{c}(\mathbf{v}_n)$$

obtained by the Minkowski sums give a decomposition of $\mathbf{c}(\mathbf{w}_1, \dots, \mathbf{w}_n)$.

If \mathfrak{k}_i is a cone containing lines in the decomposition of $\mathbf{c}(\mathbf{w}_1, \dots, \mathbf{w}_{n-1})$, then C_i also contains lines, and hence is of form (I). Otherwise, \mathfrak{k}_i must be of the form $\mathbf{c}(\mathbf{v}_1, \dots, \mathbf{v}_{n-1})$ that satisfies the properties (a)–(e) of dimension $n - 1$. It is clear that $C_i = \mathbf{c}(\mathbf{v}_1, \dots, \mathbf{v}_{n-1}, \mathbf{v}_n)$ satisfies properties (a), (b) and (d) of dimension n . By the inductive hypothesis, $\langle \mathbf{v}_1, \dots, \mathbf{v}_{n-2} \rangle = \langle \mathbf{w}_1, \dots, \mathbf{w}_{n-2} \rangle$ and $\mathbf{v}_{n-1} = \mathbf{w}_{n-1}$. Thus, we have that $\langle \mathbf{v}_1, \dots, \mathbf{v}_{n-2}, \mathbf{v}_{n-1} \rangle = \langle \mathbf{w}_1, \dots, \mathbf{w}_{n-2}, \mathbf{w}_{n-1} \rangle$ and so property (c) is satisfied. It remains to verify property (e). We note that since $\mathbf{v}_i \cdot \mathbf{v}_n = 0$, the associated matrix of C_i according to Definition 3.3.1 satisfies

$$M_n(C_i) = \begin{bmatrix} & & & 0 \\ & M_{n-1}(\mathfrak{k}_i) & & \vdots \\ 0 & \dots & 0 & 1 \end{bmatrix}.$$

By the inductive hypothesis, there exist $\epsilon_1, \dots, \epsilon_{n-1} \in \{\pm 1\}$ such that the left-hand-side of the equation in property (e) can be written as

$$\begin{aligned}
\mathbf{x}^T M_n(C_i) \mathbf{x} &= [x_1 \cdots x_{n-1}] M_{n-1}(\mathfrak{k}_i) \begin{bmatrix} x_1 \\ \vdots \\ x_{n-1} \end{bmatrix} + x_n^2 \\
&= \|\epsilon_1 x_1 \mathbf{v}_1 + \cdots + \epsilon_{n-1} x_{n-1} \mathbf{v}_{n-1}\|^2 + x_n^2 \\
&= \|\epsilon_1 \mathbf{v}_1, \dots, \epsilon_{n-1} \mathbf{v}_{n-1}, \epsilon_n \mathbf{v}_n\|^2,
\end{aligned}$$

which is equal to its right-hand side, where we set $\epsilon_n = 1$. Thus, property (e) holds.

Case 2: Suppose that \mathbf{w}_n is not orthogonal to all $\mathbf{w}_1, \dots, \mathbf{w}_{n-1}$. Without loss of generality, we may assume that $\mathbf{w}_{n-1} \cdot \mathbf{w}_n \neq 0$.

We construct a hyperplane L in order to apply Brion–Vergne decomposition Theorem 4.1.2 as follows. For $1 \leq i \leq n-2$, we define

$$\boldsymbol{\ell}_i := \mathbf{w}_i - \frac{\mathbf{w}_i \cdot \mathbf{w}_n}{\mathbf{w}_{n-1} \cdot \mathbf{w}_n} \mathbf{w}_{n-1}. \quad (4.1)$$

We remark that $\boldsymbol{\ell}_i \cdot \mathbf{w}_n = 0$ for all $i = 1, 2, \dots, n-2$. Let

$$L := \langle \boldsymbol{\ell}_1, \dots, \boldsymbol{\ell}_{n-2}, \mathbf{w}_n \rangle.$$

We find that L is a hyperplane of \mathbb{R}^n , since if there are scalars λ_i 's making

$$\mathbf{0} = \sum_{i=1}^{n-2} \lambda_i \boldsymbol{\ell}_i + \lambda_n \mathbf{w}_n = \sum_{i=1}^{n-2} \lambda_i \mathbf{w}_i - \sum_{i=1}^{n-2} \lambda_i \frac{\mathbf{w}_i \cdot \mathbf{w}_n}{\mathbf{w}_{n-1} \cdot \mathbf{w}_n} \mathbf{w}_{n-1} + \lambda_n \mathbf{w}_n,$$

then the linear independence of the \mathbf{w}_i 's implies each $\lambda_i = 0$.

Next, we decide for each i whether $\mathbf{w}_i \in L$, and we use $s_i = -1$ or 1 to indicate which open half-space that \mathbf{w}_i belongs to. It is clear that $\mathbf{w}_n \in L$. We also know that $\mathbf{w}_{n-1} \notin L$, because otherwise L would contain all $\mathbf{w}_1, \dots, \mathbf{w}_n$, a contradiction. We set $s_{n-1} = 1$. For $1 \leq i \leq n-2$, if $\mathbf{w}_i \cdot \mathbf{w}_n = 0$, then it follows from (4.1) that $\mathbf{w}_i = \boldsymbol{\ell}_i \in L$; otherwise, $\mathbf{w}_i \cdot \mathbf{w}_n \neq 0$, then we have $\mathbf{w}_i \notin L$ since

$$\mathbf{w}_i = \boldsymbol{\ell}_i + \left(\frac{\mathbf{w}_i \cdot \mathbf{w}_n}{\mathbf{w}_{n-1} \cdot \mathbf{w}_n} \right) \mathbf{w}_{n-1} \quad (4.2)$$

again by (4.1). We let accordingly

$$s_i = \begin{cases} 1, & \text{if } \mathbf{w}_i \text{ and } \mathbf{w}_{n-1} \text{ are on the same side of } L \\ -1, & \text{if } \mathbf{w}_i \text{ and } \mathbf{w}_{n-1} \text{ are on the opposite sides of } L. \end{cases}$$

Denote

$$I^+ = \{1 \leq i \leq n-1 \mid s_i = 1\} \text{ and } I^- = \{1 \leq i \leq n-1 \mid s_i = -1\}.$$

We remark that $I^- \cup I^+$ is the set of i such that $\mathbf{w}_i \in \mathbb{R}^n \setminus L$, or equivalently, the set of $1 \leq i \leq n-1$ such that $\mathbf{w}_i \cdot \mathbf{w}_n \neq 0$.

By Theorem 4.1.2, modulo indicator functions of cones containing lines, we can decompose the cone $C = \mathfrak{c}(\mathbf{w}_1, \mathbf{w}_2, \dots, \mathbf{w}_n)$ as

$$[C] \equiv \sum_{i \in I^+} [\mathbb{R}_{\geq 0} \mathbf{w}_i + \rho_i(C)] - \sum_{i \in I^-} [\mathbb{R}_{\geq 0} (-\mathbf{w}_i) + \rho_i(C)],$$

which can be rewritten as

$$[C] \equiv \sum_{i \in I^+ \cup I^-} s_i [\mathbb{R}_{\geq 0} (s_i \mathbf{w}_i) + \rho_i(C)]. \quad (4.3)$$

Therefore, it suffices to show that every cone on the right-hand side of (4.3) can be decomposed into a finite family of cones of form (I) or (II).

To this end, we let $i \in I^+ \cup I^-$ and we consider the cone

$$\mathbf{c}_i := \mathbb{R}_{\geq 0}(s_i \mathbf{w}_i) + \rho_i(C).$$

According to Definition 4.1.1,

$$\rho_i(C) = \mathbf{c}(\rho_i(\mathbf{w}_1), \dots, \rho_i(\mathbf{w}_{i-1}), \rho_i(\mathbf{w}_{i+1}), \dots, \rho_i(\mathbf{w}_n)).$$

Since $\mathbf{w}_n \in L$, we have $\rho_i(\mathbf{w}_n) = \mathbf{w}_n$. Thus,

$$\mathbf{c}_i = \mathbf{c}(s_i \mathbf{w}_i, \rho_i(\mathbf{w}_1), \dots, \rho_i(\mathbf{w}_{i-1}), \rho_i(\mathbf{w}_{i+1}), \dots, \rho_i(\mathbf{w}_{n-1}), \mathbf{w}_n). \quad (4.4)$$

Next, we determine the projections that arise on the right-hand side of (4.4), by distinguishing the cases $i = n - 1$ and $i \neq n - 1$. In the former case where $i = n - 1$, it follows from (4.2) that $\rho_i(\mathbf{w}_k) = \boldsymbol{\ell}_k$ for all $1 \leq k \leq n - 2$. Therefore, (4.4) simplifies to

$$\begin{aligned} \mathbf{c}_{n-1} &= \mathbf{c}(s_{n-1} \mathbf{w}_{n-1}, \boldsymbol{\ell}_1, \boldsymbol{\ell}_2, \dots, \boldsymbol{\ell}_{n-2}, \mathbf{w}_n) \\ &= \mathbf{c}\left(s_{n-1} \mathbf{w}_{n-1}, \mathbf{w}_1 - \frac{\mathbf{w}_1 \cdot \mathbf{w}_n}{\mathbf{w}_{n-1} \cdot \mathbf{w}_n} \mathbf{w}_{n-1}, \dots, \mathbf{w}_{n-2} - \frac{\mathbf{w}_{n-2} \cdot \mathbf{w}_n}{\mathbf{w}_{n-1} \cdot \mathbf{w}_n} \mathbf{w}_{n-1}, \mathbf{w}_n\right). \end{aligned}$$

In the latter case where $i \leq n - 2$ and $\mathbf{w}_i \cdot \mathbf{w}_n \neq 0$, we have by (4.2)

$$\mathbf{w}_{n-1} = \frac{\mathbf{w}_{n-1} \cdot \mathbf{w}_n}{\mathbf{w}_i \cdot \mathbf{w}_n} (\mathbf{w}_i - \boldsymbol{\ell}_i),$$

so

$$\begin{aligned} \rho_i(\mathbf{w}_{n-1}) &= - \left(\frac{\mathbf{w}_{n-1} \cdot \mathbf{w}_n}{\mathbf{w}_i \cdot \mathbf{w}_n} \right) \boldsymbol{\ell}_i = - \left(\frac{\mathbf{w}_{n-1} \cdot \mathbf{w}_n}{\mathbf{w}_i \cdot \mathbf{w}_n} \right) \left(\mathbf{w}_i - \frac{\mathbf{w}_i \cdot \mathbf{w}_n}{\mathbf{w}_{n-1} \cdot \mathbf{w}_n} \mathbf{w}_{n-1} \right) \\ &= \mathbf{w}_{n-1} - \left(\frac{\mathbf{w}_{n-1} \cdot \mathbf{w}_n}{\mathbf{w}_i \cdot \mathbf{w}_n} \right) \mathbf{w}_i. \end{aligned} \quad (4.5)$$

For $1 \leq k \leq n - 2$ such that $k \neq i$, we have

$$\mathbf{w}_k = \boldsymbol{\ell}_k + \frac{\mathbf{w}_k \cdot \mathbf{w}_n}{\mathbf{w}_{n-1} \cdot \mathbf{w}_n} \mathbf{w}_{n-1} = \boldsymbol{\ell}_k + \frac{\mathbf{w}_k \cdot \mathbf{w}_n}{\mathbf{w}_{n-1} \cdot \mathbf{w}_n} \cdot \frac{\mathbf{w}_{n-1} \cdot \mathbf{w}_n}{\mathbf{w}_i \cdot \mathbf{w}_n} (\mathbf{w}_i - \boldsymbol{\ell}_i).$$

It follows from (4.1) that

$$\rho_i(\mathbf{w}_k) = \boldsymbol{\ell}_k - \frac{\mathbf{w}_k \cdot \mathbf{w}_n}{\mathbf{w}_i \cdot \mathbf{w}_n} \boldsymbol{\ell}_i = \mathbf{w}_k - \frac{\mathbf{w}_k \cdot \mathbf{w}_n}{\mathbf{w}_i \cdot \mathbf{w}_n} \mathbf{w}_i. \quad (4.6)$$

Using (4.5) and (4.6), we see that (4.4) simplifies to

$$\mathbf{c}_i = \mathbf{c}\left(s_i \mathbf{w}_i, \left\{ \mathbf{w}_k - \frac{\mathbf{w}_k \cdot \mathbf{w}_n}{\mathbf{w}_i \cdot \mathbf{w}_n} \mathbf{w}_i \mid 1 \leq k \leq n - 1, k \neq i \right\}, \mathbf{w}_n\right).$$

We observe that the generators of \mathbf{c}_i in the latter case agree with those of \mathbf{c}_{n-1} in the former case, by setting $i = n - 1$.

Therefore, we can rewrite the cone \mathbf{c}_i for any $i \in I^+ \cup I^-$ in the form of

$$\mathbf{c}_i = \mathbf{c} \left(\frac{\mathbf{u}_1}{\|\mathbf{u}_1\|}, \dots, \frac{\mathbf{u}_{n-2}}{\|\mathbf{u}_{n-2}\|}, \mathbf{u}_{n-1}, \mathbf{w}_n \right),$$

where

$$\{\mathbf{u}_1, \dots, \mathbf{u}_{n-2}\} = \left\{ \mathbf{w}_k - \frac{\mathbf{w}_k \cdot \mathbf{w}_n}{\mathbf{w}_i \cdot \mathbf{w}_n} \mathbf{w}_i \mid 1 \leq k \leq n-1, k \neq i \right\} \quad (4.7)$$

$$\mathbf{u}_{n-1} = s_i \mathbf{w}_i \quad (4.8)$$

If the cone \mathbf{c}_i is already of the form (I) or (II), then no further decomposition is needed. Otherwise, we apply the inductive hypothesis on the $(n-1)$ -dimensional cone

$$\mathbf{c} \left(\frac{\mathbf{u}_1}{\|\mathbf{u}_1\|}, \dots, \frac{\mathbf{u}_{n-2}}{\|\mathbf{u}_{n-2}\|}, \mathbf{u}_{n-1} \right)$$

to get its (signed) decomposition into cones $\mathbf{k}_1, \dots, \mathbf{k}_M$ that are of the form (I) or (II). That is, each cone $\mathbf{k}_m := \mathbf{c}(\mathbf{v}_1, \dots, \mathbf{v}_{n-1})$ from $\{\mathbf{k}_1, \dots, \mathbf{k}_M\}$ either (I) contains lines, or (II) satisfies

- (i) $\|\mathbf{v}_j\| = 1$ for $j = 1, 2, \dots, n-1$
- (ii) $\mathbf{v}_{n-1} = \mathbf{u}_{n-1}$
- (iii) $\langle \mathbf{v}_1, \mathbf{v}_2, \dots, \mathbf{v}_{n-2} \rangle = \langle \mathbf{u}_1, \mathbf{u}_2, \dots, \mathbf{u}_{n-2} \rangle$
- (iv) $\mathbf{v}_j \cdot \mathbf{v}_{n-1} = 0$ for $j = 1, 2, \dots, n-3$
- (v) $\mathbf{x}^T M_{n-1}(\mathbf{k}_m) \mathbf{x} = \left\| [\epsilon_1 \mathbf{v}_1, \dots, \epsilon_{n-1} \mathbf{v}_{n-1}] \mathbf{x} \right\|^2$ holds for every $\mathbf{x} \in \mathbb{R}^{n-1}$, where $\epsilon_j = \pm 1$.

Let

$$C_m = \mathbf{k}_m + \mathbf{c}(\mathbf{w}_n) = \mathbf{c}(\mathbf{v}_1, \dots, \mathbf{v}_{n-1}, \mathbf{w}_n)$$

be the n -dimensional cone obtained by appending \mathbf{w}_n to the generators of \mathbf{k}_m . Then, the cones C_1, C_2, \dots, C_M give a decomposition of the cone \mathbf{c}_i on the right-hand side of (4.3). It is clear that if \mathbf{k}_m contain lines, then C_m also contains lines, so it is of the form (I). It remains to show that $C_m = \mathbf{c}(\mathbf{v}_1, \dots, \mathbf{v}_{n-1}, \mathbf{w}_n)$ is of the form (II), given that $\mathbf{k}_m = \mathbf{c}(\mathbf{v}_1, \dots, \mathbf{v}_{n-1})$ satisfies properties (i)–(v).

We set $\mathbf{v}_n = \mathbf{w}_n$. Then, $C_m = \mathbf{c}(\mathbf{v}_1, \dots, \mathbf{v}_{n-1}, \mathbf{v}_n)$ clearly satisfies property (a) because of (i), and property (b). Property (c) holds because

$$\langle \mathbf{v}_1, \dots, \mathbf{v}_{n-2}, \mathbf{v}_{n-1} \rangle = \langle \mathbf{u}_1, \dots, \mathbf{u}_{n-2}, \mathbf{u}_{n-1} \rangle = \langle \mathbf{w}_1, \dots, \mathbf{w}_{n-2}, \mathbf{w}_{n-1} \rangle,$$

where the first equality follows from properties (ii) and (iii), and the second equality follows from equations (4.7) and (4.8). For any $1 \leq k \leq n-1, k \neq i$, we have

$$\left(\mathbf{w}_k - \frac{\mathbf{w}_k \cdot \mathbf{w}_n}{\mathbf{w}_i \cdot \mathbf{w}_n} \mathbf{w}_i \right) \cdot \mathbf{w}_n = \mathbf{w}_k \cdot \mathbf{w}_n - \frac{\mathbf{w}_k \cdot \mathbf{w}_n}{\mathbf{w}_i \cdot \mathbf{w}_n} \mathbf{w}_i \cdot \mathbf{w}_n = 0.$$

Thus, \mathbf{w}_n is orthogonal to all $\mathbf{u}_1, \dots, \mathbf{u}_{n-2}$ by (4.7). Property (d) holds because $\mathbf{v}_n = \mathbf{w}_n$ is also orthogonal to all $\mathbf{v}_1, \dots, \mathbf{v}_{n-2}$ by property (iii). Using property (d), the associated matrix of C_m can be written in relation to the associated matrix of \mathfrak{k}_m , as

$$M_n(C_m) = \begin{bmatrix} & & & & 0 \\ & & & & \vdots \\ & & & & 0 \\ & & & & -|\mathbf{v}_{n-1} \cdot \mathbf{v}_n| \\ 0 & \cdots & 0 & -|\mathbf{v}_{n-1} \cdot \mathbf{v}_n| & 1 \end{bmatrix}.$$

Let vector $\mathbf{x} = (x_1, \dots, x_n) \in \mathbb{R}^n$. Then,

$$\mathbf{x}^T M_n(C_m) \mathbf{x} = [x_1 \cdots x_{n-1}] M_{n-1}(\mathfrak{k}_m) \begin{bmatrix} x_1 \\ \vdots \\ x_{n-1} \end{bmatrix} - 2|\mathbf{v}_{n-1} \cdot \mathbf{v}_n| x_{n-1} x_n + x_n^2.$$

By property (v), for the appropriate choice of $\epsilon_1, \dots, \epsilon_{n-1} \in \{\pm 1\}$, the first term on the right-hand side of the above equation is equal to

$$\|\epsilon_1 x_1 \mathbf{v}_1 + \cdots + \epsilon_{n-1} x_{n-1} \mathbf{v}_{n-1}\|^2.$$

By setting

$$\epsilon_n = \begin{cases} -1, & \text{if } \mathbf{v}_{n-1} \cdot \mathbf{v}_n \text{ and } \epsilon_{n-1} \text{ have the same sign} \\ 1, & \text{otherwise,} \end{cases}$$

we have that $-|\mathbf{v}_{n-1} \cdot \mathbf{v}_n| = \epsilon_{n-1} \epsilon_n (\mathbf{v}_{n-1} \cdot \mathbf{v}_n)$, and hence

$$\begin{aligned} & \mathbf{x}^t M_n(C_m) \mathbf{x} \\ &= \|\epsilon_1 x_1 \mathbf{v}_1 + \cdots + \epsilon_{n-1} x_{n-1} \mathbf{v}_{n-1}\|^2 + 2\epsilon_{n-1} \epsilon_n (\mathbf{v}_{n-1} \cdot \mathbf{v}_n) x_{n-1} x_n + \epsilon_n^2 x_n^2 \\ &= \left\| [\epsilon_1 \mathbf{v}_1, \dots, \epsilon_{n-1} \mathbf{v}_{n-1}, \epsilon_n \mathbf{v}_n] \mathbf{x} \right\|^2. \end{aligned}$$

This implies that property (e) holds as well. We showed that in Case 2, every cone obtained via B–V decomposition can be further decomposed into a finite family of cones, each of which either contains lines or has an associated matrix that is positive definite. This concludes the proof of the theorem. \square

Corollary 4.1.4. *The decomposition in Theorem 4.1.3 allows for the computation of the normalized solid angle of a simplicial cone $C \in \mathbb{R}^n$ via the power series (3.4).*

Proof. Suppose Theorem 4.1.3 yields the decomposition C_1, \dots, C_N of C such that $[C] = \sum_{i=1}^N s_i [C_i]$, where $s_i = \pm 1$. Then

$$\tilde{\Omega}_n(C) = \sum_{i=1}^N s_i \tilde{\Omega}_n(C_i).$$

For each C_i in the decomposition, if it is of the form (I), then we can apply Corollary 2.2.2 to reduce it to a lower-dimensional problem; if it is of the form (II), then Theorem 3.3.2 applies. By induction on the dimension, each $\tilde{\Omega}_n(C_i)$ can be computed. \square

We note that in order to compute the solid angle measure using Theorem 4.1.3, one must determine the cones that contain lines and take orthogonal projections to reduce dimension, which is not immediately obvious. As such, we present another decomposition method in the following section.

4.2 Second decomposition method

The decomposition Theorem 4.2.3 in this section gives a more direct way to compute the normalized solid angle measure of a simplicial cone. The resulting cones are either lower-dimensional cones or full-dimensional simplicial cones. In the former case, the cones have normalized solid angle measure 0. In the latter, the generators of the cones are explicitly given. This allows us to determine the normalized solid angle measure of the original cone, according to Corollary 4.2.4.

4.2.1 Brion–Vergne decomposition with respect to a line

We will make use another variant of Brion–Vergne (B–V) decomposition (see [8], [3]), which is with respect to a one-dimensional subspace. Each cone in the decomposition will contain a generator along the given one-dimensional subspace. This B–V decomposition is reformulated below.

Theorem 4.2.1 (Brion–Vergne decomposition with respect to a line [3, Proposition 15a], rephrased). *Let $\mathbf{w}_1, \dots, \mathbf{w}_n$ form a basis of \mathbb{R}^n and let cone $C = \mathbf{c}(\mathbf{w}_1, \dots, \mathbf{w}_n)$. Given a non-zero vector $\mathbf{r} = \sum_{i=1}^n \lambda_i \mathbf{w}_i \in \mathbb{R}^n$, let $\delta_i \in \{-1, 0, 1\}$ denote the sign of λ_i for $1 \leq i \leq n$. Then, the following relation holds, modulo indicator functions of cones containing lines.*

$$[C] \equiv \sum_{i:\delta_i \neq 0} s_i [\mathbf{c}(\epsilon_{i,1} \mathbf{w}_1, \dots, \epsilon_{i,i-1} \mathbf{w}_{i-1}, \epsilon_{i,i+1} \mathbf{w}_{i+1}, \dots, \epsilon_{i,n} \mathbf{w}_n, \delta_i \mathbf{r})],$$

where $s_i, \epsilon_{i,k} \in \{\pm 1\}$ for $1 \leq k \leq n, k \neq i$ are given by

$$s_i = \begin{cases} (-1)^{\text{card}(\{1 \leq j < i \mid \delta_j = 1\})}, & \text{if } \delta_i = 1 \\ (-1)^{\text{card}(\{i < j \leq n \mid \delta_j = -1\})}, & \text{if } \delta_i = -1 \end{cases} \quad (4.9)$$

$$\epsilon_{i,k} = \begin{cases} -1, & \text{if } \delta_i = \delta_k = 1 \text{ and } k < i, \text{ or if } \delta_i = \delta_k = -1 \text{ and } k > i \\ 1, & \text{otherwise.} \end{cases} \quad (4.10)$$

Recall that if $C = \mathbf{c}(\mathbf{w}_1, \dots, \mathbf{w}_n)$ is a simplicial cone in \mathbb{R}^n generated by some basis $\mathbf{w}_1, \dots, \mathbf{w}_n \in \mathbb{R}^n$, then its dual cone

$$C^* := \{\mathbf{y} \in \mathbb{R}^n \mid \mathbf{y} \cdot \mathbf{x} \geq 0 \forall \mathbf{x} \in C\}$$

is also simplicial. The dual cone $C^* = \mathbf{c}(\mathbf{w}_1^*, \dots, \mathbf{w}_n^*)$ is generated by some dual basis $\mathbf{w}_1^*, \dots, \mathbf{w}_n^* \in \mathbb{R}^n$ such that for every $1 \leq i, j \leq n$ and $j \neq i$,

$$\mathbf{w}_i^* \cdot \mathbf{w}_i > 0 \text{ and } \mathbf{w}_i^* \cdot \mathbf{w}_j = 0. \quad (4.11)$$

Furthermore, the dual of the dual is the cone itself, i.e., $(C^*)^* = C$. The dual of a cone containing lines is a lower dimensional cone (i.e., a cone whose affine dimension is less than n).

By first passing to the dual cone, then applying Brion–Vergne decomposition Theorem 4.2.1 with respect to a particular line, and finally taking the dual again, we obtain the following decomposition which is modulo lower dimensional cones. Furthermore, each cone in the decomposition shares at least two generators of the original cone, one being \mathbf{w}_n .

Theorem 4.2.2. *Let $\mathbf{w}_1, \dots, \mathbf{w}_n$ form a basis of \mathbb{R}^n and let cone $C = \mathbf{c}(\mathbf{w}_1, \dots, \mathbf{w}_n)$. Let $\delta_i \in \{-1, 0, 1\}$ denote the sign of $\mathbf{w}_i \cdot \mathbf{w}_n$ for $1 \leq i \leq n-1$ and set $\delta_n = 0$. Suppose that the δ_i 's are not all zero. Then, the following relation holds, modulo indicator functions of lower dimensional cones.*

$$[C] \equiv \sum_{i:\delta_i \neq 0} s_i [\mathbf{c}_i],$$

where each cone \mathbf{c}_i is generated by $\mathbf{u}_{i,k}$ ($1 \leq k \leq n$) defined as

$$\mathbf{u}_{i,k} = \begin{cases} \mathbf{w}_k, & \text{if } \delta_k = 0 \text{ or } k = i \\ \epsilon_{i,k} \left(\mathbf{w}_k - \frac{\mathbf{w}_k \cdot \mathbf{w}_n}{\mathbf{w}_i \cdot \mathbf{w}_n} \mathbf{w}_i \right), & \text{otherwise} \end{cases} \quad (4.12)$$

and the signs $s_i, \epsilon_{i,k} \in \{\pm 1\}$ are given by equations (4.9) and (4.10), respectively.

Proof. Suppose that the dual cone C^* is generated by $\mathbf{w}_1^*, \dots, \mathbf{w}_n^* \in \mathbb{R}^n$. Let

$$\mathbf{r} = \sum_{i=1}^{n-1} \left(\frac{\mathbf{w}_i \cdot \mathbf{w}_n}{\mathbf{w}_i \cdot \mathbf{w}_i^*} \right) \mathbf{w}_i^*.$$

We note that the signs δ_i agree with those defined in Theorem 4.2.1, since $\mathbf{w}_i \cdot \mathbf{w}_i^* > 0$. We apply Theorem 4.2.1 to the dual cone $C^* = \mathbf{c}(\mathbf{w}_1^*, \dots, \mathbf{w}_n^*)$, with respect to the non-zero vector \mathbf{r} , and obtain that

$$[C^*] \equiv \sum_{i:\delta_i \neq 0} s_i [\mathbf{c}(\epsilon_{i,1} \mathbf{w}_1^*, \dots, \epsilon_{i,i-1} \mathbf{w}_{i-1}^*, \epsilon_{i,i+1} \mathbf{w}_{i+1}^*, \dots, \epsilon_{i,n} \mathbf{w}_n^*, \delta_i \mathbf{r})],$$

modulo indicator functions of cones containing lines.

Since linear identities that hold for indicator functions of cones also hold for their duals, we have

$$[C] \equiv \sum_{i:\delta_i \neq 0} s_i [\mathbf{c}(\epsilon_{i,1} \mathbf{w}_1^*, \dots, \epsilon_{i,i-1} \mathbf{w}_{i-1}^*, \epsilon_{i,i+1} \mathbf{w}_{i+1}^*, \dots, \epsilon_{i,n} \mathbf{w}_n^*, \delta_i \mathbf{r})^*],$$

modulo indicator functions of lower dimensional cones.

We now show that each dual cone on the right-hand side of the above relation is generated by the $\mathbf{u}_{i,k}$'s that are defined in (4.12). To this end, we verify that

$$\mathbf{w}_i \cdot (\delta_i \mathbf{r}) > 0 \text{ and } \mathbf{w}_i \cdot (\epsilon_{i,j} \mathbf{w}_j^*) = 0 \quad \forall j \neq i, \quad (4.13)$$

and that for any $k \neq i$,

$$\mathbf{u}_{i,k} \cdot (\delta_i \mathbf{r}) = 0, \quad \mathbf{u}_{i,k} \cdot (\epsilon_{i,k} \mathbf{w}_k^*) > 0 \text{ and } \mathbf{u}_{i,k} \cdot (\epsilon_{i,j} \mathbf{w}_j^*) = 0 \quad \forall j \neq i \text{ or } k. \quad (4.14)$$

The conditions in (4.13) trivially hold because of (4.11). To show (4.14) for $k \neq i$, we first consider the case where $\delta_k = 0$, which implies that $\mathbf{w}_k \cdot \mathbf{w}_n = 0$ and $\mathbf{u}_{i,k} = \mathbf{w}_k$ by (4.12). We have

$$\mathbf{w}_k \cdot (\epsilon_{i,k} \mathbf{w}_k^*) > 0, \quad \mathbf{w}_k \cdot (\epsilon_{i,j} \mathbf{w}_j^*) = 0 \quad \forall j \neq i \text{ or } k, \text{ and}$$

$$\mathbf{w}_k \cdot (\delta_i \mathbf{r}) = \mathbf{w}_k \cdot \left(\delta_i \sum_{j=1}^{n-1} \left(\frac{\mathbf{w}_j \cdot \mathbf{w}_n}{\mathbf{w}_j \cdot \mathbf{w}_j^*} \right) \mathbf{w}_j^* \right)$$

which is equal to 0 when $k = n$, or equal to $\delta_i (\mathbf{w}_k \cdot \mathbf{w}_n) = 0$ when $k \neq n$. Now consider $k \neq i$ such that $\delta_k \neq 0$, which implies $k \neq n$. Since $\delta_i \neq 0$, we also know that $i \neq n$ and $\mathbf{w}_i \cdot \mathbf{w}_n \neq 0$. Using (4.12), we obtain that

$$\begin{aligned} \mathbf{u}_{i,k} \cdot (\delta_i \mathbf{r}) &= \epsilon_{i,k} \delta_i \left(\mathbf{w}_k - \frac{\mathbf{w}_k \cdot \mathbf{w}_n}{\mathbf{w}_i \cdot \mathbf{w}_n} \mathbf{w}_i \right) \cdot \sum_{j=1}^{n-1} \left(\frac{\mathbf{w}_j \cdot \mathbf{w}_n}{\mathbf{w}_j \cdot \mathbf{w}_j^*} \right) \mathbf{w}_j^* \\ &= \epsilon_{i,k} \delta_i \left[\frac{\mathbf{w}_k \cdot \mathbf{w}_n}{\mathbf{w}_k \cdot \mathbf{w}_k^*} (\mathbf{w}_k \cdot \mathbf{w}_k^*) - \frac{\mathbf{w}_k \cdot \mathbf{w}_n}{\mathbf{w}_i \cdot \mathbf{w}_n} \cdot \frac{\mathbf{w}_i \cdot \mathbf{w}_n}{\mathbf{w}_i \cdot \mathbf{w}_i^*} (\mathbf{w}_i \cdot \mathbf{w}_i^*) \right] = 0 \\ \mathbf{u}_{i,k} \cdot (\epsilon_{i,k} \mathbf{w}_k^*) &= \epsilon_{i,k}^2 \left(\mathbf{w}_k - \frac{\mathbf{w}_k \cdot \mathbf{w}_n}{\mathbf{w}_i \cdot \mathbf{w}_n} \mathbf{w}_i \right) \cdot \mathbf{w}_k^* = \mathbf{w}_k \cdot \mathbf{w}_k^* > 0 \\ \mathbf{u}_{i,k} \cdot (\epsilon_{i,j} \mathbf{w}_j^*) &= \epsilon_{i,k} \epsilon_{i,j} \left(\mathbf{w}_k - \frac{\mathbf{w}_k \cdot \mathbf{w}_n}{\mathbf{w}_i \cdot \mathbf{w}_n} \mathbf{w}_i \right) \cdot \mathbf{w}_j^* = 0 \quad \forall j \neq i \text{ or } k. \end{aligned}$$

Therefore, the conditions in (4.14) are all satisfied. The theorem holds. \square

4.2.2 Solid angle decomposition that includes lower dimensional cones

We present another decomposition theorem for a given full-dimensional simplicial cone whose solid angle measure is of interest. The theorem is analogous to Theorem 4.1.3. The resulting cones from Theorem 4.2.3 are either lower dimensional and hence have 0 as normalized solid angle measures, or have positive definite associated matrices so that Theorem 3.3.2 applies.

Theorem 4.2.3. *Given linearly independent unit vectors $\mathbf{w}_1, \mathbf{w}_2, \dots, \mathbf{w}_n \in \mathbb{R}^n$, the cone $\mathbf{c}(\mathbf{w}_1, \mathbf{w}_2, \dots, \mathbf{w}_n)$ can be decomposed into a finite family of cones, each of which is either*

(I) a cone of affine dimension less than n , or

(II) a full-dimensional cone generated by some vectors $\mathbf{v}_1, \dots, \mathbf{v}_n$ that satisfy the properties (a)–(e) in Theorem 4.1.3 so that its associated matrix is positive definite.

Proof. The proof is similar to that of Theorem 4.1.3. We proceed by induction on the dimension. The base case $n = 2$ is direct (same proof as in Theorem 4.1.3). Suppose that the theorem holds for dimension $n - 1$. Now consider the cone $\mathbf{c}(\mathbf{w}_1, \mathbf{w}_2, \dots, \mathbf{w}_n)$ in dimension n which is not already of the form (I) or (II).

If \mathbf{w}_n is orthogonal to all \mathbf{w}_i for $1 \leq i \leq n - 1$, then the arguments in **Case 1** of the proof of Theorem 4.1.3 (where we replace “contain lines” by “of affine dimension less than n ”) verbatim apply, so the statement is true for dimension n .

Next, we assume that \mathbf{w}_n is not orthogonal to all $\mathbf{w}_1, \dots, \mathbf{w}_{n-1}$. Let $\delta_n = 0$ and $\delta_i \in \{-1, 0, 1\}$ be the sign of $\mathbf{w}_i \cdot \mathbf{w}_n$ for $1 \leq i \leq n$. Then, the δ_i 's are not all zero. We apply Theorem 4.2.2, and obtain the (signed) decomposition

$$[C] \equiv \sum_{i:\delta_i \neq 0} s_i [\mathbf{c}_i] \text{ modulo indicator functions of lower dimensional cones,} \quad (4.15)$$

where each cone $\mathbf{c}_i = \mathbf{c}(\mathbf{u}_{i,1}, \mathbf{u}_{i,2}, \dots, \mathbf{u}_{i,n})$ is generated by the $\mathbf{u}_{i,k}$'s according to (4.12). In particular, $\mathbf{u}_{i,i} = \mathbf{w}_i$ and $\mathbf{u}_{i,n} = \mathbf{w}_n$. Thus, we can rewrite the cone \mathbf{c}_i for any $1 \leq i \leq n - 1$ such that $\delta_i \neq 0$ in the form of

$$\mathbf{c}_i = \mathbf{c}(\mathbf{u}_1, \dots, \mathbf{u}_{n-2}, \mathbf{u}_{n-1}, \mathbf{w}_n)$$

with $\{\mathbf{u}_1, \dots, \mathbf{u}_{n-2}\} = \left\{ \frac{\mathbf{u}_{i,k}}{\|\mathbf{u}_{i,k}\|} \mid 1 \leq k \leq n - 1, k \neq i \right\}$ and $\mathbf{u}_{n-1} = \mathbf{w}_i$.

If the cone \mathbf{c}_i is already of the form (I) or (II), then no further decomposition is needed. Otherwise, by the inductive hypothesis, the $(n - 1)$ -dimensional cone $\mathbf{c}(\mathbf{u}_1, \dots, \mathbf{u}_{n-2}, \mathbf{u}_{n-1})$ can be decomposed into cones $\mathbf{k}_1, \dots, \mathbf{k}_M$, such that each cone $\mathbf{k}_m := \mathbf{c}(\mathbf{v}_1, \dots, \mathbf{v}_{n-1})$ from $\{\mathbf{k}_1, \dots, \mathbf{k}_M\}$ is either (I) a cone of affine dimension less than $n - 1$, or (II) a cone with positive associated matrix satisfying the properties (i)–(v). Let

$$C_m = \mathbf{k}_m + \mathbf{c}(\mathbf{w}_n) = \mathbf{c}(\mathbf{v}_1, \dots, \mathbf{v}_{n-1}, \mathbf{w}_n)$$

be the n -dimensional cone obtained by appending \mathbf{w}_n to the generators of \mathbf{k}_m . Then, the same arguments as in the proof of Theorem 4.1.3 show that C_m has the desired properties, and that the cones C_1, \dots, C_M give a (signed) decomposition of the cone \mathbf{c}_i in the relation (4.15). This concludes the inductive step, and therefore, the theorem holds. \square

Corollary 4.2.4. *Let C be a simplicial cone in \mathbb{R}^n . Theorem 4.2.3 gives explicitly the cones C_i whose normalized solid angle measures $\tilde{\Omega}_n(C_i)$ can be computed via the power series formula (3.4) and the signs $s_i \in \{\pm 1\}$, such that the normalized solid angle measure of C satisfies*

$$\tilde{\Omega}_n(C) = \sum_{i=1}^N s_i \tilde{\Omega}_n(C_i). \quad (4.16)$$

Furthermore, the number of cones N in the decomposition is bounded above by $(n-1)!$.

Proof. Suppose that Theorem 4.2.3 yields a signed decomposition of the cone C :

$$[C] \equiv \sum_{i=1}^N s_i [C_i] \text{ modulo indicator functions of lower dimensional cones.}$$

Since the normalized solid angle measure of a lower dimensional cone with respect to \mathbb{R}^n is zero, (4.16) holds.

Each full-dimensional cone C_i resulting from the decomposition has a positive-definite matrix, so that Theorem 3.3.2 applies, and so $\tilde{\Omega}_n(C_i)$ can be computed via the power series (3.4).

Finally, we show that $N \leq (n-1)!$ by induction on n . If $n = 2$, then the base case in the proof of Theorem 4.1.3 shows that the cone C is already of the form (II), so no further decomposition is needed. Suppose that an $(n-1)$ -dimensional cone can be decomposed into at most $(n-2)!$ cones. For an n -dimensional cone C whose associated matrix is not yet positive-definite, Theorem 4.2.3 first decomposes it into the cones \mathbf{c}_i for i such that $\delta_i \neq 0$, according to (4.15). Since $\delta_n = 0$, there are at most $n-1$ such cones $\mathbf{c}_i = \mathbf{c}(\mathbf{u}_{i,1}, \dots, \mathbf{u}_{i,n})$. Subsequently, for each \mathbf{c}_i whose associated matrix is not yet positive-definite, we omit its generator $\mathbf{u}_{i,n} = \mathbf{w}_n$ in order to obtain the $(n-1)$ -dimensional cone $\mathbf{c}(\mathbf{u}_{i,1}, \dots, \mathbf{u}_{i,n-1})$, and we further decompose it into at most $(n-2)!$ cones that satisfy the desired properties by the inductive hypothesis. Therefore, the total number of cones resulting from Theorem 4.2.3 is at most $(n-1)(n-2)! = (n-1)!$. \square

4.3 Asymptotic bound on the truncation error

4.3.1 Tridiagonal associated matrices

As aforementioned, the large number of coordinates needed creates issues with computational feasibility of the power series formula (3.4) in Theorem 3.3.2. Ribando [39, p. 487] states that “... accurate series approximations will require theorems allowing us to reduce the number of terms that need computing.” Note that when $\alpha_{ij} = 0$, the only terms of $\boldsymbol{\alpha}^{\mathbf{a}}$ in the series (3.4) that are non-zero must have multiexponent \mathbf{a} whose $a_{ij} = 0$. Thus, one possibility for reducing the number of terms needed for computing is by decomposing into cones with as many pairwise orthogonal generators as possible. One particular interesting case is when $(\alpha_{ij})_{1 \leq i, j \leq n}$ is a tridiagonal matrix (i.e., $\alpha_{ij} = \mathbf{v}_i \cdot \mathbf{v}_j = 0$ whenever $i \neq j$ and $i+1 \neq j$), as we will discuss in this section.

Given linearly independent unit vectors $\mathbf{v}_1, \mathbf{v}_2, \dots, \mathbf{v}_n \in \mathbb{R}^n$, let $V \in \mathbb{R}^{n \times n}$ denote the matrix whose i -th column vector is \mathbf{v}_i . Suppose that $V^T V$ is the following symmetric and tridiagonal matrix, where $\beta_i = \mathbf{v}_i \cdot \mathbf{v}_{i+1}$ for $1 \leq i \leq n-1$.

$$V^T V = \begin{bmatrix} 1 & \beta_1 & & & \\ \beta_1 & 1 & \beta_2 & & \\ & \beta_2 & \ddots & \ddots & \\ & & \ddots & \ddots & \beta_{n-1} \\ & & & \beta_{n-1} & 1 \end{bmatrix} \quad (4.17)$$

Then, the formula (3.4) simplifies to the following multivariate power series T_{β} in $(n-1)$ -variables.

$$T_{\beta} = \frac{|\det V|}{(4\pi)^{n/2}} \sum_{\mathbf{b} \in \mathbb{N}^{n-1}} \left[\frac{(-2)^{\sum b_i}}{\prod_{i=1}^{n-1} b_i!} \Gamma\left(\frac{1+b_1}{2}\right) \Gamma\left(\frac{1+b_1+b_2}{2}\right) \cdots \right. \\ \left. \Gamma\left(\frac{1+b_{n-2}+b_{n-1}}{2}\right) \Gamma\left(\frac{1+b_{n-1}}{2}\right) \right] \beta^{\mathbf{b}}. \quad (4.18)$$

Theorem 4.3.1. *Let $C = \mathbf{c}(\mathbf{v}_1, \mathbf{v}_2, \dots, \mathbf{v}_n)$ be a cone in \mathbb{R}^n generated by the linearly independent unit vectors $\mathbf{v}_1, \mathbf{v}_2, \dots, \mathbf{v}_n$. Let V be the matrix whose column vectors are $\mathbf{v}_1, \mathbf{v}_2, \dots, \mathbf{v}_n$. Suppose that $V^T V$ is a tridiagonal matrix as in (4.17). Then, the associated matrix $M_n(C)$ has the same eigenvalues as $V^T V$.*

In particular, if $V^T V$ is tridiagonal, then $M_n(C)$ is positive definite, and the power series (4.18) converges absolutely to the normalized solid angle measure $\tilde{\Omega}_n(C)$ of the cone C .

Proof. When $V^T V$ is the symmetric and tridiagonal matrix given by (4.17), the associated matrix of C is

$$M_n(C) = \begin{bmatrix} 1 & -|\beta_1| & & & & \\ -|\beta_1| & 1 & -|\beta_2| & & & \\ & -|\beta_2| & \ddots & \ddots & & \\ & & \ddots & \ddots & -|\beta_{n-1}| & \\ & & & -|\beta_{n-1}| & 1 & \\ & & & & & \end{bmatrix}, \quad (4.19)$$

which is also symmetric and tridiagonal.

Let $P_j(\lambda)$ be the characteristic polynomial of the j -th leading principal minor of $V^T V$ for $1 \leq j \leq n$. Set $\beta_0 = 0$. We have $P_0(\lambda) = 1$, $P_1(\lambda) = 1 - \lambda$ and

$$P_j(\lambda) = (1 - \lambda)P_{j-1}(\lambda) - \beta_{j-1}^2 P_{j-2}(\lambda) \quad \text{for } 2 \leq j \leq n,$$

where the last recurrence relation is a well-known result for symmetric tridiagonal matrices (e.g., see [37]). Since the relation depends only on $\beta_{j-1}^2 = (-|\beta_{j-1}|)^2$, it is clear that the characteristic polynomial of the associated matrix is the same as that of $V^T V$. Therefore, $V^T V$ and $M_n(C)$ have the same eigenvalues.

Since the columns of V are linearly independent, for any $\mathbf{x} \neq \mathbf{0}$, we have that $\mathbf{x}^T (V^T V) \mathbf{x} = \|V\mathbf{x}\|^2 > 0$, showing that $V^T V$ is positive definite. Thus, $M_n(C)$ is also positive definite. It follows from Theorem 3.3.2 that the power series (4.18) converges absolutely to the normalized solid angle measure $\tilde{\Omega}_n(C)$ of the cone C . \square

Remark 4.3.2. We can strengthen property (d) from “ $\mathbf{v}_i \cdot \mathbf{v}_n = 0$ for $i = 1, \dots, n-2$ ” in Theorem 4.1.3 and Theorem 4.2.3 to

$$\mathbf{v}_i \cdot \mathbf{v}_j = 0 \quad \text{for all } 1 \leq i, j \leq n \text{ such that } j \neq i \text{ or } i \pm 1. \quad (\text{IId}')$$

The proofs of the two theorems hold verbatim. The new property *IId'* ensures that $V^T V$ is a tridiagonal matrix for any cone from the decomposition, so that Theorem 4.3.1 applies. Therefore, we have the following variant of Corollary 4.2.4, which takes advantage of the tridiagonal structure. We note that the number of cones resulting from the new decomposition can be larger than that of Corollary 4.2.4, but it is still upper bounded by $(n - 1)!$.

Corollary 4.3.3. *Let C be a simplicial cone in \mathbb{R}^n . Theorem 4.2.3 (with property (d) replaced by *IId'*) gives explicitly the cones C_i and the signs $s_i \in \{\pm 1\}$, such that the normalized solid angle measure of C satisfies*

$$\tilde{\Omega}_n(C) = \sum_{i=1}^N s_i \tilde{\Omega}_n(C_i).$$

The cones C_i have positive-definite and tridiagonal associated matrices, so their normalized solid angle measures $\tilde{\Omega}_n(C_i)$ can be computed via the simplified power series formula (4.18). Furthermore, the number of cones N in the decomposition is bounded above by $(n - 1)!$.

4.3.2 Eigenvalues and series truncation errors

In their study [25], Gourion and Seeger observed that a particular power series exhibited slow convergence when the associated matrix was close to being singular. Considering this observation alongside the previous Theorem 4.3.1, it is reasonable to investigate the impact of eigenvalues on the convergence of the power series.

We notice that if the linearly independent unit vectors \mathbf{v}_i 's are all pairwise orthogonal, then the normalized solid angle measure of the cone $C = \mathbf{c}(\mathbf{v}_1, \dots, \mathbf{v}_n)$ is:

$$\tilde{\Omega}_n(C) = \frac{1}{2^n}.$$

Therefore, in the following, we further assume that $n \geq 2$ and that $\mathbf{v}_i \cdot \mathbf{v}_j \neq 0$ for some $1 \leq i < j \leq n$. Let V denote the matrix whose i^{th} column is \mathbf{v}_i . Let λ_{\min} be the smallest eigenvalue of $V^T V$.

Lemma 4.3.4. *The smallest eigenvalue λ_{\min} of $V^T V$ satisfies $0 < \lambda_{\min} < 1$.*

Proof. The matrix $V^T V$ is positive definite, since for any $\mathbf{x} \neq \mathbf{0}$, we have that $\mathbf{x}^T (V^T V) \mathbf{x} = \|V \mathbf{x}\|^2 > 0$, where the last strict inequality follows from the linear independence of the columns of V . Thus, $\lambda_{\min} > 0$.

By the Cauchy interlacing theorem, λ_{\min} is less than or equal to the minimum eigenvalue of a principal submatrix of $V^T V$. In particular, by taking the principal submatrix $\begin{bmatrix} 1 & \mathbf{v}_i \cdot \mathbf{v}_j \\ \mathbf{v}_i \cdot \mathbf{v}_j & 1 \end{bmatrix}$ where $\mathbf{v}_i \cdot \mathbf{v}_j \neq 0$, we have $\lambda_{\min} \leq 1 - (\mathbf{v}_i \cdot \mathbf{v}_j)^2 < 1$. \square

For the rest of this section, we focus on the case where $V^T V$ is the tridiagonal matrix as defined in (4.17). Theorem 4.3.1 implies that the power series T_β in $n - 1$

variables as defined in (4.18) converges absolutely to the solid angle measure. For simplicity, we consider only the series part

$$\frac{(4\pi)^{n/2}}{|\det V|} T_{\beta} = \sum_{\mathbf{b} \in \mathbb{N}^{n-1}} A_{\mathbf{b}} \beta^{\mathbf{b}},$$

where, for any multiexponent $\mathbf{b} = (b_1, \dots, b_{n-1})$ in \mathbb{N}^{n-1} ,

$$A_{\mathbf{b}} := \frac{(-2)^{\sum b_i}}{\prod_{i=1}^{n-1} b_i!} \Gamma\left(\frac{1+b_1}{2}\right) \Gamma\left(\frac{1+b_1+b_2}{2}\right) \dots \Gamma\left(\frac{1+b_{n-2}+b_{n-1}}{2}\right) \Gamma\left(\frac{1+b_{n-1}}{2}\right). \quad (4.20)$$

We regard

$$T(\mathbf{x}) = \sum_{\mathbf{b} \in \mathbb{N}^{n-1}} A_{\mathbf{b}} x_1^{b_1} x_2^{b_2} \dots x_{n-1}^{b_{n-1}}$$

as a hypergeometric series of $(n-1)$ variables $\mathbf{x} = (x_1, \dots, x_{n-1})$ in Horn's sense [30].

Remark 4.3.5. We recall some standard notations and results from [30, 39] regarding the convergence of a hypergeometric series. We rephrase them below for the triadiagonal case to describe the domain of convergence of $T(\mathbf{x})$.

Let \mathbf{e}_i denote the i -th standard basis vector. For $1 \leq i \leq n-1$, we define the ratio of the neighboring coefficients

$$f_i(\mathbf{b}) := \frac{A_{\mathbf{b}+\mathbf{e}_i}}{A_{\mathbf{b}}}, \quad (4.21)$$

and introduce the limit

$$\Psi_i(\mathbf{b}) := \lim_{t \rightarrow \infty} f_i(t\mathbf{b}).$$

We can view $A_{\mathbf{b}}$, $f_i(\mathbf{b})$ and $\Psi_i(\mathbf{b})$ as functions of $\mathbf{b} \in \mathbb{R}_+^{n-1}$ instead of $\mathbf{b} \in \mathbb{N}^{n-1}$. Then, for $1 \leq i \leq n-1$, f_i is a rational function of the variables $\mathbf{b} \in \mathbb{R}_+^{n-1}$. Set $b_0 = b_n = 0$. The function Ψ_i satisfies

$$\Psi_i(\mathbf{b}) = \lim_{t \rightarrow \infty} \frac{A_{t\mathbf{b}+\mathbf{e}_i}}{A_{t\mathbf{b}}} = -\frac{\sqrt{(b_{i-1}+b_i)(b_i+b_{i+1})}}{b_i}, \quad (4.22)$$

and it is a rational and homogeneous function of degree zero.

The parameterized curve $\left(\frac{1}{|\Psi_1(\mathbf{b})|}, \dots, \frac{1}{|\Psi_{n-1}(\mathbf{b})|}\right)$ describes an hypersurface that bounds the convergence domain of the hypergeometric series $T(\mathbf{x})$. That is, if a point \mathbf{x} lies on the boundary of the convergence domain, then for some $\mathbf{b} \in \mathbb{R}_+^{n-1}$,

$$|x_i| = \frac{1}{|\Psi_i(\mathbf{b})|} \quad \forall 1 \leq i \leq n-1. \quad (4.23)$$

In addition, [39, Theorem 3.2] states that \mathbf{x} lies on the boundary of the convergence domain, if

$$\det \begin{bmatrix} 1 & -|x_1| & & & \\ -|x_1| & 1 & -|x_2| & & \\ & -|x_2| & \ddots & \ddots & \\ & & \ddots & \ddots & -|x_{n-1}| \\ & & & -|x_{n-1}| & 1 \end{bmatrix} = 0. \quad (4.24)$$

It follows from Theorem 4.3.1 that in the tridiagonal case, the minimum eigenvalue of the associated matrix $M_n(C)$ given in (4.19) is also λ_{\min} , where $0 < \lambda_{\min} < 1$ by Lemma 4.3.4, and that $\mathbf{x} = \boldsymbol{\beta}$ lies in the convergence domain of $T(\mathbf{x})$. The following lemma suggests that $1 - \lambda_{\min}$ plays a role in the convergence of $T(\mathbf{x})$.

Lemma 4.3.6. *The point $\left(\frac{\beta_1}{1-\lambda_{\min}}, \dots, \frac{\beta_{n-1}}{1-\lambda_{\min}}\right)$ lies on the boundary of the domain of convergence of the series $T(\mathbf{x})$.*

Proof. By Remark 4.3.5, it suffices to show that (4.24) holds for $\mathbf{x} = \frac{\boldsymbol{\beta}}{1-\lambda_{\min}}$, which is clearly satisfied since λ_{\min} is an eigenvalue of $M_n(C)$. \square

We show a lemma regarding the monotonicity of the functions f_i in (4.21), which will become useful later in analyzing the series truncation errors.

Lemma 4.3.7. *Let $\mathbf{b} \in \mathbb{R}_{\geq 0}^{n-1}$ and let $1 \leq i, j \leq n-1$ such that $i \neq j$. Then, $|f_i(\mathbf{b} + \mathbf{e}_j)| \geq |f_i(\mathbf{b})|$.*

Proof. If $j \neq i \pm 1$, then it follows from (4.21) and (4.20) that $|f_i(\mathbf{b} + \mathbf{e}_j)| = |f_i(\mathbf{b})|$. If $j = i \pm 1$, then the desired inequality is equivalent to

$$\frac{\Gamma\left(\frac{3+b_i+b_j}{2}\right)}{\Gamma\left(\frac{2+b_i+b_j}{2}\right)} \geq \frac{\Gamma\left(\frac{2+b_i+b_j}{2}\right)}{\Gamma\left(\frac{1+b_i+b_j}{2}\right)},$$

which holds because the Γ function is log-convex on the positive real axis. \square

We are interested in an asymptotic analysis of the truncation error of the series $T(\boldsymbol{\beta})$. Truncating the series in partial degrees (N_1, \dots, N_{n-1}) , the error term is bounded by $E(N_1, \dots, N_{n-1})$ defined below.

Definition 4.3.8. For partial degrees $(N_1, \dots, N_{n-1}) \in \mathbb{N}^{n-1}$, define the series $T(\boldsymbol{\beta})$ truncation error as

$$E(N_1, \dots, N_{n-1}) = \sum_{\mathbf{b} \in B} |A_{\mathbf{b}} \boldsymbol{\beta}^{\mathbf{b}}|,$$

where $B = \{\mathbf{b} \in \mathbb{N}^{n-1} \mid b_i \geq N_i \text{ for at least one } i\}$.

We investigate the asymptotic decay of $E(N_1, \dots, N_{n-1})$, in relation to $1 - \lambda_{\min}$.

Theorem 4.3.9. *For any ρ such that $1 - \lambda_{\min} < \rho < 1$, there exist partial degrees N_1, \dots, N_{n-1} such that for any integer $\ell \geq 1$, we have*

$$E(N_1 + \ell, \dots, N_{n-1} + \ell) \leq \rho^\ell E(N_1, \dots, N_{n-1}).$$

To simplify the notation, we will prove Theorem 4.3.9 specifically for $n = 3$, which we restate as Proposition 4.3.10 below. Note that the proof for general n follows in the exact same manner.

Proposition 4.3.10. *For any ρ such that $1 - \lambda_{\min} < \rho < 1$, there exist partial degrees N_1 and N_2 such that for any integer $\ell \geq 1$, we have*

$$E(N_1 + \ell, N_2 + \ell) \leq \rho^\ell E(N_1, N_2).$$

Proof. For the multiexponent (b_1, b_2) , the coefficient $A_{\mathbf{b}}$ in (4.20) is

$$A_{b_1, b_2} = \frac{(-2)^{b_1+b_2}}{b_1! b_2!} \Gamma\left(\frac{1+b_1}{2}\right) \Gamma\left(\frac{1+b_2}{2}\right) \Gamma\left(\frac{1+b_1+b_2}{2}\right).$$

By Lemma 4.3.6 and (4.23), there exist $x_1, x_2 \in \mathbb{R}_+$ such that

$$\frac{|\beta_1|}{1 - \lambda_{\min}} = \frac{1}{|\Psi_1(x_1, x_2)|} \quad \text{and} \quad \frac{|\beta_2|}{1 - \lambda_{\min}} = \frac{1}{|\Psi_2(x_1, x_2)|}.$$

Thus, we have

$$|\beta_1 \Psi_1(x_1, x_2)| = 1 - \lambda_{\min} \quad \text{and} \quad |\beta_2 \Psi_2(x_1, x_2)| = 1 - \lambda_{\min}. \quad (4.25)$$

Since Ψ_1, Ψ_2 are rational and homogeneous functions of degree zero by (4.22), their values only depend on the ratio between x_1 and x_2 . (We note that for general $n > 3$, each Ψ_i only depends on at most two consecutive pairwise ratios.) We express (x_1, x_2) in polar coordinates (r_0, θ_0) with $r_0 = \sqrt{x_1^2 + x_2^2}$ and $\theta_0 = \arctan(x_2/x_1)$. It follows from (4.22) that $|\Psi_1(r \cos \theta, r \sin \theta)| = \sqrt{1 + \tan \theta}$, which is increasing on $\theta \in [0, \pi/2)$, and $|\Psi_2(r \cos \theta, r \sin \theta)| = \sqrt{1 + \cot \theta}$, which is decreasing on $\theta \in (0, \pi/2]$. We obtain from (4.25) that

$$\left| \beta_1 \lim_{r \rightarrow \infty} f_1(r \cos \theta_0, r \sin \theta_0) \right| = \left| \beta_2 \lim_{r \rightarrow \infty} f_2(r \cos \theta_0, r \sin \theta_0) \right| = 1 - \lambda_{\min}. \quad (4.26)$$

Let ϵ be a small positive number. Specifically, we set

$$\epsilon := \sqrt{\frac{\rho}{1 - \lambda_{\min}}} - 1 > 0. \quad (4.27)$$

It follows from (4.26) that there exists $r_0 > 0$ such that

$$\forall r \geq r_0, \quad |\beta_i f_i(r \cos \theta_0, r \sin \theta_0)| \leq (1 - \lambda_{\min})(1 + \epsilon/2) \quad \text{for } i = 1, 2.$$

Since f_1, f_2 are rational functions, there exist θ_1, θ_2 with $\theta_2 < \theta_0 < \theta_1$ such that

$$\forall r \geq r_0 \text{ and } \theta \in [\theta_2, \theta_1], \quad |\beta_i f_i(r \cos \theta, r \sin \theta)| \leq (1 - \lambda_{\min})(1 + \epsilon) \quad \text{for } i = 1, 2.$$

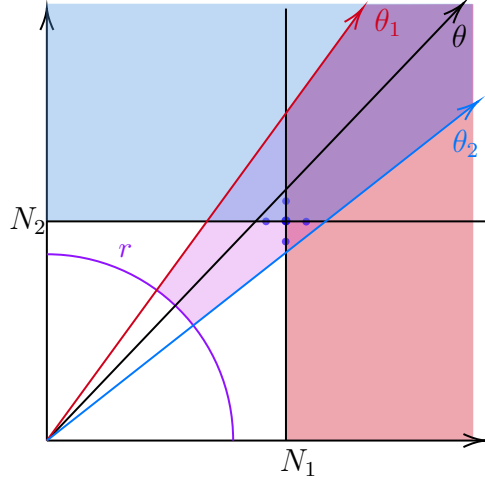


Figure 4.1: The (b_1, b_2) -plane corresponding to the proof of Proposition 4.3.10. The region bounded by rays θ_1 and θ_2 shows where the ratio bounds in (4.29) hold; The region above the horizontal line at N_2 and the ray θ_2 and the region to the right of the vertical line at N_1 and below the ray θ_1 correspond to Claim 4.3.11 (1) and (2), respectively.

Let S be the sector whose polar coordinates r, θ satisfy

$$r > r_0 \quad \text{and} \quad \theta \in [\theta_2, \theta_1].$$

Denote

$$\mu := (1 - \lambda_{\min})(1 + \epsilon) = \sqrt{(1 - \lambda_{\min})\rho} < 1. \quad (4.28)$$

We note that for $(b_1, b_2) \in \mathbb{R}_+^2$,

$$\begin{aligned} \beta_1 f_1(b_1, b_2) &= (A_{b_1+1, b_2} \beta_1^{b_1+1} \beta_2^{b_2}) / (A_{b_1, b_2} \beta_1^{b_1} \beta_2^{b_2}); \\ \beta_2 f_2(b_1, b_2) &= (A_{b_1, b_2+1} \beta_1^{b_1} \beta_2^{b_2+1}) / (A_{b_1, b_2} \beta_1^{b_1} \beta_2^{b_2}). \end{aligned}$$

Thus, for any $(b_1, b_2) \in \mathbb{R}_+^2$ that lies in the sector S ,

$$\frac{|A_{b_1+1, b_2} \beta_1^{b_1+1} \beta_2^{b_2}|}{|A_{b_1, b_2} \beta_1^{b_1} \beta_2^{b_2}|} \leq \mu \quad \text{and} \quad \frac{|A_{b_1, b_2+1} \beta_1^{b_1} \beta_2^{b_2+1}|}{|A_{b_1, b_2} \beta_1^{b_1} \beta_2^{b_2}|} \leq \mu. \quad (4.29)$$

Let (N_1, N_2) be an integer point in the interior of S such that $(N_1 \pm 1, N_2)$ and $(N_1, N_2 \pm 1)$ are also inside the sector S . Such point (N_1, N_2) exists because the conditions below can always be met by scaling.

$$\begin{aligned} N_2 \cot \theta_1 + 1 &\leq N_1 \leq N_2 \cot \theta_2 - 1 \quad \text{and} \\ N_1 \tan \theta_2 + 1 &\leq N_2 \leq N_1 \tan \theta_1 - 1. \end{aligned} \quad (4.30)$$

We illustrate the parameters and the regions in Figure 4.1.

Using (4.29) and (4.30) together with Lemma 4.3.7, we obtain the following claim.

Claim 4.3.11. *Let $(b_1, b_2) \in \mathbb{N}^2$.*

1. *If $b_1 \geq N_1$ and $b_2 \leq b_1 \tan \theta_1$, then $\frac{|A_{b_1+1, b_2} \beta_1^{b_1+1} \beta_2^{b_2}|}{|A_{b_1, b_2} \beta_1^{b_1} \beta_2^{b_2}|} \leq \mu$.*

2. *If $b_2 \geq N_2$ and $b_2 \geq b_1 \tan \theta_2$, then $\frac{|A_{b_1, b_2+1} \beta_1^{b_1} \beta_2^{b_2+1}|}{|A_{b_1, b_2} \beta_1^{b_1} \beta_2^{b_2}|} \leq \mu$.*

In order to study the truncation errors $E(N_1, N_2)$ and $E(N_1 + \ell, N_2 + \ell)$, we rewrite them as

$$E(N_1, N_2) = S_1 + S_2 + S_3 \quad (4.31)$$

and

$$E(N_1 + \ell, N_2 + \ell) \leq S'_1 + S'_2 + S'_3 + S'_4, \quad (4.32)$$

respectively, where

$$\begin{aligned} S_1 &= \sum_{\substack{b_1 \geq N_1 \\ 0 \leq b_2 < N_2}} |A_{b_1, b_2} \beta_1^{b_1} \beta_2^{b_2}|; & S_2 &= \sum_{\substack{b_2 \geq N_2 \\ 0 \leq b_1 < N_1}} |A_{b_1, b_2} \beta_1^{b_1} \beta_2^{b_2}|; \\ S_3 &= \sum_{\substack{b_1 \geq N_1 \\ b_2 \geq N_2}} |A_{b_1, b_2} \beta_1^{b_1} \beta_2^{b_2}|, \end{aligned}$$

and

$$\begin{aligned} S'_1 &= \sum_{\substack{b_1 \geq N_1 + \ell \\ 0 \leq b_2 < N_2}} |A_{b_1, b_2} \beta_1^{b_1} \beta_2^{b_2}|; & S'_2 &= \sum_{\substack{b_2 \geq N_2 + \ell \\ 0 \leq b_1 < N_1}} |A_{b_1, b_2} \beta_1^{b_1} \beta_2^{b_2}|; \\ S'_3 &= \sum_{\substack{b_1 \geq N_1 \\ b_2 \geq N_2 + \ell}} |A_{b_1, b_2} \beta_1^{b_1} \beta_2^{b_2}|; & S'_4 &= \sum_{\substack{b_1 \geq N_1 + \ell \\ b_2 \geq N_2}} |A_{b_1, b_2} \beta_1^{b_1} \beta_2^{b_2}|. \end{aligned}$$

We view each term $|A_{b_1, b_2} \beta_1^{b_1} \beta_2^{b_2}|$ in a series S_k as corresponding to the point (b_1, b_2) in the first quadrant. See Figure 4.2.

We first consider S_1 and S'_1 . Let $(b_1, b_2) \in \mathbb{N}^2$ such that $b_1 = N_1 + i$ for some $i \geq 0$ and $b_2 \leq N_2$. We compare the term corresponding to (b_1, b_2) with the term corresponding to (N_1, b_2) . Using Claim 4.3.11 (1), we have that

$$\left| \frac{A_{N_1+i, b_2} \beta_1^{N_1+i} \beta_2^{b_2}}{A_{N_1, b_2} \beta_1^{N_1} \beta_2^{b_2}} \right| = \prod_{j=0}^{i-1} \left| \frac{A_{N_1+j+1, b_2} \beta_1^{N_1+j+1} \beta_2^{b_2}}{A_{N_1+j, b_2} \beta_1^{N_1+j} \beta_2^{b_2}} \right| \leq \mu^i.$$

In particular, the above inequality holds for $i = \ell$ and any $0 \leq b_2 \leq N_2 - 1$. This implies that

$$S'_1 \leq \mu^\ell S_1. \quad (4.33)$$

Similarly, using Claim 4.3.11 (2), we obtain that

$$S'_2 \leq \mu^\ell S_2. \quad (4.34)$$

Next, we compare a term corresponding to (b_1, b_2) in S_3 to the term s corresponding to (N_1, N_2) , which is defined by

$$s := |A_{N_1, N_2} \beta_1^{N_1} \beta_2^{N_2}|.$$

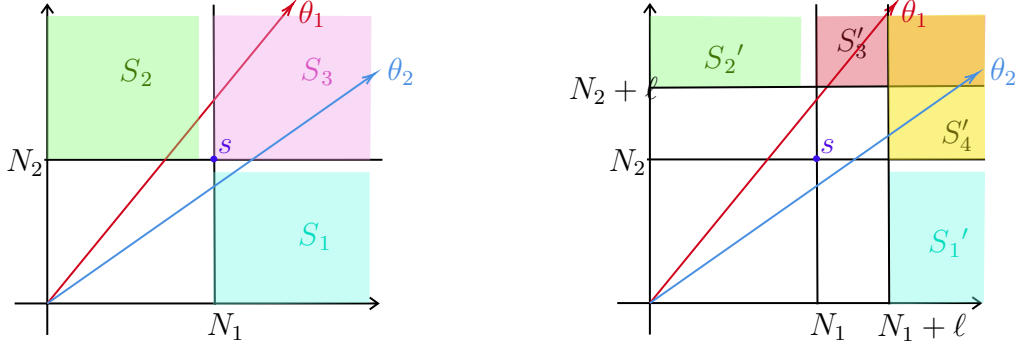


Figure 4.2: Planes of multiexponents $(b_1, b_2) \in \mathbb{N}^2$ for analyzing the series truncation errors $E(N_1, N_2)$ (left) and $E(N_1 + \ell, N_2 + \ell)$ (right). The regions indicate which series S_k the term $|A_{b_1, b_2} \beta_1^{b_1} \beta_2^{b_2}|$ belongs to in (4.31) and (4.32).

Claim 4.3.12. *Let $b_1 = N_1 + i$ and $b_2 = N_2 + j$, where i, j are non-negative integers. Then*

$$\frac{|A_{b_1, b_2} \beta_1^{b_1} \beta_2^{b_2}|}{s} \leq \mu^{i+j}.$$

Proof. Depending on whether the point (b_1, b_2) lies below or above the ray from the origin through the point (N_1, N_2) , we reduce either b_1 or b_2 by 1, as follows. By the geometric conditions in (4.30), if (b_1, b_2) is below the ray, then $b_1 - 1$ lies in the sector S , and if (b_1, b_2) is above the ray, then $b_2 - 1$ lies in the sector S . In either case, we can apply Claim 4.3.11 to obtain that the ratio between the terms corresponding to (b_1, b_2) and $(b'_1, b'_2) = (b_1, b_2 - 1)$ or $(b_1 - 1, b_2)$ is at most μ . Repeat this process until $(b'_1, b'_2) = (N_1, N_2)$. By multiplying the sequences of ratios obtained in the process, we have the desired inequality. \square

In particular, Claim 4.3.12 provides upper bounds of S'_3 and S'_4 in terms of s :

$$\begin{aligned} S'_3 &\leq s \sum_{i=0}^{\infty} \sum_{j=\ell}^{\infty} \mu^{i+j} = \frac{\mu^\ell s}{(1-\mu)^2}, \\ S'_4 &\leq s \sum_{i=\ell}^{\infty} \sum_{j=0}^{\infty} \mu^{i+j} = \frac{\mu^\ell s}{(1-\mu)^2}. \end{aligned} \tag{4.35}$$

Claim 4.3.13. *For very large N_1, N_2 , we may assume that s/S_1 is sufficiently small.*

Proof. Let $(N_1^*, N_2^*) \in \mathbb{N}^2$ be a point in the sector S such that $N_1^* \geq N_1, N_2^* = N_2 + k$ and $k := \lfloor N_2^* - N_1^* \tan \theta_2 \rfloor$ is a large integer. Define s^* to be the term corresponding to the integer point (N_1^*, N_2^*) , and define the series S_1^* accordingly. Notice that we can lower bound S_1^* by the single term t inside it, where $t := |A_{N_1^*, N_2} \beta_1^{N_1^*} \beta_2^{N_2}|$ corresponding to the point (N_1^*, N_2) . Since this point lies in S and $N_2 = N_2^* - k$, Claim 4.3.11 (2) implies that $s^*/t \leq \mu^k$. Therefore, $s^*/S_1^* \leq \mu^k$, which is sufficiently small for k large enough. \square

In particular, we take large N_1, N_2 such that $s/S_1 \leq \frac{1}{2}\epsilon(1 - \mu)^2$, or equivalently,

$$\frac{2s}{(1 - \mu)^2} \leq \epsilon S_1. \quad (4.36)$$

By combining (4.31) through (4.36), we obtain that

$$\begin{aligned} E(N_1 + \ell, N_2 + \ell) &\leq S'_1 + S'_2 + S'_3 + S'_4 \leq \mu^\ell \left(S_1 + S_2 + \frac{2s}{(1 - \mu)^2} \right) \\ &\leq \mu^\ell (S_1 + S_2 + \epsilon S_1) \leq \mu^\ell (1 + \epsilon)(S_1 + S_2 + S_3) \\ &\leq \mu^\ell (1 + \epsilon)^\ell (S_1 + S_2 + S_3) \\ &= (\mu(1 + \epsilon))^\ell E(N_1, N_2). \end{aligned}$$

Finally, according to (4.27) and (4.28),

$$\mu(1 + \epsilon) = \sqrt{(1 - \lambda_{\min})\rho} \cdot \sqrt{\frac{\rho}{1 - \lambda_{\min}}} = \rho.$$

Therefore, the desired inequality $E(N_1 + \ell, N_2 + \ell) \leq \rho^\ell E(N_1, N_2)$ holds. \square

Chapter 5 Implementation and Applications of Solid Angle Measure Approximation Methods

5.1 Implementation

In this section, we discuss the implementation of the cone decomposition of the previous chapter and Ribando’s power series for solid angle approximation.

5.1.1 Stopping Criterion

Given that T_α is an infinite series, an approximation will be given by a truncation of the series. While [39] and [26] consider truncation at a fixed degree r , we present a more dynamic truncation criterion, which we refer to as *truncation by ϵ* , for a given target absolute error parameter $\epsilon > 0$.

For a positive integer r , define S_r to be the sum of the terms in T_α that have degree r , i.e., the sum of the terms in formula (3.4) corresponding to $\mathbf{a} \in \mathbb{N}^{\binom{n}{2}}$ such that $a_1 + a_2 + \cdots + a_{n(n-1)/2} = r$. For a given polyhedral cone K , we can compute the total number of simplicial cones N whose solid angle measures will be required for computing the solid angle of K via a function called `total_num_cones`. We note that this number is dependent upon the choice of triangulation as well as type of decomposition used. Given $\epsilon > 0$, in this truncation method, for each of the N cones with convergent power series T_α , we truncate T_α at the smallest degree r such that $\frac{1}{2} (|S_{r-1}| + |S_r|) < \frac{\epsilon}{N}$.

5.1.2 Constructing Polyhedra

We will often use the Polyhedra module in SageMath to construct polyhedra as Polyhedron objects. To construct a Polyhedron object, one must provide either a V -representation of the polyhedron (vertices, rays, and lines) or an H -representation of the polyhedron (equations and inequalities presented as lists). Note that a SageMath Polyhedron object has optional parameters: `backend` and `base_ring`. For Polyhedron objects that we construct in SageMath, we use the Normaliz backend, and the Rational Field as the base ring.

5.1.3 Projecting out Lineality Space

Recall that by Corollary 2.2.2, the solid angle of a polyhedral cone is the same as the solid angle measure of the pointed cone which is its projection onto the orthogonal complement of its lineality space. Given a polyhedral cone K represented by its generators, we construct K as a Polyhedron object, which by default will compute a minimal V -representation of K . We determine an orthonormal basis of the lineality space of K . Then, we consider the extreme rays which are determined in the minimal V -representation of K . We use the orthonormal basis of the lineality space to determine the component orthogonal to the lineality space of each extreme ray.

We construct another Polyhedron object using these components as rays. This new Polyhedron object describes a pointed cone with the same solid angle measure as K .

5.1.4 Triangulation

To obtain a simplicial cone, we must triangulate the pointed cone P . The building function for triangulations in SageMath requires the input to be a point configuration. Note that a triangulation method exists for Polyhedron objects which are polytopes as well as pointed cones, whose backends are Normaliz. However, at the time of writing, it is unclear how to use the triangulation method for a Polyhedron with Normaliz backend to obtain multiple triangulations for nonsimplicial pointed cones.

We reduce triangulation of the d -cone P (whose extreme rays correspond to a vector configuration) to triangulation of a $(d - 1)$ -polytope (whose vertices give a point configuration) by positively scaling the extreme rays to obtain homogenous coordinates, where the resulting points lie on an affine hyperplane. To homogenize our vector configuration, we generate a conic combination \mathbf{n} of our extreme rays and ensure that it is not orthogonal to any of the extreme rays. We use the resulting vector as the normal vector to the affine hyperplane described by $\mathbf{n}^t \mathbf{x} = 1$. The intersection of the cone with the affine hyperplane forms a polytope. Given an extreme ray \mathbf{r} in the vector configuration, scaling by a factor of $1/(\mathbf{n} \cdot \mathbf{r})$ gives a vertex of the polytope.

We construct a PointConfiguration in SageMath of the vertices of the described polytope. To triangulate a point configuration in SageMath, one can use the internal engine, or the optional TOPCOM (Triangulations of Point Configurations and Oriented Matroids) engine. At present, the question of whether regular triangulations perform better than non-regular triangulations in the power series method remains unanswered. As such, we do not wish to restrict ourselves to only regular triangulations. We opt for the TOPCOM engine, as it is required for non-regular triangulations. TOPCOM's triangulation algorithms rely only on the combinatorial data of the point configuration, given by its oriented matroid.

Note that many different triangulations of a point configuration may exist. We considered 24 different non-simplicial cones of dimensions three through 5, and the running time of computing their solid angles, dependent on various triangulations. In Figure 5.1, each point gives the running time for solid angle computation of a non-simplicial cone using a specific triangulation. Points with the same markers correspond to different triangulations of the same non-simplicial cone. For the sake of scale, we omit running times over 1000 CPU seconds. In Figure 5.1 we see that the general trend is that an increased number of cones generally requires more time to compute a solid angle approximation via the power series method, and that small numbers of cones correspond to small computation times. For this reason, for dimensions greater than four, we choose to use the triangulation which among the up to first 500 triangulations enumerated by TOPCOM, yields the smallest N number of cones in its decomposition. The choice of 500 here is arbitrary and requires further exploration. We see clear examples where different triangulations of the same non-simplicial cone result in the same number of cones, but markedly different running times, as well as examples where a triangulation resulting in more cones has a smaller

running time. These instances underscore the limitations of this investigation, emphasizing the necessity for a deeper comprehension of factors contributing to running time for informed decisions regarding triangulation strategies.

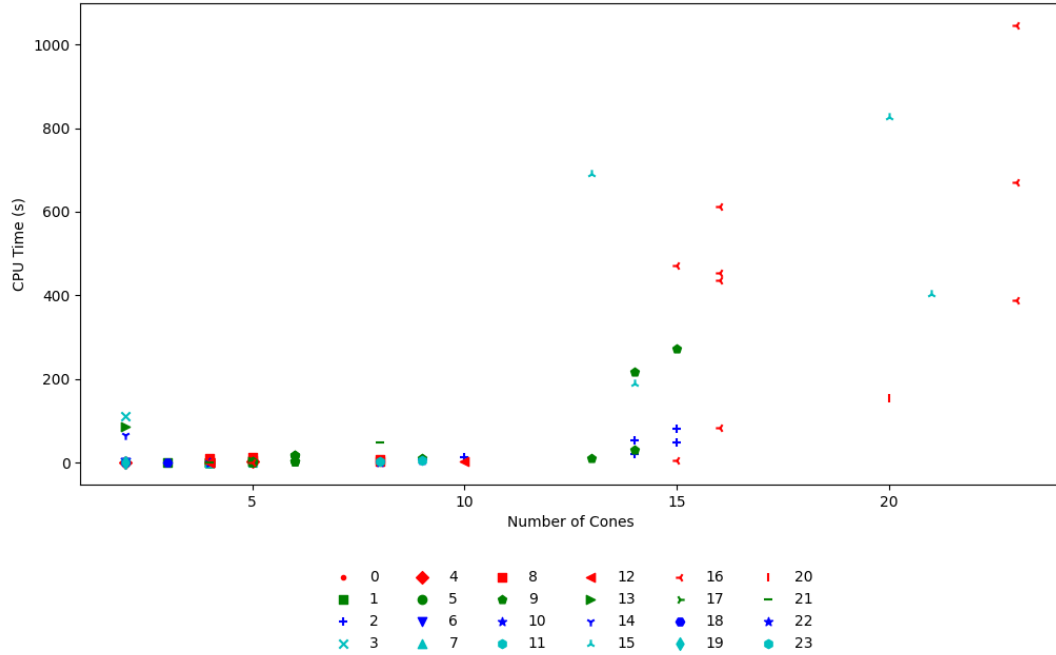


Figure 5.1: Number of cones in decomposition of triangulated cones versus running time.

The cones corresponding to the markers in Figure 5.1 and the triangulations considered are listed in in the appendix.

In our study, a triangulation of a pointed cone P is given as a list of lists of indices. Each list of indices corresponds to a simplicial cone whose extreme rays correspond to the extreme rays of P with those same indices as determined by the ordered list $P.rays_list()$.

5.1.5 Decomposition

Given a triangulation of a pointed cone P represented by indices, we represent each simplicial cone in the triangulation as a matrix, whose rows are the extreme rays of the simplicial cone. For each simplicial cone in the triangulation, we decompose it into an orthogonal direct sum of cones. For each cone in the orthogonal direct sum, we apply the decomposition in Theorem 4.2.3 via the function `generate_cones_decomposition`. The decomposition Theorem 4.2.3 is dependent upon the dot products of extreme rays, and so is still applicable to lower-dimensional cones.

Note that the decomposition is done on an ordered basis and so the order of the extreme rays of the simplicial cone matters. In particular, the last extreme ray of the simplicial cone plays a special role in that it appears in every cone in the decomposition, the extreme rays of the resulting cones in the first iteration are dependent upon their dot product with the last extreme ray, and the number of extreme rays that the last extreme ray is orthogonal to determines the number of cones in the first iteration of the decomposition, that is the number of cones \mathbf{c}_i in (4.15). Thus, to minimize this quantity, we set the last generator to be the generator which is pairwise orthogonal to the most generators of the simplicial cone.

The output of `generate_cones_decomposition` is a generator object containing a list of N ordered pairs, where for $i = 1, 2, \dots, N$ the first entry is C_i and the second is s_i as defined in (4.16).

5.1.6 Computing the Power Series

Suppose K decomposes into N simplicial cones, each having a positive definite associated matrix, and that C is one of the N cones in the decomposition. To compute the solid angle measure of K , we must compute a truncated power series for C . Given a target absolute error ϵ , we approximate the convergent power series T_{α} for C with our function `solid_angle_simplicial_and_posdef`, using truncation by ϵ . Recall that the truncation degree is dependent on ϵ and N . We first decompose C into an orthogonal direct sum of cones. By Lemma 2.2.1, the solid angle measure of C is the product of the solid angle measures of the cones in the orthogonal direct sum. Furthermore, since K has positive-definite associated matrix, it is clear that the cones in the orthogonal direct sum have positive-definite associated matrices, hence convergent power series. For each cone in the orthogonal decomposition of C , we first check if it a single ray, whose affine solid angle measure is $\frac{1}{2}$. If this is not the case, we let d be the dimension of the cone, and we normalize the extreme rays of the cone and compute the multivariable α as a list of the non-zero dot products of the extreme rays. We also keep track of the indices of the extreme rays corresponding to non-zero dot products for evaluating the Gamma function as in (3.4). We let k be the number of non-zero dot products, that is the length of α . Recall that we are able to consider only the non-zero dot products because if $\alpha_{ij} = 0$, the the only terms contributing to the sum T_{α} are those where the multiexponent \mathbf{a} satisfies $a_{ij} = 0$. Thus, rather than computing the series in $\binom{d}{2}$ coordinates, we are able to use k coordinates.

Note that in (3.4), square roots and π appear often, as a result of applying the Gamma function as well as normalizing the extreme rays. Since the square root of many values and π are interpreted in SageMath as symbolic expressions, we add as an optional parameter `base_ring` which by default is set to Real Field, with which we cast these values to, as symbolic computations are known to be costly.

For the series portion of (3.4), we re-express the series as

$$\frac{(4\pi)^{d/2}}{|\det V|} T_{\alpha} = \sqrt{\pi}^d + \sum_{m=1}^{\infty} (-2)^m \sum_{\mathbf{p} \in W_m} \frac{1}{\prod_{i=1}^k p_i!} \sum_{\mathbf{c} \in C_{\mathbf{p}}} A_{\mathbf{c}} \alpha^{\mathbf{c}},$$

where W_m is the set of all weak partitions of m into k parts, $C_{\mathbf{p}}$ is the set of all multi-permutations of the the multi-set containing the elements of \mathbf{p} , and

$$A_{\mathbf{c}} = \prod_{i=1}^d \Gamma\left(\frac{1 + \sum_{n \neq i} c_{in}}{2}\right).$$

In this way, the solid angle measure approximation of the cone is given by

$$\frac{(4\pi)^{d/2}}{|\det V|} T_{\alpha} = \sqrt{\pi}^d + \sum_{m=1}^M (-2)^m \sum_{\mathbf{p} \in W_m} \frac{1}{\prod_{i=1}^k p_i!} \sum_{\mathbf{c} \in C_{\mathbf{p}}} A_{\mathbf{c}} \alpha^{\mathbf{c}}, \quad (5.1)$$

where M is the degree at which the series satisfies the truncation criterion.

For a fixed degree m , we generate all of the weak partitions of m into k parts dynamically by fixing a minimum part of the partition, and then generating partitions with reduced m and k . We output these weak partitions as dictionaries whose keys are the entries of the partitions, and whose values are the frequency with which the entries appear in the partition. For instance, the weak partition $(3, 2, 2, 0)$ of 7 into 4 parts is stored as $\{3 : 1, 0 : 1, 2 : 2\}$. We order these dictionaries by increasing frequency. Multi-sets are often given by their frequency vector, which is a vector of the frequencies with which an element in the multi-set appears. After identifying a weak partition with a multi-set, we can obtain a frequency vector. For our example, we have frequency vector $(1, 1, 2)$. When a frequency vector is encountered for the first time, we use Aaron Williams' [45] algorithm for multi-set permutations, implemented by Erik Garrison at [20] to generate all the multipermutations of the weak partition, and we cache this result, with the key being the frequency vector and the value being the multipermutations. If another partition is encountered having the same frequency vector, its entries are mapped to the partition having cached multipermutations to generate the multipermutations of the new partition, rather than computing all of the multipermutations via Williams' algorithm.

Each $p_i!$ appearing in (5.1) is computed recursively and cached. To compute the coefficient $A_{\mathbf{c}}$ for the multiexponent \mathbf{c} , we compute $s_i = \sum_{i \neq m} c_{im}$. Then, noting that s_i is an integer, we see that we need to compute Gamma values for integers and half-integers. We have a function `recursive_gamma_si` whose input is s_i and whose output is an approximation (because we use an approximation of $\sqrt{\pi}$ depending on the `base_ring` parameter) of $\Gamma(\frac{1+s_i}{2})$. We use the recursive relation

$$\begin{aligned} \text{recursive_gamma_si}(0) &= \sqrt{\pi}, \\ \text{recursive_gamma_si}(1) &= 1, \\ \text{recursive_gamma_si}(n) &= \binom{n-1}{2} \text{recursive_gamma_si}(n-2) \text{ for } n \geq 2. \end{aligned}$$

We cache the output of `recursive_gamma_si`. In computing $\alpha^{\mathbf{c}}$, we cache the powers of the entries of α and compute these powers recursively.

5.1.7 Discussion of Optimizations to Code

Many improvements have been made over time to optimize the performance of our implementation of the power series method. The initial incarnation of the method to compute the solid angle measure of a simplicial cone takes the form of the function `solid_angle_general` in [17]. In the initial version, the multivariable α was fixed to have length $\binom{n}{2}$ where n is the dimension of the cone of interest. In the current version, we take advantage of the fact that if $\alpha_{ij} = 0$ then any term which depends on a multiexponent \mathbf{a} having $a_{ij} \neq 0$ is 0, hence does not contribute to T_α . In the initial version, to compute S_r as defined in Subsection 5.1.1, we generated all of the weak compositions of r into $\binom{n}{2}$ parts. For each composition \mathbf{a} , we computed

$$(-2)^{\sum_{1 \leq i < j \leq n} a_{ij}} \text{ and } \prod_{1 \leq i < j \leq n} a_{ij}!.$$

If two weak compositions share the same entries, then the quantities above are exactly the same, indicating numerous repeated computations. In the current iteration, we compute k , the number of nonzero entries in α . We then group weak compositions with k entries together if they are permutations of the same weak partition of a nonnegative integer m into k parts. Each group of weak compositions has the same value for $\prod_{1 \leq i < j \leq n} a_{ij}!$. We also group together weak partitions if they correspond to the same value m . These partitions, hence all of the compositions which are permutations of them, have the same value for $(-2)^{\sum_{1 \leq i < j \leq n} a_{ij}}$.

Furthermore, in the initial implementation, for each weak composition \mathbf{a} of r into $\binom{n}{2}$ parts, for $j = 1, 2, \dots, n$ the quantity

$$\Gamma\left(\frac{1 + \sum_{m \neq i} a_{im}}{2}\right) \tag{5.2}$$

as seen in (3.4) was computed, which corresponds to

$$d \times \binom{r + \binom{n}{2} - 1}{\binom{n}{2} - 1}$$

operations for each r . We observe that for all of the multiexponents used in the computations of S_1, S_2, \dots, S_k , as defined in Subsection 5.1.1, there exist only k distinct values that (5.2) can assume. Therefore, it is pragmatic to store these values in a cache rather than recalculating them. Additionally, both the Gamma and factorial functions exhibit recursive properties, making it advantageous to exploit this characteristic. In the initial iteration, we neither cached the Gamma nor factorial values nor utilized recursive computation. However, in the present iteration, we implement both strategies.

To illustrate the improvement in performance, we consider how `solid_angle_general` performs versus how the current improved version of it performs. The Corner and Opposite cones (defined in the next section) are simplicial cones with positive definite associated matrices. Over 5 runs, the `solid_angle_general` function with target

absolute error $\epsilon = 0.0001$, required an average of 37.68 and 0.22 CPU seconds respectively. In our current version, the average computation time was 0.21 and 0.02 CPU seconds respectively. The Weyl chamber D_5 (discussed in the next section) is a 5-dimensional simplicial cone without positive definite associated matrix and so requires decomposition. Using `solid_angle_general` to compute the solid angle measure approximation of each cone in the decomposition, using T_α truncated at degree 15, required an average of 327.86 CPU seconds. The current version required an average of 1.26 CPU seconds.

5.2 Computational Experiments

All experiments were run on a 1.4 GHz Quad-Core Intel Core i5, 8GB RAM PC. We utilized MATLAB R2023a and SageMath 10.0 [44].

5.2.1 Simplicial Cones with Known Solid Angles

Irreducible root systems have been studied extensively (see [7, 31]). Given an irreducible root system $\Phi \subset \mathbb{R}^n$, the *Coxeter arrangement* corresponding to Φ is the arrangement of hyperplanes which are orthogonal to the roots in Φ , that is, the reflecting hyperplanes of the associated finite Coxeter group. The complement of the set of hyperplanes in a Coxeter arrangement is disconnected. Each connected component is isometric and called a *region* of the hyperplane arrangement.

We will focus primarily on a certain type of Coxeter group, namely Weyl groups, which are finite reflection groups. Given $\alpha \in \Phi$, the reflection about the hyperplane perpendicular to α is the map

$$s_\alpha(\mathbf{x}) = \mathbf{x} - 2 \frac{\mathbf{x} \cdot \alpha}{\alpha \cdot \alpha} \alpha.$$

The Weyl group of Φ is the finite group generated by all such s_α 's. For Weyl groups, the regions of the corresponding hyperplane arrangements are called *Weyl chambers*. It is well known that the Weyl group acts freely and transitively on Weyl chambers. Thus, the normalized solid angle measure of a single Weyl chamber is $\frac{1}{|W|}$, where $|W|$ is the number of Weyl chambers, which is also the order of the associated Weyl group. To construct a single Weyl chamber, we construct the cone that is bounded by the hyperplanes orthogonal to a fixed set of simple roots. Note that after projecting out the lineality space of Weyl chambers, we have simplicial cones.

We also consider a class of obtuse cones (cones which are larger than orthants) of the form cone $(\mathbf{e}_1, \mathbf{e}_2, \dots, \widehat{\mathbf{e}}_i, \dots, \mathbf{e}_n, -\mathbf{e}_1 - \mathbf{e}_2 - \dots - \mathbf{e}_n)$ for $1 \leq i \leq n$, which all have normalized solid angle measure $\frac{2^n - 1}{2^n}$. We will refer to cones of this form as type I_n . The case of I_4 is discussed in [27]. Type I_n cones are simplicial cones.

Other cones with known solid angle measures arise in the literature. We list the cones appearing in [38] below with their normalized solid angle measure:

$$\text{Standard} = \text{cone} \left((-1, 1, -1, -1), (-1, -1, -1, 1), (2, 0, 0, 0), (0, 0, 0, 2) \right)$$

$$\text{Corner} = \text{cone} \left((1, -1, -1, -1), (0, 2, 0, 0), (0, 0, 2, 0), (0, 0, 0, 2) \right)$$

$$\text{Opposite} = \text{cone} \left((1, -1, -1, -1), (-1, -1, -1, 1), (-1, 1, -1, -1), (2, 0, 0, 0) \right),$$

with

$$\tilde{\Omega}_4(\text{Standard}) = \frac{5}{48}, \quad \tilde{\Omega}_4(\text{Corner}) = \frac{15}{64}, \quad \text{and} \quad \tilde{\Omega}_4(\text{Opposite}) = \frac{11}{192}.$$

Note that the Corner cone is isometric to I_4 and so has the same solid angle measure. Another four-dimensional cone is considered in [27] where the authors compute its solid angle measure to be $\frac{17}{96}$. The cone is

$$\text{HW} = \text{cone} \left((0, 1, 0, 0), (-1, -1, -1, 1), (-1, -1, -1, -1), (1, 0, 0, 0) \right).$$

Richard Ehrenborg [13] determined an alternative method to obtain the normalized solid angle measures of the four aforementioned cones through the lens of Weyl chambers. The Coxeter arrangement associated to the Weyl group of the B_4 root system comprises the hyperplanes defined by equations

$$\begin{aligned} x_i &= 0, & \text{for } 1 \leq i \leq 4 \\ x_i \pm x_j &= 0, & \text{for } 1 \leq i < j \leq 4. \end{aligned}$$

The hyperplanes defining the facets of the Standard, Corner, and HW cones are in the above arrangement. Thus, each of these three cones is formed from multiple Weyl chambers of the B_4 arrangement, of which there are 384 isometric chambers. Consider the set of permutations of the points $(s_1 1, s_2 2, s_3 3, s_4 4)$ where $s_1, s_2, s_3, s_4 \in \{\pm 1\}$. Each chamber is characterized by the presence of exactly one such point. Consequently, it is straightforward to compute the normalized solid angle measure of the Standard, Corner and HW cones as $\frac{n}{384}$ where n is the number of such points which lie in each cone respectively.

The Coxeter arrangement associated to the Weyl group of the F_4 root system comprises the 24 hyperplanes defined by the equations

$$\begin{aligned} x_i &= 0, & \text{for } 1 \leq i \leq 4, \\ x_i \pm x_j &= 0, & \text{for } 1 \leq i < j \leq 4, \\ x_1 \pm x_2 \pm x_3 \pm x_4 &= 0. \end{aligned}$$

The facets of the Opposite cone lie on hyperplanes in this arrangement. This hyperplane arrangement divides \mathbb{R}^4 into 1152 isometric chambers, each characterized by the presence of exactly one point in the following list:

$$\begin{aligned} &\text{Permutations of } (s_1 1, s_2 5, s_3 7, s_4 9), \\ &\text{Permutations of } (s_1 2, s_2 4, s_3 6, s_4 10), \\ &\text{Permutations of } (s_1 1, s_2 3, s_3 5, s_4 11), \end{aligned}$$

where $s_1, s_2, s_3, s_4 \in \{\pm 1\}$. The Opposite cone contains 16, 22, and 28 points from each set respectively. Consequently, its normalized solid angle measure is $\frac{66}{1152}$.

We consider the absolute error of the approximation given by the power series method for the aforementioned simplicial cones with known solid angle measures, for dimensions two through five. In Figure 5.2, the dashed line represents the line

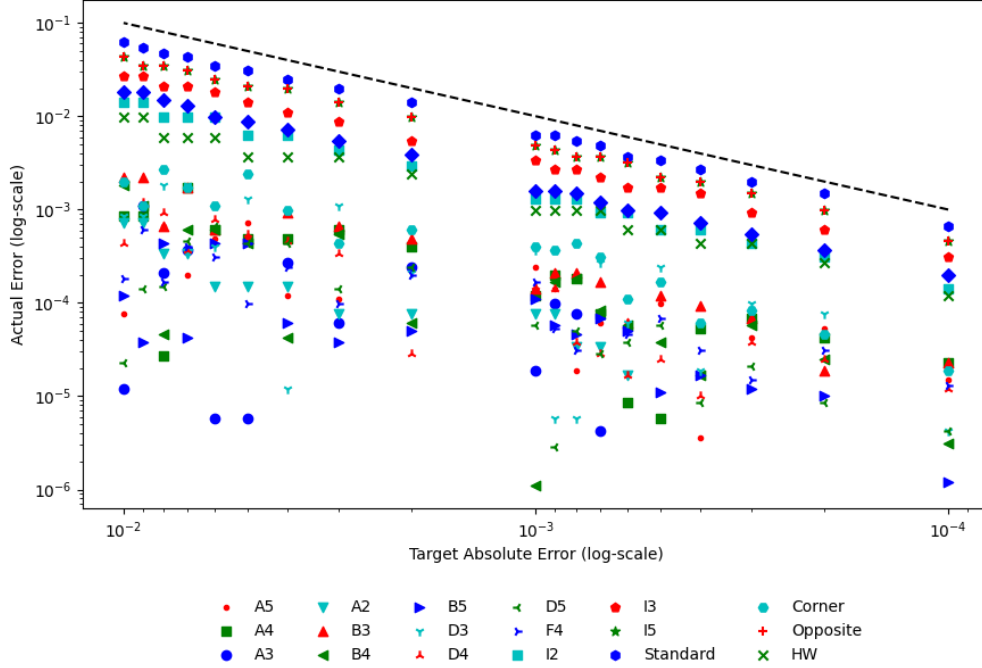


Figure 5.2: Target Absolute Error versus Absolute Error for polyhedral cones with known solid angle measures on log-log scale.

Actual Error = 10(Target Absolute Error). We see that for the cases considered, the error is always strictly less than this, indicating that the power series method gives an approximation whose error is of the order of the given target absolute error parameter ϵ . While these findings provide an empirical foundation for our stopping criterion, they also underscore a notable limitation of both this study and the power series method. The stopping criterion alone does not ensure accuracy, and increasing the target absolute error parameter may not necessarily result in improved accuracy. Therefore, additional exploration is essential to identify the conditions under which the power series method can reliably provide an estimate with an error lower than a specified target absolute error parameter.

5.2.2 Outer Normal Cones of Group-Facet Polytopes

In this section, we report computational results for approximating solid angle measures of outer normal cones of reduced group facet polytopes at their vertices. In the tables that follow, Gom is the number of Facet in Table $P(G_q, (f))$ of [21]. Facet is the facet of of $P(q, f)$ corresponding to the vertex of interest. The bold values correspond to the indices of the chosen set I from the partition of indices as discussed in Section 2.3. Cones is the total number of cones in the power series method decomposition. PS gives the approximation via the power series method with truncation

by target absolute error parameter $\epsilon = 1e - 4$, rounded to the fourth decimal place. The choice of ϵ is based on the fact that the shooting experiment data comes from a shooting experiment with 10,000 shots. For cones having dimension at most four, when applicable, we consider multiple triangulations for the power series method and report in the table the estimate corresponding to the fastest running time. For higher dimensions, we select the triangulation having the smallest number of cones in the decomposition. SSS is the shooting experiment size reported in [41] normalized by a factor of $\frac{1}{10,000}$. As aforementioned, the Cousins–Vempala algorithm is randomized, and the authors of [9] report the average of at least 100 trials in experiments conducted in [9]. As such, we use 100 trials in our experiments. CV is the average solid angle measure approximation obtained from performing 100 trials of the Cousins–Vempala algorithm.

The times are CPU times in seconds, rounded to nearest hundredth of a second. The Time for PS appears directly to the right of it and is the average of three runs of the power series method. The Time for CV appears in the last column and is the average time per trial. That is, the total time spent on computing the CV approximation should be understood as 100 times the listed time.

Table 5.1: Solid angle measures of outer normal cones at vertices of $\tilde{\Pi}(7, 6)$

Gom	Facet						Cones	PS	Time	CV	Time
1	1	2	3	4	5	6	1	0.3238	0.01	0.3245	68.66
4	9	4	6	8	3	12	2	0.2500	0	0.2500	53.77
3	4	8	5	2	6	10	2	0.2500	0	0.2500	52.39
2	6	5	4	3	2	8	1	0.1762	0.01	0.1763	40.11

Since the outer normal cones considered in Table 5.1 are two-dimensional, their exact measures are known. The PS values agree with the exact values rounded to the fourth decimal place. For this case, the power series method is both faster and more accurate than the Cousins–Vempala algorithm. In this example, we see that the most important facet is the mixed integer cut for $P(7, 6)$. The mixed integer cut for a master cyclic group polyhedron is defined in [16], where it is discussed as being a class of frequently hit facets in the shooting experiment.

Table 5.2: Solid angle measures of outer normal cones at vertices of $\tilde{\Pi}(8, 7)$

Gom	Facet							Cones	PS	Time	SSS	CV	Time
1	1	0	1	0	1	0	1	2	0.3051	0.13	0.3081	0.3050	151.93
2	1	2	3	0	1	2	3	2	0.1933	0.06	0.1915	0.1931	92.76
5	1	2	3	4	5	6	7	2	0.1667	0.04	0.1682	0.1669	79.14
7	9	10	3	12	5	6	15	3	0.1250	0	0.1283	0.1250	70.22
4	3	2	1	4	3	2	5	1	0.0811	0.01	0.0815	0.0811	39.11
3	1	2	1	2	1	2	3	1	0.0650	0.02	0.0633	0.0651	29.25
6	7	6	5	4	3	2	9	1	0.0636	0.02	0.0591	0.0633	29.09

In Table 5.2, we see that all three solid angle approximation methods give rise to the same order of importance. We also observe that the two most important facets are those from homomorphic liftings as described in Theorem 1.2.4, which are known to perform well in shooting experiments. In particular, it is noted in [16, 24] that for q not prime, the facets from homomorphic liftings receive a disproportionately high number of hits in shooting experiments. Since the outer normal cones are three-dimensional, we are able to ascertain the exact solid angle measures of the outer normal cones. The PS values agree with the exact measures rounded to the fourth decimal place for all the vertices except $(1, 0, 1)$ where the exact measure rounded to the fourth decimal place is 0.3053. The first two most important facets are from homomorphic lifting. The third most important is from the mixed integer cut.

Table 5.3: Solid angle measures of outer normal cones at vertices of $\tilde{\Pi}(9, 8)$

Gom	Facet				Cones				PS	Time	SSS	CV	Time	
1	1	2	0	1	2	0	1	2	2	0.2958	0.12	0.2915	0.2963	114.63
3	1	2	3	4	5	6	7	8	2	0.1817	0.05	0.1860	0.1814	88.98
5	4	8	12	7	2	6	10	14	2	0.1666	0.03	0.1675	0.1667	88.93
7	16	5	12	10	8	15	4	20	3	0.1250	0.00	0.1256	0.1250	48.03
4	8	7	6	5	4	3	2	10	1	0.1019	0.01	0.1008	0.1020	39.87
6	11	4	6	8	10	12	5	16	1	0.0650	0.02	0.0664	0.0651	27.35
2	2	1	3	2	1	3	2	4	1	0.0636	0.02	0.0622	0.0636	27.32

In Table 5.3, the three approximation methods give the same order of importance for the three-dimensional cones. The power series method is faster than the CV algorithm. The exact normalized solid angle measures rounded to the fourth decimal place are the same as the approximations given by the power series method except at Facets 1 and 5, where the exact measures rounded to the fourth decimal place are 0.2961 and 0.1667 respectively. The two most important facets are from homomorphic lifting and the mixed integer cut.

Table 5.4: Solid angle measures of outer normal cones at vertices of $\tilde{\Pi}(10, 9)$

Gom	Facet									Cones	PS	Time	SSS	CV	Time
1	1	0	1	0	1	0	1	0	1	8	0.2861	0.85	0.2757	0.2854	162.34
3	1	2	3	4	0	1	2	3	4	14	0.1533	325.24	0.1572	0.1522	72.65
4	4	3	2	6	0	4	3	2	6	4	0.1309	0.26	0.1312	0.1290	65.42
9	1	2	3	4	5	6	7	8	9	5	0.1272	1.05	0.1322	0.1263	77.67
12	9	18	7	6	15	14	3	12	21	4	0.0833	0.04	0.0837	0.0839	50.08
11	3	6	4	2	5	3	1	4	7	2	0.0535	0.64	0.0526	0.0532	26.60
10	9	8	7	6	5	4	3	2	11	2	2.94	1.39	0.0411	0.0446	26.51
5	4	3	2	1	5	4	3	2	6	5	0.0353	6.21	0.0358	0.0357	24.14
6	2	4	6	3	5	2	4	6	8	1	0.0259	1.00	0.0254	0.0273	18.79
7	6	7	3	4	5	6	2	3	9	1	0.0236	0.08	0.0256	0.0240	16.03
8	6	2	3	4	5	6	7	3	9	1	0.0208	6.92	0.0217	0.0205	14.73
2	1	2	1	2	1	2	1	2	3	1	0.0158	31.16	0.0158	0.0156	10.81

In Table 5.4, we see that the ranking of facets is the same for the PS and CV values. However, the shooting experiment differs in its rankings of Facets 4 and 9 as well as Facets 6 and 7. The power series method is faster for approximating the solid angle measures of the four-dimensional outer normal cones. We once again observe that the the two most important facets come from homomorphic lifting and mixed integer cuts.

Table 5.5: Solid angle measures of outer normal cones at vertices of $\tilde{\Pi}(11, 10)$

Gom	Facet										Cones	PS	Time	SSS	CV	Time
1	1	2	3	4	5	6	7	8	9	10	3	0.1332	0.45	0.1354	0.1332	73.28
7	4	8	12	16	9	2	6	10	14	18	5	0.1272	1.38	0.1291	0.1273	71.36
13	9	18	16	3	12	21	8	6	15	24	4	0.0908	0.06	0.0935	0.0908	72.88
2	10	9	8	7	6	5	4	3	2	12	8	0.0894	3.23	0.0872	0.0895	56.35
16	16	21	4	20	14	8	24	7	12	28	4	0.0833	0.05	0.0816	0.0832	54.94
17	25	6	20	12	15	18	10	24	5	30	3	0.0809	0.01	0.0813	0.0810	48.68
3	8	5	2	10	7	4	12	9	6	14	2	0.0627	0.73	0.0579	0.0627	47.22
5	6	12	7	2	8	14	9	4	10	16	2	0.0605	0.16	0.0646	0.0605	34.59
11	20	7	16	14	12	10	8	17	4	24	1	0.0411	0.04	0.0403	0.0410	24.82
6	15	8	12	5	9	13	6	10	3	18	1	0.0399	0.05	0.0404	0.0401	35.65
9	13	4	6	8	10	12	14	16	7	20	1	0.0370	0.03	0.0402	0.0370	25.68
4	6	12	7	13	8	3	9	4	10	16	5	0.0351	2.16	0.0297	0.0353	24.81
8	4	8	12	5	9	13	6	10	14	18	1	0.0286	0.16	0.0276	0.0286	19.34
14	9	18	5	14	12	10	19	6	15	24	1	0.0236	0.09	0.0250	0.0236	21.69
18	14	6	20	12	15	18	10	24	16	30	1	0.0190	0.16	0.0187	0.0190	13.21
15	18	14	10	6	13	20	16	12	8	26	1	0.0176	646.49	0.0173	0.0175	11.07
10	13	15	6	8	10	12	14	5	7	20	1	0.0158	33.52	0.0162	0.0158	15.90
12	9	18	16	14	12	10	8	6	15	24	2	0.0134	0.18	0.0140	0.0137	13.55

In Table 5.5, we see that the order of importance given by the power series method and the CV–algorithm agree. The order of importance given by the shooting experiment disagrees with the two other methods for Facets 3 and 5 and Facets 11 and 6. The power series method is faster than the CV–algorithm for these four dimensional cones. We once again observe that the facet corresponding to the mixed integer cut is the most important cut.

5.2.3 Outer Normal Cones of Blockers of Master Cyclic Group Polyhedra

In this section, we report computational results for approximating solid angle measures of outer normal cones at vertices of the blocking polyhedra of master cyclic group polyhedra. Since these polyhedra are of blocking type, and therefore contained in the nonnegative orthant, the approximations are normalized so that an orthant has measure 1. In the tables, Gom is the number of Facet in Table $P(G_q, (f))$ of [21]. Facet is the facet of $P(q, f)$ corresponding to the vertex of interest. Cones is the total number of cones in the power series method decomposition. PS gives the approximation via the power series method with truncation by target absolute error parameter $\epsilon = 1e - 3$. Note that the output of the power series method is scaled by a factor of $2^{|I|}$ as solid angle approximations from shooting experiments are normalized so that an orthant has measure 1. The choice of ϵ is based on the fact that the shooting experiment data comes from a shooting experiment with 1,000 shots. For cones having dimension at most four, when applicable, we consider multiple triangulations for the power series method and report in the table the estimate corresponding to the fastest running time. HSS is the shooting experiment size reported in [32] normalized by a factor of $\frac{1}{1000}$. CV is the average solid angle approximation from 100 trials of the Cousins–Vempala algorithm. The times are CPU times in seconds. The Time for PS is the average of three runs of the power series method. As aforementioned, the Cousins–Vempala algorithm is randomized, and the authors of [9] report the average of at least 100 trials in every experiment. The Time for CV is the average time of per trial. That is, the total time spent on computing the CV approximation should be understood as 100 times the listed time.

Table 5.6: Solid angle measures of outer normal cones at vertices of $\Pi(7, 6) + \mathbb{R}_{\geq 0}^6$

Gom	Facet						Cones	PS	Time	HSS	CV	Time
1	1	2	3	4	5	6	4	0.325	0.17	0.332	0.323	1.87
4	9	4	6	8	3	12	2	0.251	0.02	0.253	0.248	1.53
3	4	8	5	2	6	10	4	0.247	0.21	0.245	0.246	1.68
2	6	5	4	3	2	8	2	0.172	0.05	0.170	0.170	1.39

In Table 5.6, the order or importance given by each of the three approximation methods is consistent. For these four-dimensional cones, we see that the power series method is faster than the Cousins–Vempala algorithm. In this example, we see that the most important facet is the mixed integer cut for $P(7, 6)$. The mixed integer cut for a master cyclic group polyhedron is defined in [16], where it is discussed as being a class of frequently hit facets in the shooting experiment.

An important observation here is that while the order of importance of facets is the same, the approximations in Table 5.6 differ from those in Table 5.1, suggesting that the Shim and Gomory shooting experiments are not equivalent.

Table 5.7: Solid angle measures of outer normal cones at vertices of $\Pi(8, 2) + \mathbb{R}_{\geq 0}^7$

Gom	Facet							Cones	PS	Time	HSS	CV	Time
1	1	2	1	0	1	2	1	4	0.342	0.13	0.367	0.340	4.95
3	3	6	5	4	3	2	1	4	0.325	0.16	0.312	0.325	4.44
2	3	6	1	4	3	2	5	4	0.325	0.16	0.321	0.322	4.69

In Table 5.7, we see that none of the three methods agree on the rankings of Facets 2 and 3. The PS approximations suggest that Facet 2 and Facet 3 are equally important. The CV approximations suggest that Facet 3 is more important than Facet 2, while the shooting experiment suggests the opposite. Note that all three methods rank the facet from homomorphic lifting as most important. We see that the power series method is faster on these 4-dimensional cones. When considering the outer normal cones corresponding to Facet 2 and Facet 3, we have that they are

$$C_2 = \text{cone}((-2, -1, 0, 0), (-1, 0, 0, -1), (-1, 0, 0, 0), (0, -1, -1, 0), (0, 0, -1, 0))$$

$$C_3 = \text{cone}((-1, 0, 0, -1), (0, -1, -1, 0), (0, -1, 0, -2), (0, 0, -1, 0), (0, 0, 0, -1))$$

respectively. Swapping the first and fourth coordinates of each extreme ray corresponds to an isometry between C_2 and C_3 . Thus, Facet 2 and Facet 3 subtend solid angles of equal measure and are therefore equally important, as predicted by the power series method.

Table 5.8: Solid angle measures of outer normal cones at vertices of $\Pi(8, 4) + \mathbb{R}_{\geq 0}^7$

Gom	Facet							Cones	PS	Time	HSS	CV	Time
4	3	2	1	4	1	2	3	2	0.250	0.02	0.259	0.249	1.21
1	1	2	3	4	1	2	3	2	0.250	0.02	0.259	0.247	1.21
3	3	2	1	4	3	2	1	2	0.250	0.02	0.254	0.245	1.23
2	1	2	3	4	3	2	1	2	0.250	0.02	0.228	0.245	1.23

In Table 5.8, we see that the power series method suggests that all four facets are equally important. The shooting experiment suggests Facets 4 and 1 are equally important, but more important than Facets 3 and 2. However, the volume approximation method suggests that Facets 3 and 2 are equally important. One can show that the 4 outer normal cones corresponding to this facet are isometric to each other. Labelling the cones C_4, C_1, C_3 and C_2 as corresponding to Facets 4, 1, 3 and 2 respectively, we have that:

$$C_4 = \text{cone}((-1, -1, 0, 0), (0, -1, 0, 0), (0, 0, -1, -1), (0, 0, -1, 0))$$

$$C_1 = \text{cone}((-1, -1, 0, 0), (-1, 0, 0, 0), (0, 0, -1, -1), (0, 0, -1, 0))$$

$$C_3 = \text{cone}((-1, -1, 0, 0), (0, -1, 0, 0), (0, 0, -1, -1), (0, 0, 0, -1))$$

$$C_2 = \text{cone}((-1, -1, 0, 0), (-1, 0, 0, 0), (0, 0, -1, -1), (0, 0, 0, -1)).$$

Swapping the first and second coordinates of each extreme ray of C_2 shows it is isometric to C_1 . Swapping the third and fourth coordinates of each extreme ray of C_3 shows it is isometric to C_1 . Swapping the first and second coordinates and the third and fourth coordinates of each extreme ray of C_4 shows it is isometric to C_1 . Thus, the four cones are isometric. Therefore, the power series estimate is the exact measure. Furthermore, the power series method is once again faster than the CV algorithm on these four-dimensional cones.

Table 5.9: Solid angle measures of outer normal cones at vertices of $\Pi(8, 7) + \mathbb{R}_{\geq 0}^7$

Gom	Facet							Cones	PS	Time	HSS	CV	Time
1	1	0	1	0	1	0	1	86		> 1 day	0.303	0.309	23.34
2	1	2	3	0	1	2	3	41		> 1 day	0.230	0.192	17.53
5	1	2	3	4	5	6	7	68		> 1 day	0.144	0.166	11.44
7	9	10	3	12	5	6	15	6	0.124	0.16	0.120	0.124	9.82
4	3	2	1	4	3	2	5	18	0.102	51969.90	0.092	0.082	8.34
3	1	2	1	2	1	2	3	7	0.061	1221.40	0.068	0.061	6.28
6	7	6	5	4	3	2	9	25		> 1 day	0.043	0.063	4.31

Table 5.9 shows that the power series method is not efficient at approximating solid angle measures for the six dimensional cones. In particular, the computation appears to be encumbered by large numbers of cones in the decompositions. In contrast, the CV algorithm computes approximations relatively fast. Note that of the three approximations that the power series method is able to compute within 24 hours, 2 match exactly with the CV values.

Table 5.10: Solid angle measures of outer normal cones at vertices of $\Pi(9, 3) + \mathbb{R}_{\geq 0}^8$

Gom	Facet								Cones	PS	Time	HSS	CV	Time
1	2	4	6	5	4	3	2	1	6	0.163	0.27	0.159	0.163	27.02
3	5	1	6	2	4	3	2	4	6	0.163	0.13	0.152	0.163	25.26
5	2	4	6	2	1	3	5	4	6	0.162	0.15	0.151	0.164	25.72
2	2	4	6	2	4	3	2	4	3	0.125	0.02	0.138	0.124	24.29
7	10	2	12	4	5	6	7	8	9	0.112	1339.67	0.129	0.110	23.50
8	4	8	12	7	2	6	10	5	9	0.111	420.93	0.115	0.111	20.64
6	7	5	12	10	8	6	4	2	10	0.098	13.06	0.116	0.111	21.16
4	4	2	6	4	2	3	4	2	28		> 1 day	0.040	0.051	7.81

In Table 5.10, G_9 is the number of Facet in Table $P(G_9, (6))$ of [21]. $P(9, 6)$ and $P(9, 3)$ have the same structure by Theorem 1.2.3. The table shows many discrepancies in the ranking of facets. Notably, none of the three methods agree on which of the six dimensional cones has the largest solid angle measure, thus none of the methods agree on which facet is the most important. The CV method ranks Facet 5 as the most important, while the shooting experiment ranks Facet 1 as the most important, and the PS method ranks Facets 1 and 3 as the most important.

Table 5.11: Solid angle measures of outer normal cones at vertices of $\Pi(9, 8) + \mathbb{R}_{\geq 0}^8$

Gom	Facet								Cones	PS	Time	HSS	CV	Time
1	1	2	0	1	2	0	1	2	52		> 1 day	0.312	0.300	22.87
3	1	2	3	4	5	6	7	8	50		> 1 day	0.170	0.183	14.06
5	4	8	12	7	2	6	10	14	68		> 1 day	0.173	0.167	13.21
7	16	5	12	10	8	15	4	20	6	0.124	0.21	0.115	0.126	9.73
4	8	7	6	5	4	3	2	10	23		> 1 day	0.094	0.100	8.44
2	2	1	3	2	1	3	2	4	25		> 1 day	0.079	0.063	7.67
6	11	4	6	8	10	12	5	16	7	0.061	608.73	0.057	0.062	5.72

In Table 5.11, we see that the power series method cannot efficiently approximate all of the solid angle measures of the six dimensional cones under consideration. We see that we can only approximate the measures of two outer normal cones of $\Pi(9, 8) + \mathbb{R}_{\geq 0}^8$ using the power series method. As with Table 5.2, these results suggest that solid angle measure approximation via the power series method is encumbered by a larger number of cones coming out of the decomposition. In contrast, the Cousins–Vempala algorithm does not take long to compute approximations. Note that the two approximations obtained using the power series method are within 0.002 of the corresponding CV approximations, but differ quite drastically from those given by the shooting experiment. Furthermore, note that the shooting experiment and the CV method rank a facet from homomorphic lifting as being the most important facet. However, the methods do not agree on rankings for Facets 3 and 5.

Table 5.12: Solid angle measures of outer normal cones at vertices of $\Pi(10, 2) + \mathbb{R}_{\geq 0}^9$

Gom	Facet									Cones	PS	Time	HSS	CV	Time
1	2	4	1	3	0	2	4	1	3	31		> 1 day	0.198	0.209	15.75
2	3	6	4	2	0	3	6	4	2	41		> 1 day	0.177	0.191	14.45
5	4	8	7	6	5	4	3	2	1	52		> 1 day	0.199	0.183	15.84
7	6	12	3	4	10	6	2	8	9	6	0.163	0.28	0.168	0.163	14.21
3	3	6	4	2	5	3	1	4	2	17	0.136	8114.87	0.141	0.126	12.38
4	4	8	2	6	5	4	3	2	6	3	0.086	0.08	0.077	0.086	7.39
6	6	12	3	4	5	6	7	8	9	14		> 1 day	0.040	0.041	4.56

In Table 5.12, Gom is the number of Facet in Table $P(G_{10}, (8))$ of [21]. $P(10, 8)$ and $P(10, 2)$ have the same structure by Theorem 1.2.3. We see that the power series method cannot efficiently approximate all of the solid angle measures of the six dimensional cones under consideration. We see that we can only approximate the measures of three outer normal cones of $\Pi(10, 2) + \mathbb{R}_{\geq 0}^9$ using the power series method. As with Table 5.2 and Table 5.11, these results suggest that solid angle measure approximation via the power series method is encumbered by a larger number of cones coming out of the decomposition. In contrast, the Cousins–Vempala algorithm does not take long to compute approximations. It is interesting to observe that of the three approximations obtained via the power series method, two match exactly with that of the CV approximations. Furthermore, these two approximations are obtained much faster via the power series method than the CV algorithm. We see that the CV values rank a facet from homomorphic lifting as most important whereas the shooting experiment ranks a facet from the mixed integer cut as most important.

Appendices

Appendix A: SageMath Program

The following program is to approximate solid angle measures for polyhedral cones. Below, we include two main functions for computing solid angle measures of simplicial cones, and solid angle measures of simplicial cones with positive definite associated matrices respectively. A simplicial cone should be represented as a matrix whose rows give the extreme rays of the cone. The code, including the helper functions called in the two main functions, can be accessed at [17].

```
def solid_angle_measure(simplicial_cone, deg=100000, eps=1e-6,
    ↪ base_ring=RR, decompose_to_tridiag=False, verbose=False):
r"""
Return an estimate of the sum of the normalized solid angle
↪ measure of the cones generated by the row vectors of the
↪ matrices in the given list of matrices, based on a truncated
↪ form of Jason Ribando's formula (see note).

INPUT:

- ``simplicial_cone`` -- a matrix or a list that is convertible
↪ to a matrix; the row vectors of ``M`` span the cone for
↪ which we compute its solid angle.

- ``deg`` -- integer (default: `100`); ``deg`` is the maximum
↪ sum of the powers of the  $\alpha_{ij}$ 's in the summation
↪ (i.e. it is the maximum sum of the terms in the
↪ multiexponent.)

- ``eps`` -- positive real number (default: `1e-6`); this
↪ parameter is used to determine when the summation stops. In
↪ terms of the partial sum, when  $s_n - s_{n-1} < \epsilon$ , we
↪ stop adding terms to the partial sum sequence.

- ``base_ring`` -- a sub-field of the reals implemented in Sage
↪ (default: RR). The base_ring parameter determines the field
↪ in which arithmetic is done.

- ``decompose_to_tridiag`` -- boolean (default: False). Whether
↪ each cone in the decomposition should have a tridiagonal
↪ associated matrix.
```

- `verbose` -- (optional) boolean(default: False). Whether to
→ print out intermediate data.

OUTPUT:

- an estimate of the sum of the normalized solid angle measures
→ of the given simplicial cone

EXAMPLES:

This example shows the measure of the solid angle spanned by the
→ vectors `[1,0]` and `[-1,-1]`. Note that it agrees with
→ the value obtained by the arctan formula.::

```
sage: logging.disable(logging.INFO)
sage: A = matrix([[1,0],[-1,-1]])
sage: solid_angle_measure(A, eps=1e-6)
0.374998211389711
```

This example shows the measure of the solid angle spanned by the
→ vectors `[2, sqrt(2), 3]`, `[-1, 1, 2]`, and `[-3, 0,`
→ `5/4]`, with `deg` set to `20` and `eps` set to
→ `1e-6`. The relative error compared to value `0.01183`
→ obtained by the arctan formula is `<0.5%`.::

```
sage: A = matrix(RR, [[2, sqrt(2), 3], [-1, 1, 2], [-3, 0, ↵
5/4]])
sage: a = solid_angle_measure(A, deg=50, eps=1e-6)
sage: b = solid_angle_3d(A)
sage: abs(a-b)/b < 5e-5
True
```

The following are examples of estimations of the solid angle
→ measure of a cone in `\RR^5` using different `deg`
→ values.::

```
sage: A = matrix([[1,1,0,0,0], [-1,3,0,-4,1], [5,0,0,-1,0], ↵
[0,0,-2,1,4], [0,0,0,0,1]])
sage: solid_angle_measure(A, deg=10)
0.00533087907335968
```

```
sage: solid_angle_measure(A, deg=12)
0.00487047236050033
```

```
sage: solid_angle_measure(A, deg=18)
0.00407911422649577
```

TESTS:

In the following examples, we consider cones formed by Coxeter
 → arrangements in various dimensions of various types. The
 → hyperplanes of a Coxeter arrangement of type B_n
 → subdivide R^n into $n! \cdot 2^n$ isometric cones, each with
 → normalized solid angle measure $1/(n! \cdot 2^n)$.

We consider cones formed by the B_2 arrangement in R^2 .
 → The expected value is $1/(2! \cdot 2^2) = 1/8$:

```
sage: B2 = matrix([[1,1],[1,0]])
sage: solid_angle_measure(B2)
0.125000319734726
```

We consider cones formed by the B_3 arrangement in R^3 .
 → The expected value is $1/(3! \cdot 2^3) = 1/48$:

```
sage: B3 = matrix([[1,0,0],[1,1,0],[1,1,1]])
sage: solid_angle_measure(B3)
0.0208338480731115
```

We consider cones formed by the B_4 arrangement in R^4 .
 → The expected value is $1/(4! \cdot 2^4) = 1/384$:

```
sage: B4 = matrix([[1,0,0,0],[1,1,0,0],[1,1,1,0],[1,1,1,1]])
sage: solid_angle_measure(B4)
0.00260509099329648
```

The hyperplanes of a Coxeter arrangement of type D_n (n at
 → least 4) subdivide R^n into $n! \cdot 2^{(n-1)}$ isometric
 → cones, each with normalized solid angle measure
 → $1/(n! \cdot 2^{(n-1)})$.

We consider cones formed by the D_4 arrangement in R^4 .
 → The expected value is $1/(4! \cdot 2^3) = 1/192$:

```
sage: D4 = matrix([[1,0,0,0],[1,1,0,0],[1,1,1,1],[1,1,1,-1]])
sage: solid_angle_measure(D4, eps=1e-4)
0.00523328191018306
```

.. NOTE::

*This function decomposes the cone of interest into cones
↪ with positive definite associated matrices, hence into
↪ cones whose solid angles are computable via Ribando's
↪ formula.*

"""

*# since number nonzero parts may be different, we clear the
multipermutation cache*

`multipermute.clear_cache()`

`multipermute_by_frequency_dict = {}`

`solid_angle_prod = 1`

decompose the cone into an orthogonal direct sum

`for orth_cone in generate_orthogonal_parts(simplicial_cone):`

*# decompose to cones with positive definite associated
matrices*

`if decompose_to_tridiag:`

`if verbose:`

`↪ print(list(generate_tridiag_cones_decomposition(orth_cone)))`

`t = sum(s*solid_angle_simplicial_and_posdef(c, deg=deg,`

`↪ eps=eps, base_ring=base_ring, space="affine",`

`↪ tridiag=True, verbose=verbose,`

`↪ multipermute_by_frequency_dict=`

`multipermute_by_frequency_dict)`

`for (c, s) in`

`↪ generate_tridiag_cones_decomposition(orth_cone))`

`else:`

`if is_M_alpha_posdef(orth_cone) == True:`

`if verbose is True:`

`print([orth_cone, 1])`

`t = solid_angle_simplicial_and_posdef(orth_cone,`

`↪ deg=deg, eps=eps, base_ring=base_ring,`

`↪ space="affine", tridiag=False, verbose=verbose,`

`↪ multipermute_by_frequency_dict=`

`multipermute_by_frequency_dict)`

`else:`

`if verbose:`

`print(list(generate_cones_decomposition(orth_cone)))`

`t = sum(s*solid_angle_simplicial_and_posdef(c,`

`↪ deg=deg, eps=eps, base_ring=base_ring,`

`↪ space="affine", verbose=verbose,`

`↪ multipermute_by_frequency_dict=`

`multipermute_by_frequency_dict)`

```

        for (c, s) in
            ↪ generate_cones_decomposition(orth_cone)
solid_angle_prod *= t
logging.info('Solid angle measure is %s.', solid_angle_prod)
logging.info(' ')
return(solid_angle_prod)

def solid_angle_simplicial_and_posdef(M, eps=1e-6, deg=1000000000,
    ↪ space="ambient", tridiag=False, base_ring=RR, verbose=False,
    ↪ multipermute_by_frequency_dict={}):
    r"""
    Return an estimate of the normalized solid angle measure of the
    cone spanned by the row vectors of the given matrix ``A``, based
    on a truncated form of Jason Ribando's formula (see note).

    INPUT:

    - ``M`` -- a matrix or a list that is convertible to a matrix;
    ↪ the row vectors of ``M`` span the cone for which we compute
    ↪ its solid angle. The cone is assumed to have positive
    ↪ definite associated matrix.

    - ``eps`` -- positive real number (default: ``1e-6``); this
    ↪ parameter is used to determine when the summation stops. In
    ↪ terms of the partial sum, when  $s_n - s_{n-1} < \epsilon$ , we
    ↪ stop adding terms to the partial sum sequence.

    - ``deg`` -- integer (default: ``100``); ``deg`` is the maximum
    ↪ sum of the powers of the  $\alpha_{ij}$ 's in the summation
    ↪ (i.e. it is the maximum sum of the terms in the
    ↪ multiexponent.)

    - ``space`` -- either "ambient" (by default) or "affine",
    ↪ indicating with respect to which space the solid angle of
    ↪ the cone is considered.

    - ``tridiag`` -- boolean (default: False). Whether the associated
    ↪ matrix of the cone is tridiagonal or not.

    - ``base_ring`` -- a sub-field of the reals implemented in Sage
    ↪ (default: RR). The base_ring parameter determines the field
    ↪ in which arithmetic is done.

```

- `verbose` -- (optional) boolean(default: False). Whether to
 ↪ print out intermediate data for the power series, such as
 ↪ the degree, term, and partial sums.

OUTPUT:

- an estimate of the normalized solid angle measure spanned by
 ↪ the row vectors given in `M`.

EXAMPLES:

This example shows the measure of the solid angle spanned by the
 ↪ vectors `[1,0]` and `[-1,-1]`. Note that it agrees with
 ↪ the value obtained by the arctan formula.::

```
sage: logging.disable(logging.INFO)
sage: M = matrix([[1,0],[-1,-1]])
sage: solid_angle_simplicial_and_posdef(M, eps=1e-9) # abs→
tol 2e-9
0.375
```

This example shows that when the vectors are linearly dependent,
 ↪ the measure of the solid angle with respect to the ambient
 ↪ space is 0::

```
sage: M = matrix([[2,0,0], [0,3,0], [-4,-4,0]])
sage: solid_angle_simplicial_and_posdef(M, space="ambient")
WARNING:root:cone not full-dimensional
0
```

This example shows the measure of the solid angle spanned by the
 ↪ vectors `[2, sqrt(2), 3]`, `[-1, 1, 2]`, and `[-3, 0,`
 ↪ `5/4]`, with `deg` set to `20` and `eps` set to
 ↪ `1e-6`. The relative error compared to value `0.01183`
 ↪ obtained by the arctan formula is `<0.5%`.::

```
sage: M=matrix(RR, [[2, sqrt(2), 3], [-1, 1, 2], [-3, 0,↪
5/4]])
sage: a = solid_angle_simplicial_and_posdef(M, deg=20,
↪ eps=1e-6)
sage: b = solid_angle_3d(M)
sage: abs(a-b)/b < 0.005
True
```

This example shows an estimation of the measure of the solid
 ↪ angle spanned by vectors \mathbb{R}^5 , with different deg
 ↪ values.::

```
sage: A = [[1,1,0,0,0],[-1,3,0,-4,1],[5,0,0,-1,0],
.....:      [0,0,-2,1,4],[0,0,0,0,1]]
sage: solid_angle_simplicial_and_posdef(A, eps=-1, deg=10)
↪ # abs tol 1e-15
0.00533087907335968
```

```
sage: solid_angle_simplicial_and_posdef(A, eps=-1, deg=12) #↪
long time (18 s), abs tol 1e-15
0.00487047236050033
```

TESTS:

The example below is based on Example 3.4 in Gourion and Seeger
 ↪ (see note). For the matrix A below, the authors used
 ↪ truncated forms of Ribando's formula, testing $\text{deg} =$
 ↪ $0, 1, 2, 5, 10, 20$, and 40 . The estimates they obtained were
 ↪ $0.097403, 0.067204, 0.082871, 0.079939, 0.080930, 0.080878,$
 ↪ and 0.080878 respectively. The authors normalized their
 ↪ measurement with respect to a half space. Thus, the function
 ↪ should return estimates that are half of the above values.
 ↪ Below, we show that this is the case. We observe that the
 ↪ last two returns are equal, showing that $\text{eps}=1e-6$ is too
 ↪ large when $\text{deg}=40$.::

```
sage: A = matrix([[1/2, -1/2, -1/2, 1/2],[1/2, 1/10, 7/10,
↪ 1/2],
.....:      [-4/7, 4/7, 1/7, 4/7], [-4/11, -5/11, 8/11,
↪ 4/11]])
sage: solid_angle_simplicial_and_posdef(A, deg=1)
↪ # abs tol 1e-15
0.0336018459286235
```

```
sage: solid_angle_simplicial_and_posdef(A, deg=2)
↪ # abs tol 1e-15
0.0431921854297128
```

```
sage: solid_angle_simplicial_and_posdef(A, deg=5)
↪ # abs tol 1e-15
0.0399696621189179
```

```
sage: solid_angle_simplicial_and_posdef(A, deg=10)
↪ # abs tol 1e-15
0.0404638509737549
```

```
sage: solid_angle_simplicial_and_posdef(A, deg=20) # abs
↪ tol 1e-15
0.0404387819367501
```

```
sage: solid_angle_simplicial_and_posdef(A, deg=40) # abs
↪ tol 1e-15
0.0404387819367501
```

.. NOTE::

*This function uses the formula given in Ribando's 2006 paper
↪ entitled "Measuring Solid Angles Beyond Dimension Three."
↪ More specifically, it is a truncated form of the multi-
↪ variate power series given in Theorem 2.2.*

*In Gourion and Seeger's 2010 paper entitled "Deterministic
↪ and stochastic methods for computing volumetric moduli
↪ of convex cones, the authors look at the volumetric
↪ modulus/ normalized volume of convex polyhedral cones,
↪ in comparison to a half space. See Theorem 4.1 and
↪ Remark 4.2.*

"""

```
Start_Time = time.process_time()
if not hasattr(M, 'nrows'):
    M = matrix(M)
if space == "ambient" and M.rank() < M.ncols():
    logging.warning("cone not full-dimensional")
return 0
prod = 1
br_pi = base_ring(pi)
sqrt_pi = base_ring(sqrt(br_pi))
trunc_degs = []

for A in generate_orthogonal_parts(M):
    # is M has positive-definite block associated matrix, it's ↪
    blocks have positive-definite associated matrices
    d = A.nrows()

    # if cone is 1 ray, affine solid angle is 1/2
    if d == 1:
        prod *= base_ring(1/2)
```



```

    trunc_degs.append(0)
continue
# the only multivariables contributing to the sum are the
nonzero ones
v = matrix([A[i]/A[i].norm() for i in range(d)]) # leave as
    ↪ norm, otherwise lose 0s in vtv
dot_prod_matrix = v * v.transpose()

# find the values for the multivariable alpha
if tridiag: # if tridiag is True, we only consider the
    tridiagonal part of the dot product matrix
    nonzero_inds = [(i, i+1) for i in range(d - 1) if
        ↪ dot_prod_matrix[i][i+1] != 0]
else:
    nonzero_inds = [(i, j) for i in range(d - 1) for j in
        ↪ range(i + 1, d) if dot_prod_matrix[i][j] != 0]
alpha = [base_ring(dot_prod_matrix[i, j]) for (i, j) in
nonzero_inds]
number_nonzero_parts = len(alpha)

# if all dihedral angles are 0, the cone is an orthant
if number_nonzero_parts == 0:
    prod *= base_ring(1/2) ** d
    trunc_degs.append(0)
    continue

# compute the constant and use it to determine the threshold
for truncation
const = base_ring(sqrt((dot_prod_matrix).determinant())) / ((2
    ↪
    * sqrt_pi) ** d)
threshold = eps / const

# zero term for power series
partial_sum = sqrt_pi ** d

two_to_deg = 1
prev_sum_deg_n = partial_sum
if verbose:
    logging.info('Degree:, Current Term:, Partial Sum:, Avg of
        ↪ Terms:')
for n in range(1, deg + 1):
    two_to_deg *= -2

```

```

sum_deg_n = sum(sum_partition(partition, alpha, sqrt_pi,
↪ base_ring, nonzero_inds, number_nonzero_parts,
↪ multipermute_by_frequency_dict) for partition in
↪ weak_partitions(n, number_nonzero_parts))
partial_sum += (two_to_deg * sum_deg_n)
if verbose:
    logging.info([n, (const * sum_deg_n), (const *
↪ partial_sum), (const * 0.5 * (abs(two_to_deg *
↪ sum_deg_n) + abs(two_to_deg/2 *
↪ prev_sum_deg_n)))]))
# check if we should truncate the series at degree n
if (0.5 * (abs(two_to_deg * sum_deg_n) + abs(two_to_deg/2 *
↪ prev_sum_deg_n))) < threshold:
    trunc_degs.append(n)
    break
prev_sum_deg_n = sum_deg_n
prod *= base_ring(const * (partial_sum))
Execution_Time = time.process_time() - Start_Time
logging.info('Simplicial cone with positive-definite associated
↪ matrix \n%s\n truncated at degrees %s. Took %s CPU s to
↪ compute solid angle %s.', sage_input(matrix(M)), trunc_degs,
↪ Execution_Time, prod)
logging.info(' ')
return prod

```

Appendix B: Cones and Triangulations

Unless otherwise stated, we consider all of the triangulations for the cones below. When a subset of triangulations is considered, we give the extreme rays of the cone as an ordered list and a list of the considered triangulations.

0. Outer normal cone of $\tilde{\Pi}(9, 8)$ at vertex $(1/8, 1/4, 3/8)$
1. Outer normal cone of $\tilde{\Pi}(11, 10)$ at vertex $(1/10, 1/5, 3/10, 2/5)$
2. Outer normal cone of $\tilde{\Pi}(11, 10)$ at vertex $(2/9, 4/9, 2/3, 8/9)$
3. Outer normal cone of $\tilde{\Pi}(11, 10)$ at vertex $(3/8, 3/4, 7/16, 13/16)$
4. Outer normal cone of $\tilde{\Pi}(11, 10)$ at vertex $(3/8, 3/4, 7/16, 1/8)$
5. Outer normal cone of $\tilde{\Pi}(11, 10)$ at vertex $(3/8, 3/4, 2/3, 1/8)$
6. Outer normal cone of $\tilde{\Pi}(11, 10)$ at vertex $(4/7, 5/14, 1/7, 5/7)$
7. Outer normal cone of $\tilde{\Pi}(11, 10)$ at vertex $(4/7, 3/4, 1/7, 5/7)$

8. Outer normal cone of $\tilde{\Pi}(11, 10)$ at vertex $(5/6, 3/4, 2/3, 7/12)$
9. Outer normal cone of $\tilde{\Pi}(10, 9)$ at vertex $(1/9, 2/9, 1/3, 4/9)$
10. Outer normal cone of $\tilde{\Pi}(10, 9)$ at vertex $(3/7, 6/7, 1/3, 2/7)$
11. Outer normal cone of $\tilde{\Pi}(10, 9)$ at vertex $(3/7, 6/7, 4/7, 2/7)$
12. Outer normal cone of $\tilde{\Pi}(10, 9)$ at vertex $(2/3, 1/2, 1/3, 1)$
13. Outer normal cone of $\tilde{\Pi}(10, 9)$ at vertex $(2/3, 1/2, 1/3, 1/6)$
14. Outer normal cone of $\tilde{\Pi}(10, 9)$ at vertex $(9/11, 8/11, 7/11, 6/11)$
15. Outer normal cone of $\tilde{\Pi}(10, 9)$ at vertex $(1/4, 1/2, 3/4, 1)$

- Ordered rays:

$$[-2, 1, 0, 0], [-1, -1, 1, 0], [-1, 0, -1, 1], [0, -2, 0, 1], \\ [0, 1, 2, 0], [0, 2, 0, 1], [1, 0, 1, 1]$$

- Triangulations:

- $[0, 1, 2, 4], [0, 2, 4, 5], [1, 2, 3, 4], [2, 3, 4, 5], [3, 4, 5, 6]$
- $[0, 1, 2, 4], [0, 2, 4, 5], [1, 2, 3, 4], [2, 3, 4, 6], [2, 4, 5, 6]$
- $[0, 1, 2, 4], [0, 2, 4, 5], [1, 2, 3, 6], [1, 2, 4, 6], [2, 4, 5, 6]$
- $[0, 1, 2, 6], [0, 1, 4, 6], [0, 2, 5, 6], [0, 4, 5, 6], [1, 2, 3, 6]$

16. Outer normal cone of $\tilde{\Pi}(10, 9)$ at vertex $(1, 0, 1, 0)$

- Ordered rays:

$$[-1, -1, 1, 0], [-1, 0, 0, -2], [0, -2, 0, 1], [0, -1, -1, -1], \\ [0, 1, 2, 0], [1, 0, 1, 1], [1, 1, 0, -1], [2, 0, -1, 0]$$

- Triangulations:

- $[0, 1, 2, 4], [1, 2, 3, 4], [1, 3, 4, 6], [2, 3, 4, 5], [2, 3, 5, 7], [3, 4, 5, 6], [3, 5, 6, 7]$
- $[0, 1, 3, 4], [0, 2, 3, 4], [1, 3, 4, 6], [2, 3, 4, 5], [2, 3, 5, 7], [3, 4, 5, 6], [3, 5, 6, 7]$
- $[0, 1, 2, 4], [1, 2, 3, 4], [1, 3, 4, 6], [2, 3, 4, 5], [2, 3, 5, 7], [3, 4, 5, 7], [3, 4, 6, 7]$
- $[0, 1, 2, 4], [1, 2, 3, 5], [1, 2, 4, 5], [1, 3, 5, 6], [1, 4, 5, 6], [2, 3, 5, 7], [3, 5, 6, 7]$
- $[0, 1, 2, 4], [1, 2, 3, 4], [1, 3, 4, 6], [2, 3, 4, 6], [2, 3, 6, 7], [2, 4, 5, 6], [2, 5, 6, 7]$
- $[0, 1, 3, 4], [0, 2, 3, 4], [1, 3, 4, 6], [2, 3, 4, 5], [2, 3, 5, 7], [3, 4, 5, 7], [3, 4, 6, 7]$
- $[0, 1, 2, 4], [1, 2, 3, 4], [1, 3, 4, 6], [2, 3, 4, 7], [2, 4, 5, 7], [3, 4, 6, 7]$
- $[0, 1, 2, 4], [1, 2, 3, 4], [1, 3, 4, 7], [1, 4, 6, 7], [2, 3, 4, 5], [2, 3, 5, 7], [3, 4, 5, 7]$
- $[0, 1, 2, 4], [1, 2, 3, 6], [1, 2, 4, 5], [1, 2, 5, 6], [1, 4, 5, 6], [2, 3, 6, 7], [2, 5, 6, 7]$
- $[0, 1, 2, 5], [0, 1, 4, 5], [1, 2, 3, 5], [1, 3, 5, 6], [1, 4, 5, 6], [2, 3, 5, 7], [3, 5, 6, 7]$

17. Outer normal cone of $\tilde{\Pi}(8, 7)$ at vertex $(1/7, 2/7, 3/7)$
18. Outer normal cone of $\tilde{\Pi}(8, 7)$ at vertex $(1/3, 2/3, 1)$
19. Outer normal cone of $\tilde{\Pi}(8, 7)$ at vertex $(1, 0, 1)$
20. Outer normal cone of $\tilde{\Pi}(12, 11)$ at vertex $(1/3, 2/3, 1/3, 2/3, 1/3)$
21. Cone isometric to a four-dimensional orthant
 - rays = $[[2, 0, 1, 0], [1, 0, 0, 1], [0, 1, 1, 0], [0, 0, 2, 1], [0, 0, 1, 0]]$
22. Cone which contains two copies of the Weyl chamber F_4
 - rays = $[[1, 0, 0, 0], [1, 1, 0, 0], [2, 1, 1, 0], [3, 1, 1, 1], [3, 1, 1, -1]]$
23. Cone which contains two copies of the Weyl chamber B_4
 - rays = $[[1, 0, 0, 0], [1, 1, 0, 0], [1, 1, 1, 0], [1, 1, 1, 1], [1, 1, 0, 1]]$

Bibliography

- [1] K. Aomoto. Analytic structure of Schläfli function. *Nagoya Math. J.*, 68:1–16, 1977.
- [2] J. Aráoz, L. Evans, R. E. Gomory, and E. L. Johnson. Cyclic groups and knapsack facets. *Math. Program.*, 96(2, Ser. B):377–408, 2003.
- [3] V. Baldoni, N. Berline, M. Köppe, and M. Vergne. Intermediate sums on polyhedra: computation and real Ehrhart theory. *Mathematika*, 59(1):1–22, 2013.
- [4] I. Bárány and Z. Füredi. Computing the volume is difficult. *Discrete Comput. Geom.*, 2(4):319–326, 1987.
- [5] M. Beck and S. Robins. Solid angles. In *Computing the Continuous Discretely: Integer-Point Enumeration in Polyhedra*, chapter 11, pages 179–190. Springer New York, New York, NY, 2007.
- [6] M. Beck, S. Robins, and S. V. Sam. Positivity theorems for solid-angle polynomials. *Beiträge Algebra Geom.*, 51(2):493–507, 2010.
- [7] N. Bourbaki. *Lie Groups and Lie Algebras: Chapters 4–6*. Springer-Verlag Berlin Heidelberg, 1989.
- [8] M. Brion and M. Vergne. Residue formulae, vector partition functions and lattice points in rational polytopes. *J. Amer. Math. Soc.*, 10(4):797–833, 1997.
- [9] B. Cousins and S. Vempala. A practical volume algorithm. *Math. Program. Comput.*, 8(2):133–160, 2016.
- [10] B. Cousins and S. Vempala. MATLAB code Volume-and-sampling (version 2.2.1). <https://in.mathworks.com/matlabcentral/fileexchange/43596-volume-and-sampling>, 2022.
- [11] S. Dash and O. Günlük. Valid inequalities based on the interpolation procedure. *Math. Program.*, 106(1, Ser. A):111–136, 2006.
- [12] M. Dyer, A. Frieze, and R. Kannan. A random polynomial-time algorithm for approximating the volume of convex bodies. *J. Assoc. Comput. Mach.*, 38(1):1–17, 1991.
- [13] R. Ehrenborg. private communication, Mar. 2024.
- [14] G. Elekes. A geometric inequality and the complexity of computing volume. *Discrete Comput. Geom.*, 1(4):289–292, 1986.
- [15] F. Eriksson. On the measure of solid angles. *Math. Mag.*, 63(3):184–187, 1990.

- [16] L. A. Evans. *Cyclic group and knapsack facets with applications to cutting planes*. PhD thesis, Georgia Institute of Technology, 2002.
- [17] A. Fitisone and Y. Zhou. SageMath code for computing solid angles of polyhedral cones. <https://github.com/yuan-zhou/solid-angle-code>, 2023.
- [18] A. Fitisone and Y. Zhou. Solid angle measure of polyhedral cones. eprint arXiv: 2304.11102 [math.MG], 2023.
- [19] L. Fukshansky and S. Robins. Bounds for solid angles of lattices of rank three. *J. Combin. Theory Ser. A*, 118(2):690–701, 2011.
- [20] E. Garrison. Permutations of a multiset. <https://github.com/ekg/multichoose/blob/master/multipermute.py>, 2010.
- [21] R. E. Gomory. Some polyhedra related to combinatorial problems. *Linear algebra and its applications*, 2(4):451–558, 1969.
- [22] R. E. Gomory and E. L. Johnson. Some continuous functions related to corner polyhedra. *Math. Programming*, 3:23–85, 1972.
- [23] R. E. Gomory and E. L. Johnson. T-space and cutting planes. volume 96, pages 341–375. 2003.
- [24] R. E. Gomory, E. L. Johnson, and L. Evans. Corner polyhedra and their connection with cutting planes. *Math. Program.*, 96(2, Ser. B):321–339, 2003.
- [25] D. Gourion and A. Seeger. Deterministic and stochastic methods for computing volumetric moduli of convex cones. *Comput. Appl. Math.*, 29(2):215–246, 2010.
- [26] D. Gourion and A. Seeger. Deterministic and stochastic methods for computing volumetric moduli of convex cones. *Comput. Appl. Math.*, 29(2):215–246, 2010.
- [27] M. Hajja and P. Walker. The measure of solid angles in n -dimensional Euclidean space. *Internat. J. Math. Ed. Sci. Tech.*, 33(5):725–729, 2002.
- [28] M. Herceg, M. Kvasnica, C. Jones, and M. Morari. Multi-Parametric Toolbox 3.0. In *Proc. of the European Control Conference*, pages 502–510, Zürich, Switzerland, July 17–19 2013. <http://control.ee.ethz.ch/~mpt>.
- [29] R. Heylen and P. Scheunders. Multidimensional pixel purity index for convex hull estimation and endmember extraction. *IEEE Transactions on Geoscience and Remote Sensing*, 51(7):4059–4069, 2013.
- [30] J. Horn. Ueber die Convergenz der hypergeometrischen Reihen zweier und dreier Veränderlichen. *Math. Ann.*, 34(4):544–600, 1889.
- [31] J. E. Humphreys. *Introduction to Lie Algebras and Representation Theory*, volume 9. Springer-Verlag New York, 1972.

- [32] B. K. Hunsaker. *Measuring Facets of Polyhedra to Predict Usefulness in Branch-and-Cut Algorithms*. PhD thesis, Georgia Institute of Technology, 2003.
- [33] Z. Kabluchko and D. Zaporozhets. Absorption probabilities for Gaussian polytopes and regular spherical simplices. *Adv. in Appl. Probab.*, 52(2):588–616, 2020.
- [34] H. W. Kuhn. *On the origin of the Hungarian Method, History of mathematical programming; a collection of personal reminiscences (JK Lenstra, AHG Rinnooy Kan, and A. Schrijver, eds.)*. North Holland, Amsterdam, 1991.
- [35] M. S. Mariani, Z.-M. Ren, J. Bascompte, and C. J. Tessone. Nestedness in complex networks: observation, emergence, and implications. *Phys. Rep.*, 813:1–90, 2019.
- [36] O. Mazonka. Solid angle of conical surfaces, polyhedral cones, and intersecting spherical caps, 2012.
- [37] B. N. Parlett. *The symmetric eigenvalue problem*. Society for Industrial and Applied Mathematics, 1998.
- [38] J. M. Ribando. *Probabilistic methods for efficient triangulations of the n-cube*. PhD thesis, University of California, San Diego, 2000.
- [39] J. M. Ribando. Measuring solid angles beyond dimension three. *Discrete Comput. Geom.*, 36(3):479–487, 2006.
- [40] A. Schrijver et al. *Polyhedral combinatorics*. CWI, 1987.
- [41] S. Shim. *Large scale group network optimization*. PhD thesis, Georgia Institute of Technology, 2009.
- [42] S. Shim and E. L. Johnson. Cyclic group blocking polyhedra. *Math. Program.*, 138(1-2, Ser. A):273–307, 2013.
- [43] J. Stoer and C. Witzgall. *Convexity and optimization in finite dimensions. I*. Die Grundlehren der mathematischen Wissenschaften, Band 163. Springer-Verlag, New York-Berlin, 1970.
- [44] The Sage Developers. *SageMath, the Sage Mathematics Software System (Version 9.6)*, 2022. <https://www.sagemath.org>.
- [45] A. Williams. Loopless generation of multiset permutations using a constant number of variables by prefix shifts. In *Proceedings of the Twentieth Annual ACM-SIAM Symposium on Discrete Algorithms*, pages 987–996. SIAM, Philadelphia, PA, 2009.

Vita

Allison Marie Fitisone

Place of Birth:

- Pago Pago, American Samoa

Education:

- University of Kentucky, Lexington, KY
Ph.D. in Mathematics, expected May 2024
M.A. in Mathematics, May 2021
- Berea College, Berea, KY
B.A. in Mathematics, May 2017
summa cum laude

Professional Positions:

- Graduate Teaching Assistant, University of Kentucky Fall 2019–Spring 2024
- Mathematics Teacher, South Pacific Academy Fall 2017–Spring 2019
- Teaching Assistant, Berea College Fall 2015–Spring 2017

Publications & Preprints:

- "Solid angle measure of polyhedral cones," with Yuan Zhou, arXiv:2304.11102 (submitted)